Structural Insights into the Regulation of the L-type Voltage-gated Channel $Ca_V1.2$ by Half-Calcified Calmodulin (CaM) and Calcium-binding Protein 1 (CaBP1)

By

IAN SALVESON

DISSERTATION

Submitted in partial satisfaction of the requirements for the degree of

DOCTOR OF PHILOSOPHY

in

Chemistry

in the

OFFICE OF GRADUATE STUDIES

of the

UNIVERSITY OF CALIFORNIA

DAVIS

Approved:

_____

James B. Ames, Chair

_____

Justin Siegel

_____

Johannes Hell

Committee in Charge

2023

ABSTRACT

The L-type voltage gated calcium channel $Ca_V1.2$ is expressed in smooth and cardiac muscle, as well as in neurons where it regulates neuronal excitability and synaptic transmission. Mutations that disrupt channel regulation are linked to various disorders including cardiac arrythmia, Timothy's Syndrome and epilepsy. Calmodulin (CaM) and calcium-binding protein 1 (CaBP1) are both key modulators of $Ca_V1.2$ activity. Under basal resting conditions (cytosolic Ca^{2+} concentration equal to 100 nM), both CaM and CaBP1 promote channel opening. Under high calcium conditions (cytosolic Ca^{2+} concentration greater than 1 μM), Ca^{2+}-bound CaBP1 further activates the channel in a process called calcium dependent facilitation (CDF); whereas Ca^{2+}-saturated CaM deactivates the channel upon influx of calcium in a process termed calcium dependent inactivation (CDI). Calcium-free calmodulin (apo-CaM) was previously proposed to bind to $Ca_V1.2$ and promote channel activation under low calcium conditions, in contrast Ca^{2+}-saturated CaM ($4Ca^{2+}$-bound CaM) acts as a channel deactivator under high calcium conditions. After analyzing channel electrophysiology and in-vitro binding data as well as nuclear magnetic resonance (NMR) spectra, I conclude that a half-calcified form of CaM (with the C-terminal lobe bound to Ca^{2+} and the N-terminal lobe devoid of Ca^{2+}, called Ca_2/CaM_{12}) is present under basal conditions and is likely responsible for basal channel activation. I used NMR to solve the structure of Ca_2/CaM_{12} complexed with a peptide fragment of the channel, known as the IQ motif (residues 1646-1665). The NMR spectrum of Ca_2/CaM_{12} bound to the IQ peptide structure reveals that the calcium-bound CaM C-terminal lobe interacts with the IQ peptide and the calcium-free CaM N-terminal lobe does not contact the IQ. Based on the structure, I identified hydrophobic residues on CaM (residues A89, F93, V109, M110, L113, M125, and M146) and the IQ motif (I1654, Y1657, and F1658) that are important for the binding interaction. The IQ mutations (I1654A, Y1657D and

F1658D) each significantly weakened IQ binding to CaM as measured by isothermal titration calorimetry (ITC) and fluorescence polarization. Additionally, these IQ mutations decrease the $Ca_V1.2$ channel open probability determined by electrophysiology analysis (performed in collaboration with Dr. Johannes Hell), demonstrating that this binding interaction is important for the basal channel activation. The IQ mutations also prevent $Ca_V1.2$ channel inactivation under high calcium conditions and abolish CDI. The results suggest that half-calcified CaM binding to the IQ serves two functional roles: (1) to promote channel activation under basal conditions and (2) to enable channel pre-association with CaM that is essential for rapid channel inactivation during CDI. Our new model is contrary to a previously proposed model in which apo-CaM was suggested to support activation of the $Ca_V1.2$ channel. This earlier model involving apoCaM is inconsistent with our finding that the $Ca_V1.2$ mutant K1662E (that disables apoCaM binding to $Ca_V1.2$) has no effect on channel open probability. Also, co-expression of $Ca_V1.2$ with CaM_{1234} mutant (that disables Ca^{2+} binding) in HEK293 cells abolishes basal channel activation in contrast to the 300% increase in channel open probability that occurs when $Ca_V1.2$ is co-expressed with wild type CaM.

Calcium-binding protein 1 (CaBP1) shares high sequence similarity (56%) to CaM; however, the two EF-hands in the N-lobe of CaBP1 have mutations in the binding loop that prevent Ca^{2+}-binding. This lack of Ca^{2+} binding to the N-lobe makes CaBP1 a functional analog of half-calcified CaM. Indeed, the calcified C-lobe of CaBP1 binds to the IQ motif of $Ca_V1.2$ and promotes Ca2+-dependent channel activation (called CDF) and prevents inactivation of the channel (CDI) in the presence of high calcium. On the basis of sequence similarity between CaBP1 and CaM, I was able to generate a structural model of CaBP1 bound to the IQ peptide by docking the crystal structure of CaBP1 to the IQ motif using the HADDOCK protein docking software. I then

performed NMR structural studies on the CaBP1 C-terminal lobe bound to the IQ peptide that revealed intermolecular contacts consistent with those of the docked structure and suggested CaBP1 hydrophobic residues (A107, F111, M128, L131, I144, and M165) make close contact with IQ residues (1654, Y1657, and F1658). The CaBP1 mutation I144E and IQ mutations (I1654D, Y1657D, K1662E and F1658) each weaken IQ binding to CaBP1 and validate the structural model. The NMR-derived structural model of Ca_2/CaBP1-IQ closely resembles the Ca_2/CaM_{12}-IQ structure. Hydrophobic CaBP1 residues I99, A107, F111, M128, L132, V136, I144, V148, M164, and M165 form a hydrophobic pocket that interacts with IQ residues I1654, Y1657, F1658, and F1661. Additionally, IQ residue K1662, forms a salt bridge with CaBP1 residue D140, which may explain why the K1662E mutation causes 4-fold weaker binding to CaBP1. I propose a structural mechanism for Ca^{2+}-dependent facilitation of $Ca_V1.2$ promoted by CaBP1 in which Ca^{2+} binding to the third and fourth EF-hands of CaBP1 are essential for $Ca_V1.2$ channel activation and for abolishing CDI by preventing CaM binding. Future electrophysiology studies are needed to test whether a CaBP1 mutant that disables Ca^{2+} binding to EF3 and EF4 ($CaBP1_{34}$) can both decrease basal channel open probability and abolish CDF.

Table of Contents

ABSTRACT 2

Table of Contents 5

Chapter 1: Introduction

1.1 L-type Voltage Gated Ca^{2+} Channel $Ca_V1.2$ 6

1.2 Calmodulin 10

1.3 CaBP1 13

1.4 Differential regulation of $Ca_V1.2$ by CaM and CaBP1 15

Chapter 2: Modulation of $Ca_V1.2$ by Half-calcified Calmodulin

2.1 Half-calcified CaM Binds to $Ca_V1.2$ Under Basal Conditions 19

2.2 NMR studies of Half-calcified Calmodulin 24

2.3 NMR Structure of Half-calcified Calmodulin 27

2.4 Validating the NMR Structure of Half-calcified Calmodulin by Mutagenesis 32

2.5 Mutations to the IQ motif and their effects on $Ca_V1.2$ Channel Electophysiology 35

2.6 CaM Expression Effects on Channel Activity 38

2.7 Discussion 40

2.8 Experimental Procedures 44

Chapter 3: Structural Insights into $Ca_V1.2$ Channel Activation by CaBP1

3.0 CaBP1 is a Homolog of CaM that Activates $Ca_V1.2$ 54

3.1 Structural Comparison of CaBP1 and CaM 55

3.2 IQ Binding to CaBP1 Enhances its Ca^{2+}-binding Affinity 58

3.3 Molecular Docking of CaBP1 Binding to IQ using HADDOCK 59

3.4 NMR Structural Studies of the Ca_2/CaBP1-IQ Complex 64

3.5 NMR-Refined HADDOCK Docking Structure Calculation 70

3.6 Mutational Analysis of Binding Contacts in Ca_2/CaBP1-IQ 74

3.7 Ca^{2+}-dependent Activation of $Ca_V1.2$ Promoted by CaBP1 76

3.8 Experimental Procedures 80

3.9 References 84

Chapter 1

Introduction

1.1 L-type Voltage Gated Ca^{2+} Channel $Ca_V1.2$

Calcium is an important and ubiquitous second messenger, affecting a wide range of processes from vesicle secretion and muscle contraction to learning and memory.[1–3] Intracellular calcium signaling is based on the large concentration gradient between cytosolic (≈100nM) and extracellular (≈1mM) calcium concentrations. This gradient is maintained by pumps, exchangers and intracellular Ca^{2+} sequestration, allowing a rapid influx of calcium upon regulated calcium channel opening. Ion channel opening caused by neuronal stimulation causes a rapid influx of calcium that increases intracellular calcium levels into the micromolar range and triggers a wide range of calcium-dependent processes. However, prolonged or excessive elevation of intracellular calcium is toxic to the cell. As a result, Ca^{2+} transporters must be tightly regulated, and dysregulation of Ca^{2+} homeostasis has been linked to various neurological and psychiatric disorders.[2,4–6]

The L-type voltage-gated calcium channel $Ca_V1.2$ is found in excitable cells, such as neurons, cardiac myocytes and smooth muscle. These channels are comprised of a regulatory cytosolic β-subunit and extracellular α2-subunit and δ-subunit, and a transmembrane α1-subunit which forms the channel pore, with both the N- and C-termini located inside the cell (**Fig. 1.1.1A**).[4,7] The α1-subunit includes 4 repeating, transmembrane domains containing 6 membrane-spanning helices(S1-S6), which together form a 4-fold symmetric structure that surrounds the

central channel pore. One helix (S4), with positively charged residues in every third position, is found in each of the transmembrane domains controls the voltage gating of the channel.[8] Under basal conditions, these helices are drawn in by the negative internal resting membrane potential. Upon membrane depolarization, the helices move in a spiral motion with each positively charged residue making sequential isoenergetic ion pairs with negative charges. The movement of these helices results in the opening of the channel pore.[8]

Once the $Ca_V1.2$ channel is open, a rapid influx of calcium binds to the regulatory protein calmodulin (CaM) and the CaM-bound channel becomes inactivated, in a process known as calcium dependent inactivation (CDI) (**Fig. 1.1.1B**). These moving Ca^{2+} ions can be measured as a current and can be compared to currents of Ba^{2+}. Ba^{2+} can also pass through $Ca_V1.2$ but Ba^{2+} does not bind to CaM, meaning any decrease in channel current is due to voltage dependent inactivation (VDI) (gray trace in **Fig. 1.1.1B**). The difference in these traces is CDI (black trace in **Fig. 1.1.1B**). Calmodulin binding to the Ca_V1 channel isoforms is essential for CDI, and CaM has been shown to bind to a short sequence of amino acids ($Ca_V1.2$ residues 1646-1665 in the intracellular C-terminal domain of the channel that is highly conserved across Ca_V1 isoforms, known as the IQ motif (**Fig. 1.1.1A**, green). The IQ mutation, I1654A or deletion of this site disables calmodulin binding and CDI. [4,9]

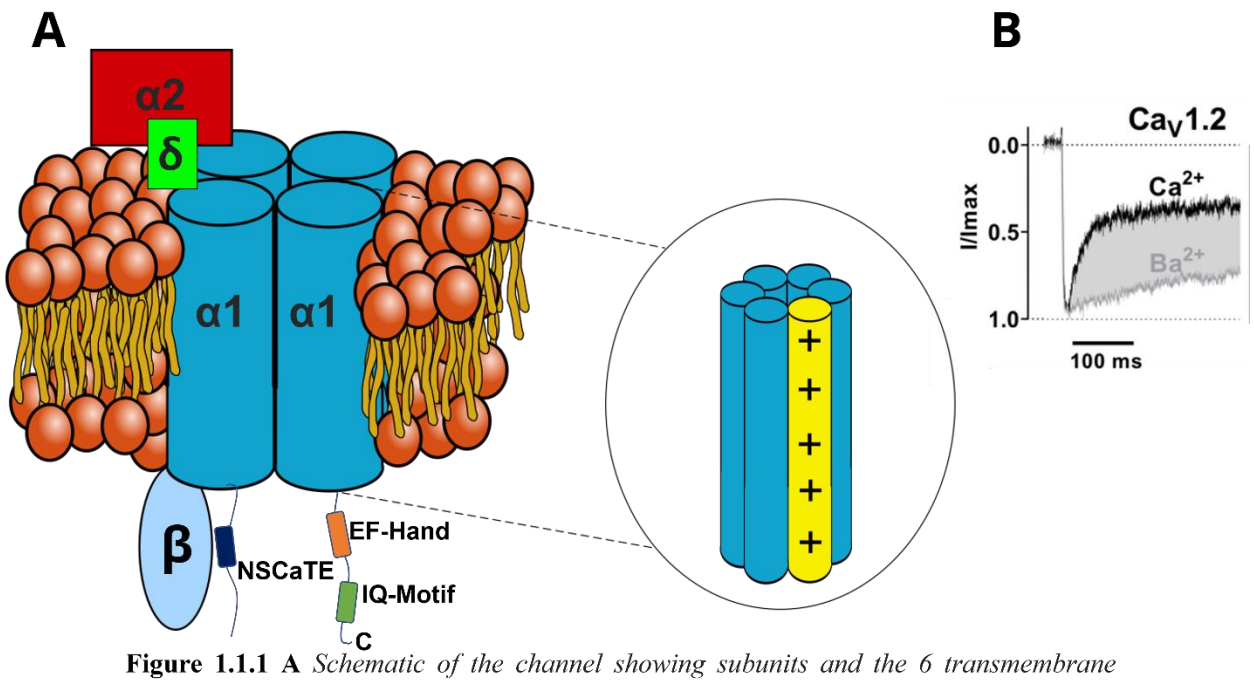

Figure 1.1.1 A *Schematic of the channel showing subunits and the 6 transmembrane helices making up each piece of the α-subunit, highlighting the positively charged S4 helix.* **B** *Sample of Ca^{2+} CDI trace (black) and a Ba^{2+} VDI(grey) trace.*

Cryo-EM structures were solved recently for $Ca_V1.1$[10] and $Ca_V1.2$ (**Fig. 1.1.2**).[11] These Structures were all determined in the absence of a membrane voltage and in the absence of CaM, suggesting that the channel is in the inactivated state with structural features that are key for understanding the mechanism of CDI. First, the channel has two EF hand motifs (residues 1520-1620 that resemble a CaM lobe) in the C-terminal end of the structure (**Fig. 1.1.2**, highlighted yellow) that interact with the intracellular loop connecting the third and fourth transmembrane domains, termed the III-IV inactivation gate (**Fig. 1.1.2**, purple). This EF-hand/III-IV complex is located near the cytosolic opening of the channel and may serve as a plug that could block or modulate Ca^{2+} influx. The CryoEM structure ends at $Ca_V1.2$ residue 1638 and all residues downstream of A1638 (including the IQ-motif, residues 1646-1665 and proximal/distal regulatory domains) are dynamically disordered or otherwise not defined in the cryoEM structure. The lack of electron density for the IQ motif suggests that in the inactivated state, the IQ motif may be solvent exposed and/or dynamically disordered.

Figure 1.1.2 *Cryo-EM structure of the inactivated $Ca_V1.2$ channel. The α1, β, and α2 subunits are shown in blue, cyan and red, respectively. The C-terminal EF-hand is shown in yellow. The 3-4 linker helix is shown in purple.*

1.2 Calmodulin

Calmodulin (CaM) is a highly conserved 16.7kDa calcium binding protein found in all eukaryotic cells and human CaM is 100% identical in amino acid sequence with CaM from fruit flies and more than 90% identical in sequence to yeast CaM. CaM is an essential gene in humans, flies and yeast, which is encoded by three separate genes(CALM1-3) in humans, each encoding the exact same amino acid sequence.[12,13] This genetic redundancy is indicative of the importance of proper CaM expression. Pathological CaM variants have been discovered on each CALM gene with some mutations isolated from multiple genes. A summary of mutations and associated disease are shown in **Figure 1.2.1.**[13] Many of the CaM mutations (D96V, N98I, D130S, D132E, D134H, Q136P) occur in the EF-hand Ca^{2+} binding loops that disable or weaken Ca^{2+} binding to either EF3 or EF4.[13] Thus, Ca^{2+} binding to EF3 and EF4 in CaM is essential for its binding to many target proteins as demonstrated by CaM binding to $Ca_V1.2$ described in Chapter 2.

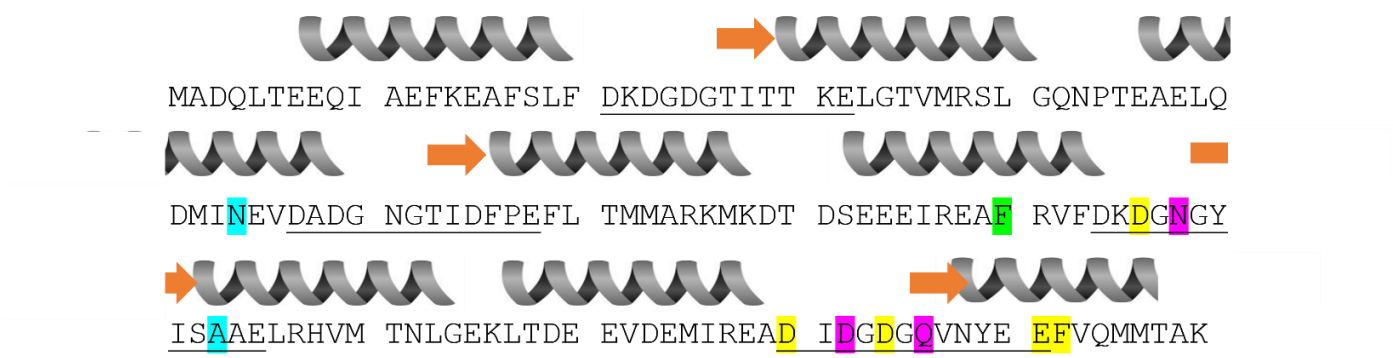

Figure 1.2.1 *Amino acid sequence of calmodulin is shown with secondary structure indicated. Helices indicate a-helix and beta strands are shown as arrows. Ca^{2+} binding EF-hand loops are indicated by underlined residues. Highlighted residues indicate documented mutations, with disease in blue (catecholaminergic polymorphic ventricular tachycardia), green (idiopathic ventricular fibrillation), yellow (long QT syndrome, and purple (both long QT syndrome and Brugada syndrome).*

CaM has two independently folded lobes (N-lobe and C-lobe) connected by a flexible linker with each lobe containing two calcium-binding EF-hand motifs in which EF-hands 1 and 2 form the N-lobe, and EF-hands 3 and 4 form the C-lobe.[4,14,15] These EF-hand motifs are 29-residue helix-loop-helix structures (**Fig. 1.2.2**) that coordinate the binding of calcium to a 12-residue calcium binding loop with a consensus sequence of (OXOXOGXIXXXE), with O designating a residue with a side chain containing oxygen that chelates the bound Ca^{2+} (see D21, D25, D23 in **Fig. 1.2.2**) and X is any residue. The glutamate at the twelfth position in the loop is especially important for binding calcium as the carboxylate side chain forms a bidentate coordination with the bound Ca^{2+} (see E32 in **Fig. 1.2.2**). The EF-hands in the C-lobe (EF3 and EF4) of calmodulin binds calcium with a 1 μM dissociation constant compared to the 10 μM dissociation constant for Ca^{2+} binding to the EF-hands in the N-lobe.[16,17] Consequently, the Ca^{2+} will bind to the C-lobe before the N-lobe in a sequential fashion at equilibrium, which explains the formation of half-calcified CaM described in Chapter 2. Upon binding calcium, the lobes of CaM undergo separate conformational changes (**Fig. 1.2.3**) referred to as a closed-to-open transition.[18] The Ca^{2+}-induced opening of the EF-hands leads to the exposure of a hydrophobic pocket that allows CaM to bind

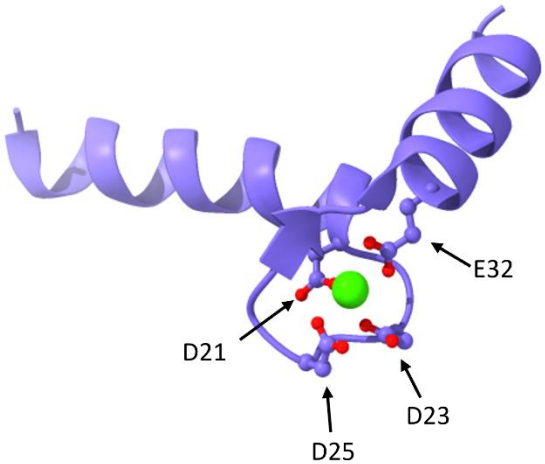

Figure 1.2.2 *Structure of the first EF-hand of calmodulin bound to calcium. Oxygen containing residues at positions 1, 3, 7 and 12 of the loop are coordinating the calcium with the glutamate at position 12 making a bidentate contact.*

to and modulate the activity of hundreds of targets in response to a rise in intracellular calcium levels.

The high degree of flexibility in the interdomain linker between these two lobes allows for CaM to bind to a wide variety of targets, including enzymes, ion channels, and transcription factors.[13] More than two dozen structures are known for CaM bound to different target proteins including myosin light chain kinase,[19] CaM-dependent kinase,[20] calcineurin,[21] transient receptor potential channels,[22] ryanodine receptors,[23] cyclic-nucleotide gated channels,[24] voltage-gated Na^+ channels,[25] voltage-gated Ca^{2+} channels,[26] estrogen receptors,[27] and creatine kinase.[28] In each case, CaM adopts a unique structure in which both CaM lobes bind to opposite sides of a target helix and form a collapsed structure (see structures of CaM/MLCK[19] and CaM/RyR2[23]). Alternatively, each CaM lobe can bind independently to distinct target binding sites (see structures of CaM/ER,[27] CaM/CNGB1,[24] and CaM/CK[28]). The Ca^{2+}-dependent plasticity of the two CaM lobes explains how CaM can accommodate and bind tightly to hundreds of different target proteins. In addition to its role in calcium signaling, CaM has also been implicated in a number of cellular processes

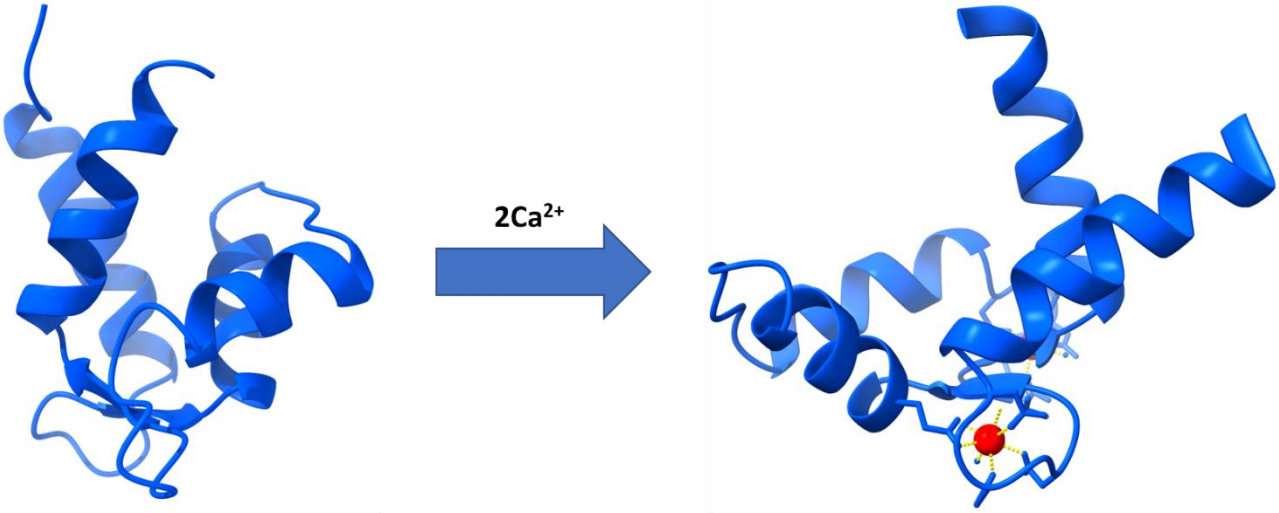

Figure 1.2.3 *The N-lobe of apocalmodulin (PDB 1qx5) shown on the left. Shown on the right is the $2Ca^{2+}$-calmodulin N-lobe (PDB: 3oxq). The induced conformation change upon binding of calcium to the N-lobe of calmodulin reveals residues in the hydrophobic core of the channel. This same conformational change is also seen in the C-lobe of calmodulin upon binding calcium.*

including cell proliferation, apoptosis, and cytoskeletal dynamics. As a result, mutations in CaM have been linked to diseases including cancer and neurodegenerative disorders.[2,4–6,13,29,30]

1.3 CaBP1

Calcium-binding protein 1 (CaBP1), has been shown to modulate the Ca^{2+}-sensitive activity of L-type channels,[31] and the transient receptor potential channel, TRPC5.[32] CaBP1 is widely expressed in the brain and is closely related in sequence to CaM (**Fig. 1.3.1**). The two proteins share 56% sequence identity and similar structural folds. Like CaM, CaBP1 has two independent lobes containing a total of 4 EF-hand motifs in which the third and fourth EF-hands bind calcium with high affinity. However, the first and second EF-hands, located in the N-lobe, do not bind calcium under physiological conditions because these EF-hands lack key oxygen containing residues in the EF hand loops that are required for the coordination of calcium (highlighted red in **Fig. 1.3.1**). In the first EF-hand, the canonical glutamate at the twelfth position in the EF-hand loop is replaced with aspartate that significantly weakens calcium binding and allows for the high affinity binding of Mg^{2+} with space for a water molecule to bridge the interaction..[4,9] Thus the first EF-hand binds constitutively to Mg^{2+} that stabilizes its structure.[33] In the second EF-hand, a Gly substitution at the 5-position in the EF-hand loop lacks an oxygen containing side chain, and therefore disables Ca^{2+} binding to EF2. The lack of Ca^{2+} binding at EF1 and EF2 and the binding of Ca^{2+} at EF3 and EF4 was verified in the crystal structure of CaBP1 that shows Ca^{2+} bound only at EF3 and EF4.[9] In essence, Ca^{2+}-saturated CaBP1 with Ca^{2+} bound at EF3 and EF4 is structurally similar to half-calcified CaM in which Ca^{2+} is bound only at EF3 and EF4 (see Chapter 2). This may explain why Ca^{2+}-bound CaBP1 activates $Ca_V1.2$ analogous to that of half-calcified CaM (see Chapter 2).

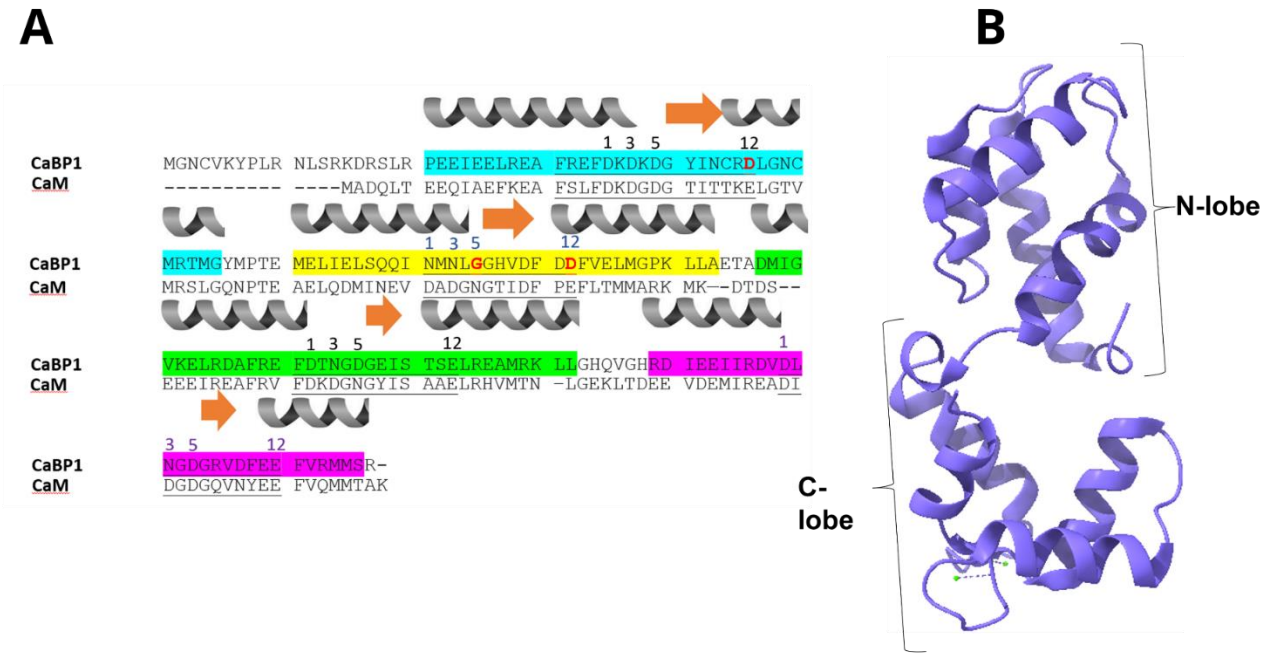

Figure 1.3.1 A *A sequence alignment comparing CaBP1 and calmodulin. The secondary structure is shown above the sequence with helices shown in grey and beta sheets represented by orange arrows. Each EF1, EF2, EF3, and EF4 are highlighted in cyan, yellow, green, and magenta, respectively. Key calcium coordinating positions 1, 3, 5, and 12 for each EF hand loop are indicated. CaBP1 residues that weaken or disable calcium binding to the first and second EF hand are highlighted in red.* **B** *A crystal structure of Ca^{2+}-bound CaBP1 with an Ca^{2+}-free, closed N-lobe and a Ca^{2+}-bound, open C-lobe (PDB: 3OX6).*

The binding of CaBP1 to L-type channels can both increase the channel open probability and prevent CDI. Unlike CaM, CaBP1 binding to $Ca_V1.2$ causes channel activation at high cytosolic Ca^{2+} levels, known as Ca^{2+}-dependent facilitation or CDF.[9] CaBP1 has been suggested to bind to multiple sites within $Ca_V1.2$,[34] and CaBP1 binding to the IQ-motif is essential for CDF.[35] The CaBP1 binding to the IQ-motif under basal conditions[36] may serve to block CaM binding to $Ca_V1.2$, which may explain how CaBP1 prevents CDI. Mutations or alterations in CaBP1 expression have been associated with neurological and psychiatric disorders including Alzheimer's disease, bipolar disorder, and schizophrenia.[5]

1.4 Differential regulation of $Ca_V1.2$ by CaM and CaBP1

The Ca^{2+}-dependent regulation of $Ca_V1.2$ by CaM and CaBP1 is essential for proper channel function: CaBP1 increases $Ca_V1.2$ channel open probability at high Ca^{2+} levels (CDF), whereas CaM causes channel inactivation at high Ca^{2+} levels (CDI). The binding of CaM and CaBP1 to the IQ domain ($Ca_V1.2$ residues 1646-1665) is required for CDI and CDF, respectively. Thus, both CaM and CaBP1 compete for binding to the IQ, and the deletion of the IQ disables their respective effects on channel activity. Ca^{2+} binding to calmodulin is required for channel inactivation.[4,9] Likewise, Ca^{2+} binding to CaBP1, is essential for its ability to increase the channel open probability (see Chapter 3).

Calmodulin has been shown to increase the activity of the $Ca_V1.2$ channel under low-calcium conditions and to deactivate the channel under high calcium conditions upon channel opening in a process known as calcium dependent inactivation (CDI).[4,9,37,38] Thus, CaM acts as both an accelerator (at low Ca^{2+} levels) and a brake (high Ca^{2+} levels) to control $Ca_V1.2$ channel opening.[39,40] Ca^{2+} influx through $Ca_V1.2$ channels cause CDI,[41] mediated by CaM binding to the IQ-motif. The rapid kinetics of CDI requires CaM to be pre-associated with the L-type channel under basal conditions.[42] ApoCaM has been suggested to be pre-associated with L-type channels,[36] which may increase the basal channel open probability.[37] It is widely believed that under the low calcium concentrations of the basal state, that the calcium-free form of CaM (ApoCaM) is responsible for channel preassociation and activation.[37,38] An atomic-level NMR structure of the interaction between ApoCaM and the IQ motif of the channel has been solved and reveals that the C-lobe of Ca^{2+}-free CaM makes contact with the channel (Fig. 1.4.1), whereas the Ca^{2+}-free N-lobe does not.[43]

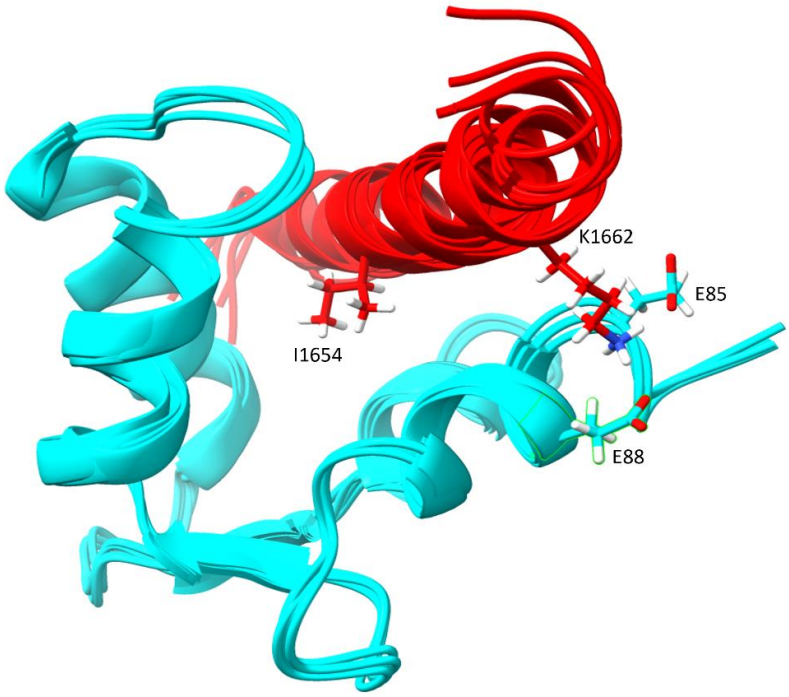

Figure 1.4.1 *The NMR structure (PDB: 6CTB) of apocalmodulin C-lobe (shown in cyan) bound to the IQ motif of $Ca_V1.2$(shown in red). The key contacts include the interaction include I1654 of the peptide which points down into the hydrophobic core of calmodulin and the salt bridge formed between K1662 of the peptide and E85/E88.*

The Yue lab has proposed a model to explain how apoCaM might activate $Ca_V1.3$.[26] The Ca^{2+}-free CaM C-lobe is known to bind the IQ motif.[43] The Yue lab model proposes that the Ca^{2+}-free CaM N-lobe may bind to the channel EF-hand to stabilize the high open probability channel state under basal conditions.[39] However, there are zero known atomic resolution structures of the Ca^{2+}-free CaM N-lobe bound to any target protein. The structural model of Ca^{2+}-free CaM N-lobe bound to CaV1.3 as proposed[26] has not been experimentally verified and is not supported by any structural evidence. The Yue lab model furthermore proposes that Ca^{2+} influx caused by voltage-dependent channel opening, produces a rise in intracellular Ca^{2+} concentration that in turn causes Ca^{2+}-saturated CaM to bind to CaV1.3 at two different sites: The Ca^{2+}-bound N-lobe binds to the NSCaTE domain (**Fig. 1.4.2**) and the Ca^{2+}-bound C-lobe binds to the IQ motif (**Fig. 1.4.3**) to stabilize $Ca_V1.3$ in the inactivated channel state. Atomic-level structures are known for apoCaM

bound to the IQ[43] and for Ca^{2+}/CaM bound to IQ[44,45] and NSCaTE[46] domains. However, structures are not yet known for CaM bound to the full-length L-type channel. In chapter 2, I present evidence that argues against L-type channel activation by apoCaM. Instead, I present evidence that a half-calcified form of CaM (with Ca^{2+} bound to the CaM C-lobe but not bound to the N-lobe) exists under basal conditions and binds tightly to the IQ-motif to cause channel activation under basal conditions

A high-resolution crystal structure of Ca^{2+}-saturated CaM (with $4Ca^{2+}$ bound) bound to the

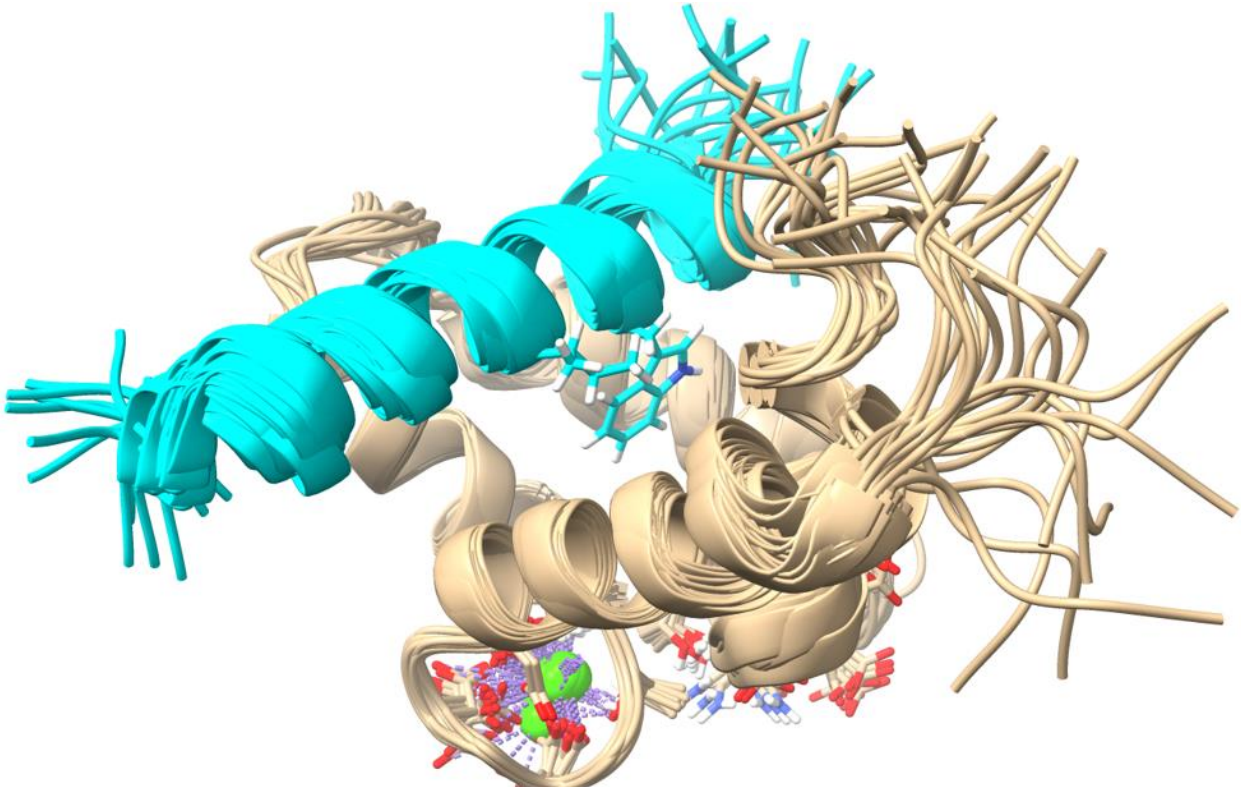

Figure 1.4.2 *Structure of the N-lobe of calmodulin (beige) bound to the NSCaTE domain of the channel (cyan) (PDB: 2LQC). Key interactions include the I56 and W52 which point downwards into the hydrophobic core of calmodulin.*

IQ peptide has been solved (**Fig. 1.4.3**) and suggests how CaM binding may stabilize the inactivated state of the channel.[44] In the crystal structure, both calcium-bound lobes of CaM interact with opposite sides of the channel, and hydrophobic residues I1654, Y1657, and F1658 of the IQ motif make contact with the hydrophobic pocket created by the Ca^{2+}-bound, open CaM C-

lobe. On the opposite side of the IQ, aromatic residues Y1649 and F1652 contact hydrophobic pocket of the Ca^{2+}-bound, open CaM N-lobe.

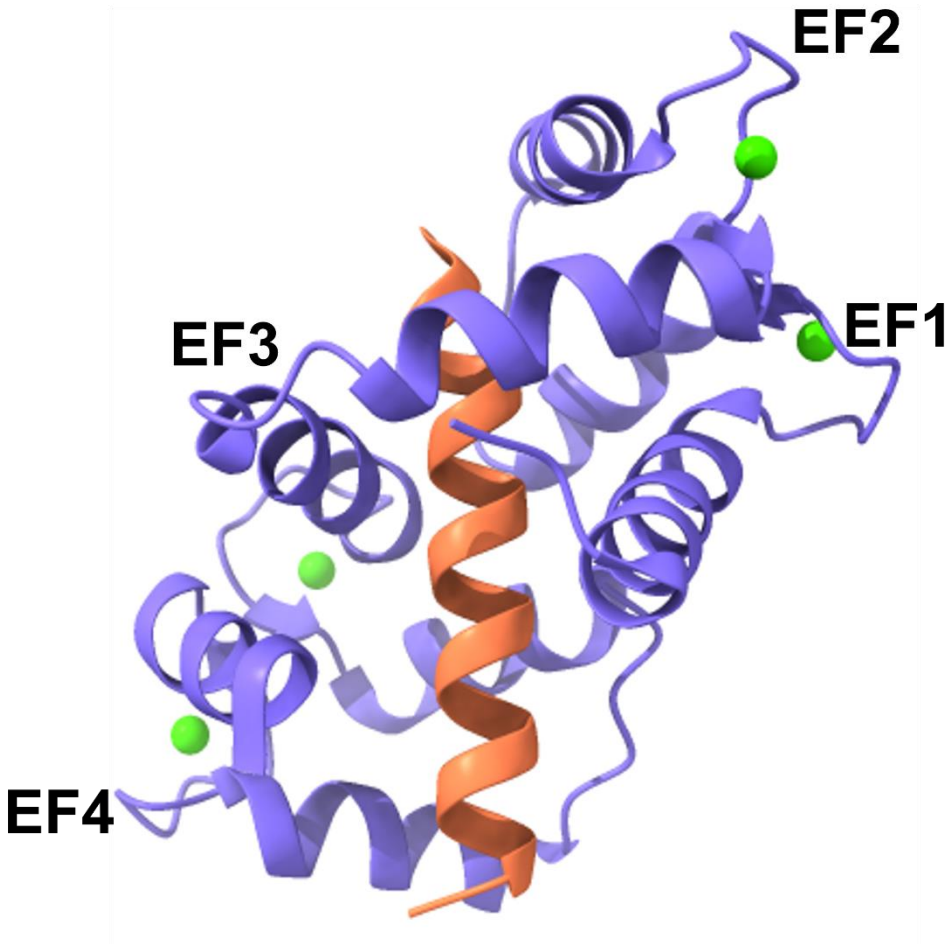

Figure 1.4.3 *Crystal Structure of Ca_4/CaM (purple) bound to the IQ motif (pink) (PDB: 2BE6).*

Chapter 2

Modulation of $Ca_V1.2$ by Half-calcified Calmodulin

2.1 Half-calcified CaM Binds to $Ca_V1.2$ Under Basal Conditions

Previous studies suggested that $Ca_V1.2$ is preassociated with apoCaM under basal conditions ($[Ca^{2+}]$ = 100 nM).[37] ApoCaM binds to the IQ peptide (in the absence of salt) with sub-micromolar affinity as measured by isothermal titration calorimetry.[36] However, under physiological salt levels, the affinity of apoCaM for the channel peptide decreases to 10 μM.[43,47] Single molecule FRET assays measured that apoCaM binds to the full-length $Ca_V1.2$ channel with a 10-fold greater affinity than binding to the peptide.[48] Thus, apoCaM is predicted to bind to the full channel with a K_D of ~1 μM, putting the interaction outside the physiological range of free CaM concentration in neurons and cardiomyocytes, measured to be less than 100 nM.[43,49] This relatively low affinity $Ca_V1.2$ binding to apoCaM indicates that only 10% of $Ca_V1.2$ is bound to apoCaM under basal conditions.

The NMR structure of apoCaM bound to the $Ca_V1.2$ IQ-motif shows an intermolecular salt bridge between K1662 of the channel peptide and CaM residue E88.[43] Fluorescence polarization studies show that the mutation K1662E significantly weakens apoCaM binding to the peptide. However, patch clamp recordings show that the mutation K1662E does not affect the single-channel open probability of the channel.[43] These results indicate that the apoCaM interaction with $Ca_V1.2$ is probably not physiologically relevant. As a result, I conclude that $Ca_V1.2$ may not be

preassociated with apoCaM as previously suggested by [36–38]. Instead, I propose that under basal conditions, $Ca_V1.2$ is more likely bound to a half-calcified form of CaM in which the CaM C-lobe is bound to Ca^{2+} and the CaM N-lobe is in the Ca^{2+}-free state. This hypothesis is tested by the experiments and analysis presented below.

The micromolar Ca^{2+} affinity of the CaM C-lobe (CaMC) in the absence of $Ca_V1.2$ ($K_1 = 10^{12}$ M^{-2})[16] implies that less than 10% of CaM would bind to Ca^{2+} under basal Ca^{2+} levels.[16] However, the nanomolar binding of the IQ peptide to the Ca^{2+}-bound CaM C-lobe ($K_2 = 10^7$ M^{-1} in Fig. 2.1.1A) and the micromolar binding of the IQ peptide to the Ca^{2+}-free CaM C-lobe ($K_3 = 10^{-5}$ M in Fig. **2.1.1A**) causes the apparent Ca^{2+} affinity of CaMC-IQ (CaM C-lobe bound to IQ) to increase by 100-fold ($K_{tot} = K_1 \times K_2 \times K_3 = 10^{14}\ M^{-2}$ in **Fig. 2.1.1A**) relative to the Ca^{2+} affinity of the free CaM C-lobe ($K_1 = 10^{12}$ M^{-2} in **Fig. 2.1.1A**). Correspondingly, the micromolar binding of the IQ peptide to the Ca^{2+}-bound CaM N-lobe ($K_2 = 10^6$ M^{-1} in **Fig. 2.1.1B**) and sub-millimolar binding of the IQ peptide to Ca^{2+}-free CaM N-lobe ($K_3 = 10^{-4}$ M in **Fig. 2.1.1B**) causes the apparent Ca^{2+} affinity of CaMN-IQ (CaM N-lobe bound to IQ) to increase by 100-fold ($K_{tot} = K_1 \times K_2 \times K_3 = 10^{12}\ M^{-2}$ in **Fig. 2.1.1B**) relative to the Ca^{2+} affinity of the free CaM N-lobe ($K_1 = 10^{10}$ M^{-2} in **Fig. 2.1.1B**). The apparent Ca^{2+} dissociation constants of CaMN-IQ and CaMC-IQ are calculated to be 1 μM and 100 nM, respectively (**Fig. 2.1.1**).[4,47]

A

$$2Ca^{2+} + CaMC \xrightarrow{K_1=10^{12}\,M^{-2}} Ca_2/CaMC \quad (18)$$

$$Ca_2/CaMC + IQ \xrightarrow{K_2=10^{7}\,M^{-1}} Ca_2/CaMC - IQ \quad (14)$$

$$CaMC - IQ \xrightarrow{K_3=10^{-5}\,M} CaMC + IQ \quad (14)$$

$$CaMC - IQ + 2Ca^{2+} \xrightarrow{K_{tot}=K_1\times K_2\times K_3} Ca_2/CaMC - IQ$$

$$CaMC\ apparent\ K_D = \sqrt{\frac{1}{K_{tot}}} = 100 \pm 20\ nM$$

B

$$2Ca^{2+} + CaMN \xrightarrow{K_1=10^{10}\,M^{-2}} Ca_2/CaMN \quad (18)$$

$$Ca_2/CaMN + IQ \xrightarrow{K_2=10^{6}\,M^{-1}} Ca_2/CaMN - IQ \quad (14)$$

$$CaMN - IQ \xrightarrow{K_3=10^{-4}\,M} CaMN + IQ \quad (14)$$

$$CaMN - IQ + 2Ca^{2+} \xrightarrow{K_{tot}=K_1\times K_2\times K_3} Ca_2/CaMN - IQ$$

$$CaMN\ apparent\ K_D = \sqrt{\frac{1}{K_{tot}}} = 1.0 \pm 0.5\ \mu M$$

Figure 2.1.1 *Apparent Ca^{2+}-binding affinity of the CaM C-lobe bound to the IQ motif (**A**) and the CaM N-lobe bound to the IQ motif (**B**).*

The binding analysis in **Fig. 2.1.1** suggests that under basal conditions, some fraction of CaM would exist in a half-calcified state in which 2 Ca^{2+} are bound to the C-lobe while the N-lobe would remain calcium free. Using the apparent Ca^{2+} dissociation constants of CaMC-IQ and CaMN-IQ (**Fig. 2.1.1**), the Ca^{2+} occupancy of CaM (bound to the IQ) was calculated as a function of the free Ca^{2+} concentration and provided concentration profiles of apoCaM, half-calcified CaM (Ca_2/CaM) and Ca^{2+}-saturated CaM (Ca_4/CaM) each bound to IQ and plotted as a function of free Ca^{2+} concentration (**Fig. 2.1.2**). The concentration profiles indicate that at basal Ca^{2+} levels (100 nM), nearly half of the $Ca_V1.2$ channels would be bound to half-calcified CaM (red trace in **Fig. 2.1.2**) in which 2 Ca^{2+} are bound to the CaM C-lobe and the CaM N-lobe is in the Ca^{2+}-free state.

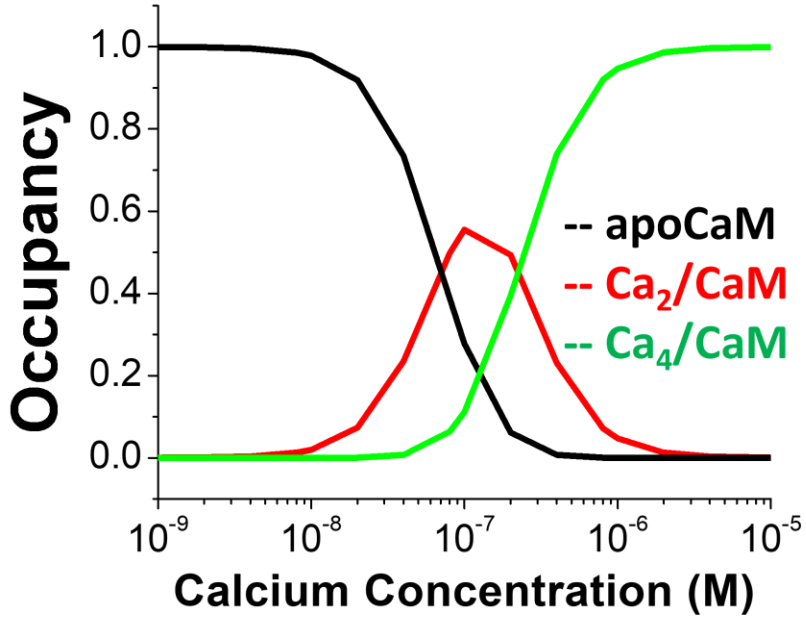

Figure 2.1.2 *Concentration profiles of apoCaM-IQ (black), Ca_2/CaM-IQ (red), and Ca_4/CaM-IQ (green) shown as a function of free Ca^{2+} concentration*

The Ca^{2+} binding analysis above (Fig. 2.1.1A) and Ca^{2+}-dependent occupancy profiles (Fig. 2.1.2) suggest that the CaM C-lobe (bound to the IQ) can bind to Ca^{2+} in the nanomolar range to form Ca_2/CaM under basal conditions. To experimentally measure the Ca^{2+} affinity of the CaM C-lobe in the context of full-length CaM, I prepared a CaM mutant (D21A/D23A/D25A/E32Q/D57A/D59A/N61A/E68Q, called CaM_{12}) that substitutes Ala in place of negatively charged residues in EF1 and EF2 that bind to Ca^{2+}, which completely abolishes Ca^{2+} binding to the CaM N-lobe.

The calcium binding affinity of the CaM_{12} mutant in the presence of the IQ peptide was measured by isothermal titration calorimetry (ITC) (**Figure 2.1.3)**. The Ca^{2+} binding isotherm at 27° C showed biphasic binding (**Fig. 2.1.3A**), suggesting sample heterogeneity, possibly caused by self-association of the IQ motif. The major binding component of the isotherm shows a stoichiometry of 1.7 ± 0.3 Ca^{2+} per CaM-IQ complex that represents Ca^{2+} binding to EF3 and EF4

in the CaM C-lobe. Fitting the isotherms to a two-site model results in an apparent Ca^{2+}-binding dissociation constant of 60 ± 20 nM, which is similar to the apparent affinity predicted in **Figure 2.1.1A** and agrees with previous Ca^{2+}-binding measurements by UV fluorescence.[50] At 37º the Ca^{2+} binding isotherm becomes monophasic with a dissociation constant of 72 ± 20 nM (**Fig. 2.1.3B**), which again is consistent with the affinity predicted in **Fig. 2.1.1A**. The high affinity Ca^{2+} binding to the CaM_{12} C-lobe implies at least 50% of the CaM_{12}/IQ complex will have two Ca^{2+} bound to the C-lobe under basal conditions.

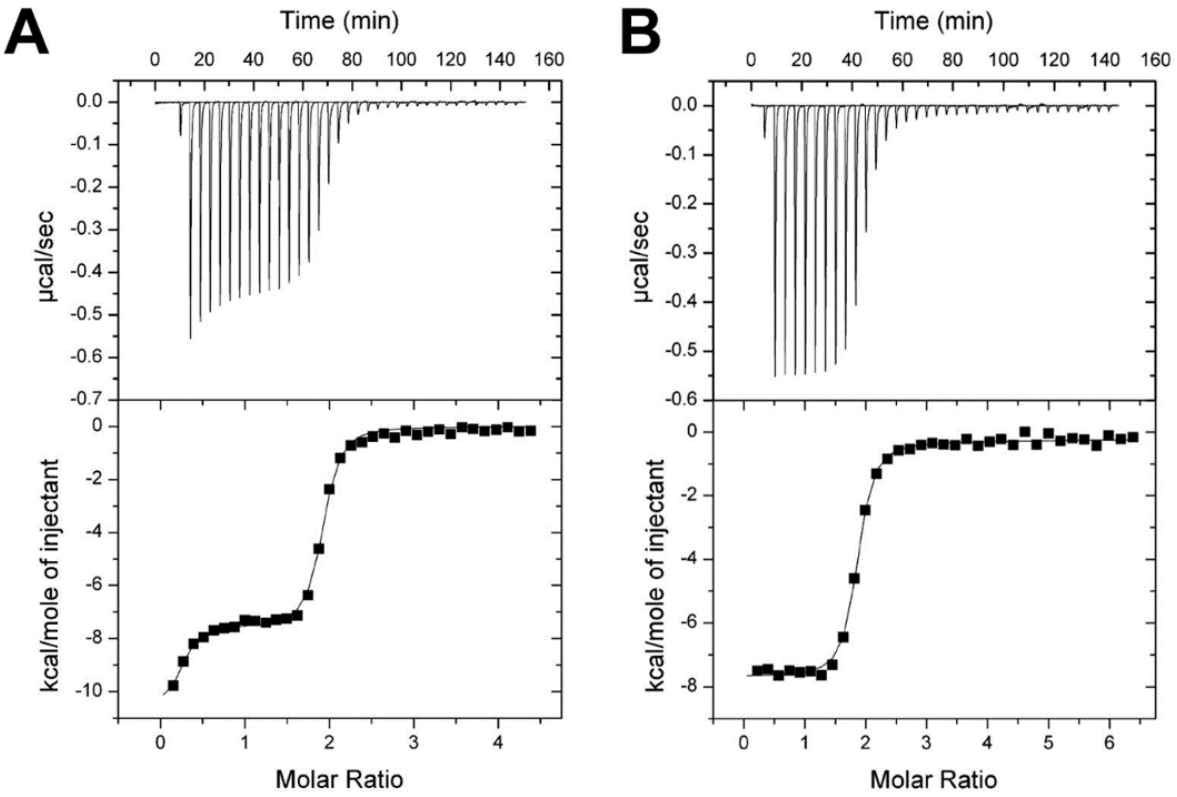

Figure 2.1.3 *ITC measurements of CaM12-IQ binding Ca^{2+} at 27º C (**A**) and 37º C (**B**). The molar ratio is defined as moles of titrant (Ca^{2+}) divided by the moles of CaM_{12}.*

2.2 NMR Studies of Half-calcified Calmodulin

The fractional occupancy of the apoCaM (38%), Ca_2/CaM (55%) and Ca_4/CaM (7%) indicate a complex mixture of these species under basal conditions when Ca_2/CaM reaches its maximal level (**Fig. 2.1.2**). In order to isolate Ca_2/CaM for structural analysis (and eliminate any occupancy by apoCaM and Ca_4/CaM), NMR structural studies were performed on the CaM_{12} mutant (D21A/D23A/D25A/E32Q/D57A/D59A/N61A/E68Q) bound to the IQ peptide (called Ca_2/CaM_{12}-IQ). The NMR HSQC spectrum of ^{15}N-labeled CaM_{12} bound to unlabeled IQ peptide (**Fig. 2.2.1**) exhibits well-resolved amide resonances that provide a residue-specific fingerprint of the structure. The backbone amide NMR assignments of Ca_2/CaM_{12}-IQ are shown as residue labeled peaks in **Figure 2.2.1** and were published in 2019.[51] More than 92% of the main chain ^{13}C resonances (^{13}Cα, ^{13}Cβ, and ^{13}CO), 90% of backbone amide resonances (^{1}HN, ^{15}N), and 74% of methyl side chain resonances were assigned. The unassigned residues (14-15, 30-32, 43, 59-61, 75, 78, 94) had overlapped backbone amide resonances and/or weak NMR intensities that obscured their assignment. In particular, the EF-hand loop residues in EF1 (residues 30-32) and EF2 (residues 58-61) could not be assigned due to weak NMR intensities, perhaps caused by conformational disorder in these Ca^{2+}-free binding loops. A complete listing of the chemical shift assignments (^{1}H, ^{15}N, ^{13}C) of Ca_2/CaM_{12} bound to unlabeled Cav1.2 IQ peptide have been deposited in the BioMagResBank (http://www.bmrb.wisc.edu) under accession number 27692 and were published in 2019.[51]

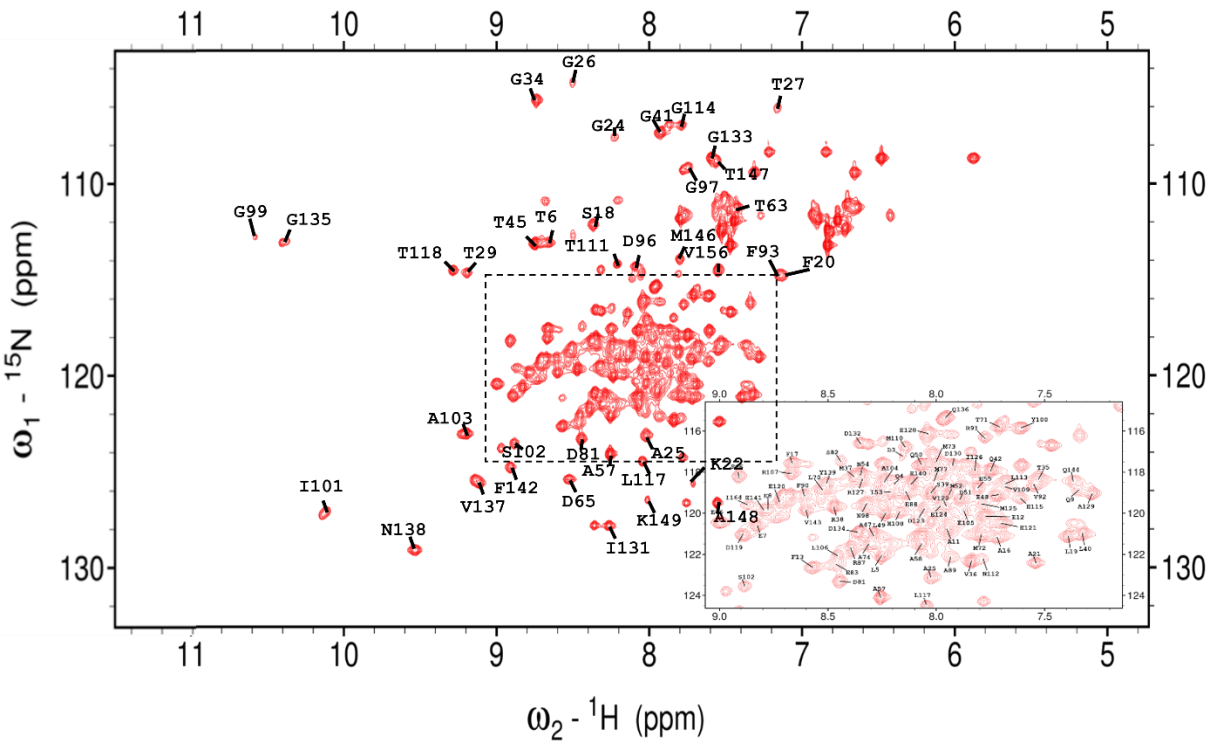

Figure 2.2.1 *^{15}N-HSQC of CaM$_{12}$-IQ with backbone amide assignments.*

Figure 2.2.2 shows the ^{15}N-HSQC spectrum of the CaM$_{12}$ (red) is a composite of the spectra of apoCaM (black) and Ca$_2$/CaMC-IQ (blue). The resolved and assigned resonances of the CaM$_{12}$ C-lobe (G99, I101, V103, G114, T118, G133, G135, N138, T147) match those of Ca^{2+}-saturated CaM C-lobe bound to the IQ peptide (**Fig. 2.2.2A**), indicating that the structure of CaM$_{12}$ C-lobe must be similar to that of wild type Ca^{2+}-bound CaM C-lobe bound to the IQ,[52] implying that CaM$_{12}$ C-lobe is bound to the IQ. The CaM$_{12}$ N-lobe resonances (assigned to S18, L19, F20, A21, G24, G26, T27, G34, G41, E46, D65, F66) overlay closely with those of apoCaM in the absence of the IQ motif (Fig. 2.2.2B), indicating that the structure of CaM$_{12}$ N-lobe must be similar to that of the Ca^{2+}-free CaM N-lobe in the absence of the IQ, implying that the CaM$_{12}$ N-lobe is not bound to the IQ. Thus, the structure of the Ca$_2$/CaM$_{12}$-IQ complex is predicted to have a closed,

Ca^{2+}-free N-lobe making no contact with peptide and an open, Ca^{2+}-bound C-lobe that is bound to the IQ.

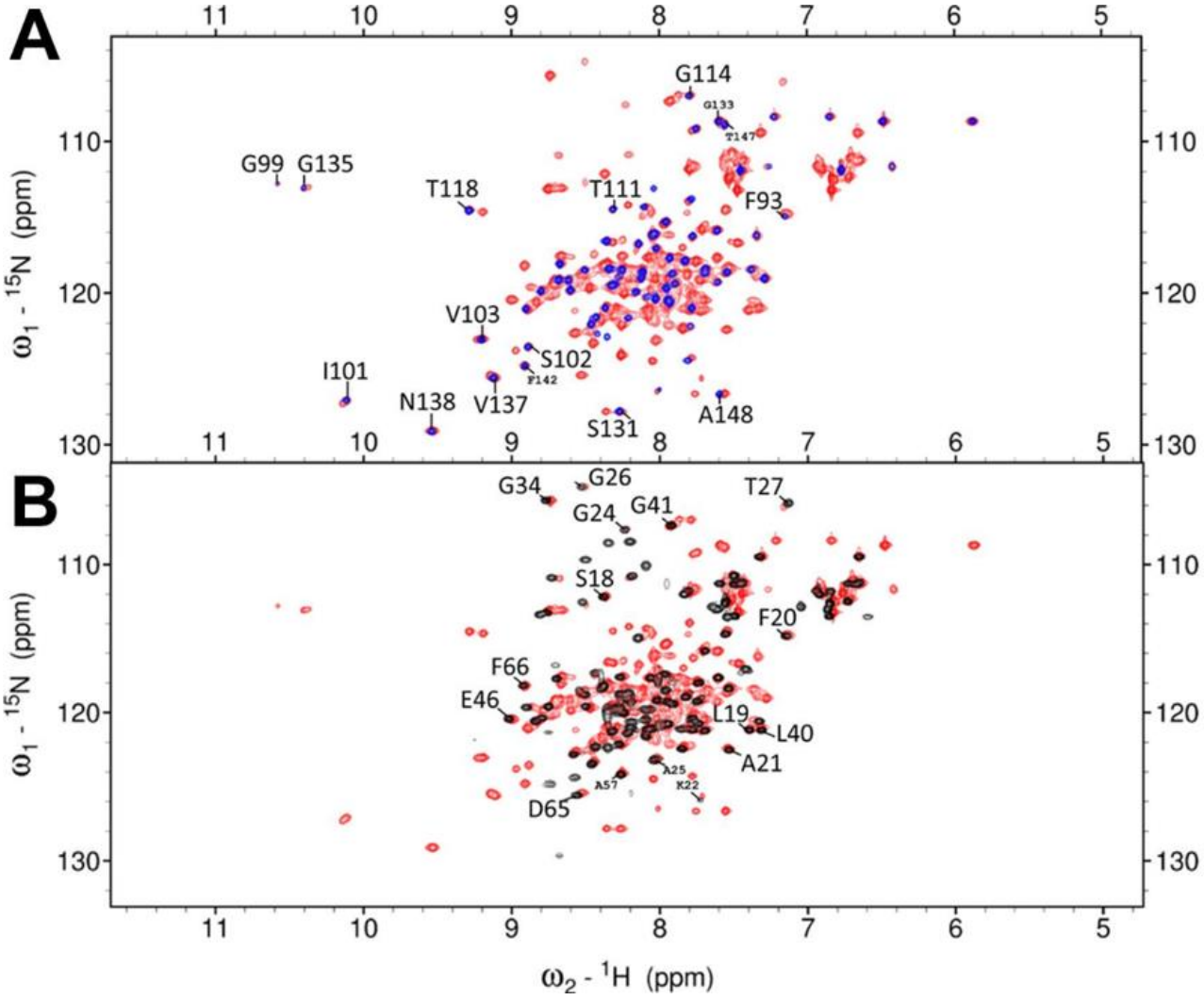

Figure 2.2.2 A *Overlay of the ^{15}N-HSQC of Ca_2/CaM12-IQ(red) with the ^{15}N-HSQC of Ca_2/CaMC-IQ(blue). Select C-lobe residues are labeled to demonstrate overlap.* **B** *Overlay of the ^{15}N-HSQC of Ca_2/CaM12-IQ(red) with the ^{15}N-HSQC of apoCaM(black) in the presence of the IQ motif.*

The binding of Ca^{2+} to CaM_{12} (at EF3 and EF4) causes the amide proton of the conserved glycine at EF-hand loop position 6 to be hydrogen bonded with the side chain carboxylate oxygen of the EF-hand residue at position 1, which causes a dramatic deshielding of the amide proton from glycine at position 6. The downfield amide chemical shifts of G99 and G135 imply that EF3 and EF4 must have Ca^{2+} bound. The amide proton chemical shifts of the corresponding glycines in

EF1 (G26) and EF2 (G62) are not downfield shifted and appear within the normal range of glycine amide chemical shifts, indicating that EF1 and EF2 of CaM_{12} do not have calcium bound under saturating levels of Ca^{2+}.

2.3 NMR Structure of Half-calcified Calmodulin

NMR spectral assignments for the Ca_2/CaM12-IQ complex (**Fig. 2.2.2**) have been previously deposited in the BMRB(accession number 27692).[51] These assignments were used to obtain NMR structural restraints in the form of NOESY derived interatomic distances[53], residual dipolar coupling (RDC) data derived long-range orientational restraints[54] (**Fig. 2.3.1)**, and dihedral angles using TALOS+.[55]

These restraints were used to calculate NMR-derived structures of Ca_2/CaM12 bound to the IQ peptide using restrained molecular dynamics simulations within Xplor-NIH.[56] The resulting ensemble of NMR-derived structures is shown in **Figure 2.3.2** along with NMR structural statistics shown in **Table 2.3.1**. The two lobes of Ca_2/CaM12 are folded independently and do not appear to interact as seen in previous structures of apoCaM.[57–59] The RMSD of the individual lobes was calculated from the main chain atom coordinates of each lobe separately and was calculated to be 0.83 ± 0.09 Å for the C-lobe and 0.9 ± 0.1 Å for the N-lobe. PROCHECK-NMR was used to assess the quality of the ensemble[60], with 93% of residues showing in favorable or allowed regions from the Ramachandran plot.

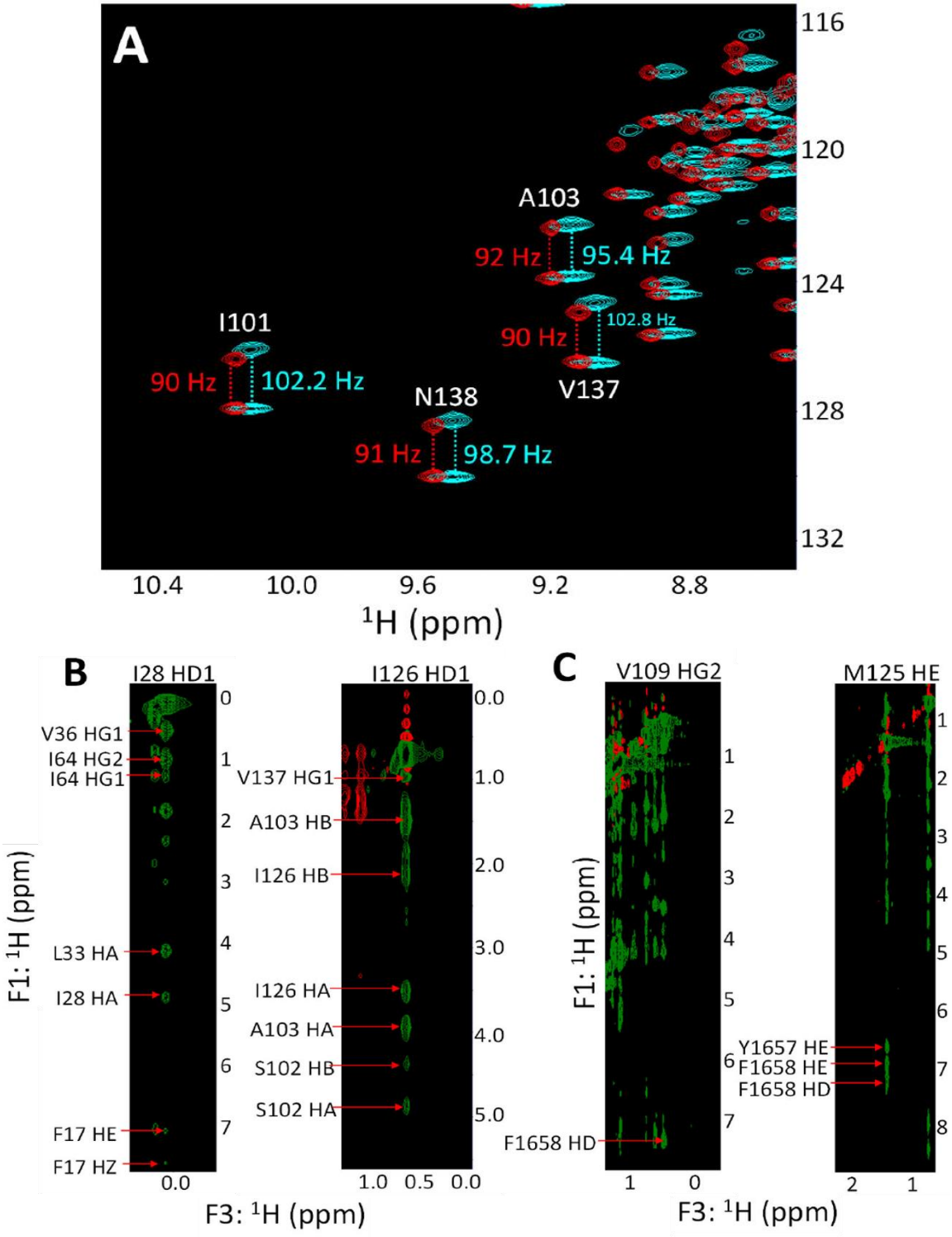

Figure 2.3.1 A *Representative IPAP-HSQC spectrum of ^{15}N-labeled Ca$_2$/CaM12 bound to unlabeled IQ peptide.* **B** *Representative strip plot analysis of three-dimensional ^{13}C-edited NOESY-HSQC.* **C** *Representative ^{13}C-filtered NOESY-HSQC spectra of ^{13}C-labeled Ca2/CaM**12'** bound to unlabeled IQ peptide.*

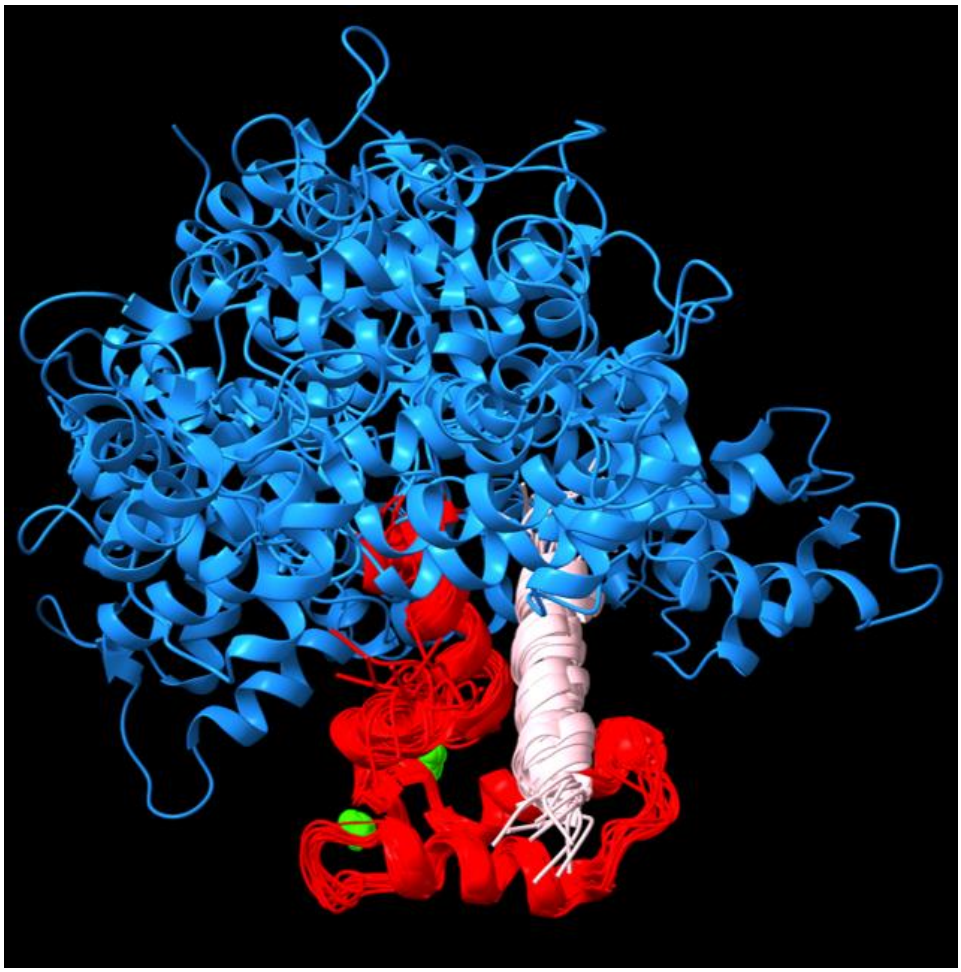

Figure 2.3.2 *An overlay of calculated structure ensemble for Ca_2/CaM12 (PDB: 7L8V) bound to the IQ peptide. The C-lobe residues of CaM are shown in red, the N-lobe residues in blue, and the IQ peptide is shown in pink.*

The main chain structure of the lowest energy calculated structure of the Ca_2/CaM-IQ complex is shown below in **Figure 2.3.3**. The interaction of the Ca^{2+}-bound CaM C-lobe with the IQ motif in the complex appears similar to the that of the Ca_4/CaM-IQ crystal structure (**Fig. 2.3.4**, purple)[44], with the IQ motif helical structure (**Fig. 2.3.3**, pink) being verified by NMR. The Ca_2/CaM12-IQ structure shows hydrophobic residues I1654, Y1657, F1658, and F1661 making extensive contact with the hydrophobic pocket formed by CaM C-lobe residues A89, F93, V109, M110, L113, M125, and M146.

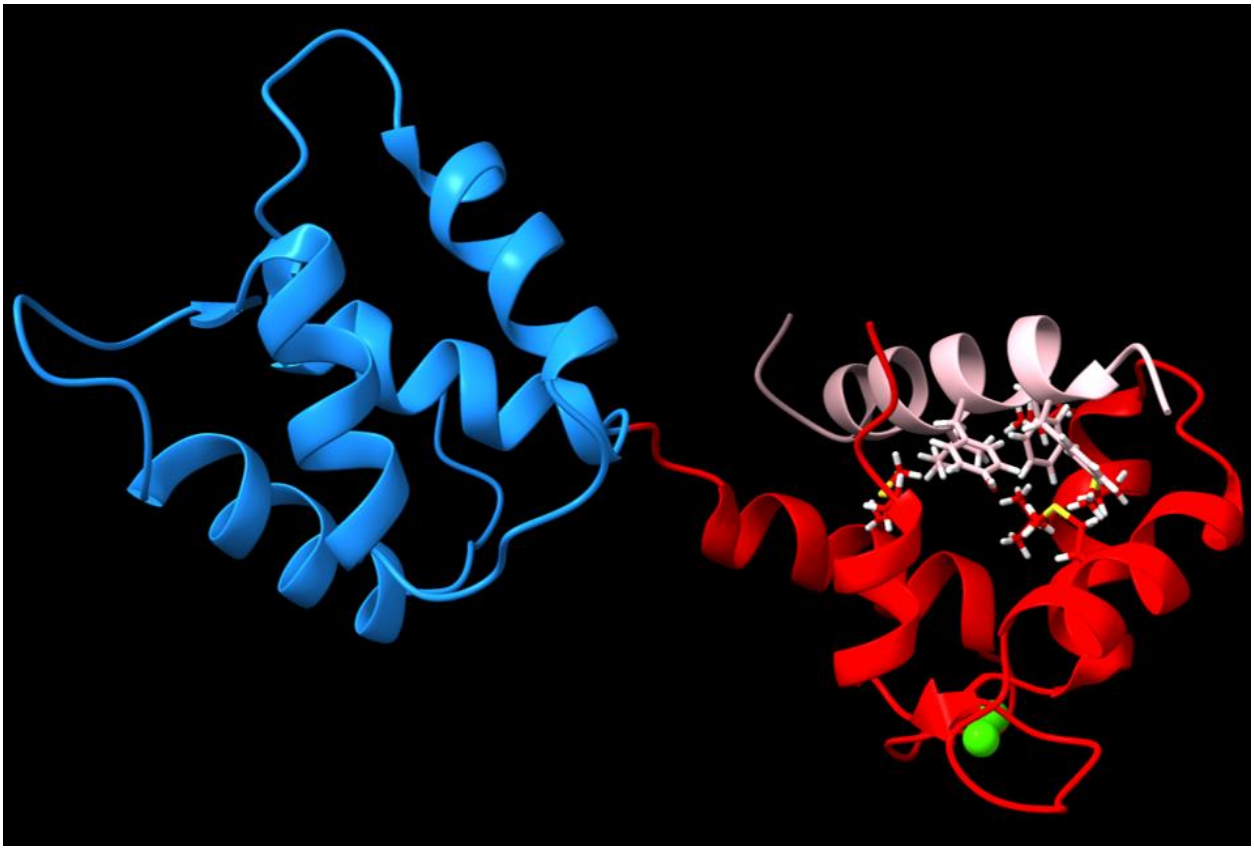

Figure 2.3.3 *The lowest energy calculated structure of the Ca_2/CaM12-IQ complex, shown as a ribbon diagram. The C-lobe residues of CaM are shown in red, the N-lobe residues in blue, and the IQ peptide is shown in pink.*

The Ca^{2+}-free CaM N-lobe of the Ca_2/CaM_{12}-IQ adopts a closed conformation like that observed for apoCaM.[59] The structure of the wild type Ca^{2+}-free N-lobe is overlaid in **Figure 2.2.4A** (dark pink). The Ca^{2+}-free CaM_{12} N-lobe does not make contact with the IQ peptide, unlike what is seen in the Ca^{2+}-bound N-lobe of the Ca_4/CaM-IQ crystal structure, where the hydrophobic residues F13, F69, M73 of the N-lobe make contact with the aromatic IQ residues F1648, Y1649, and F1652.[44,45,52]

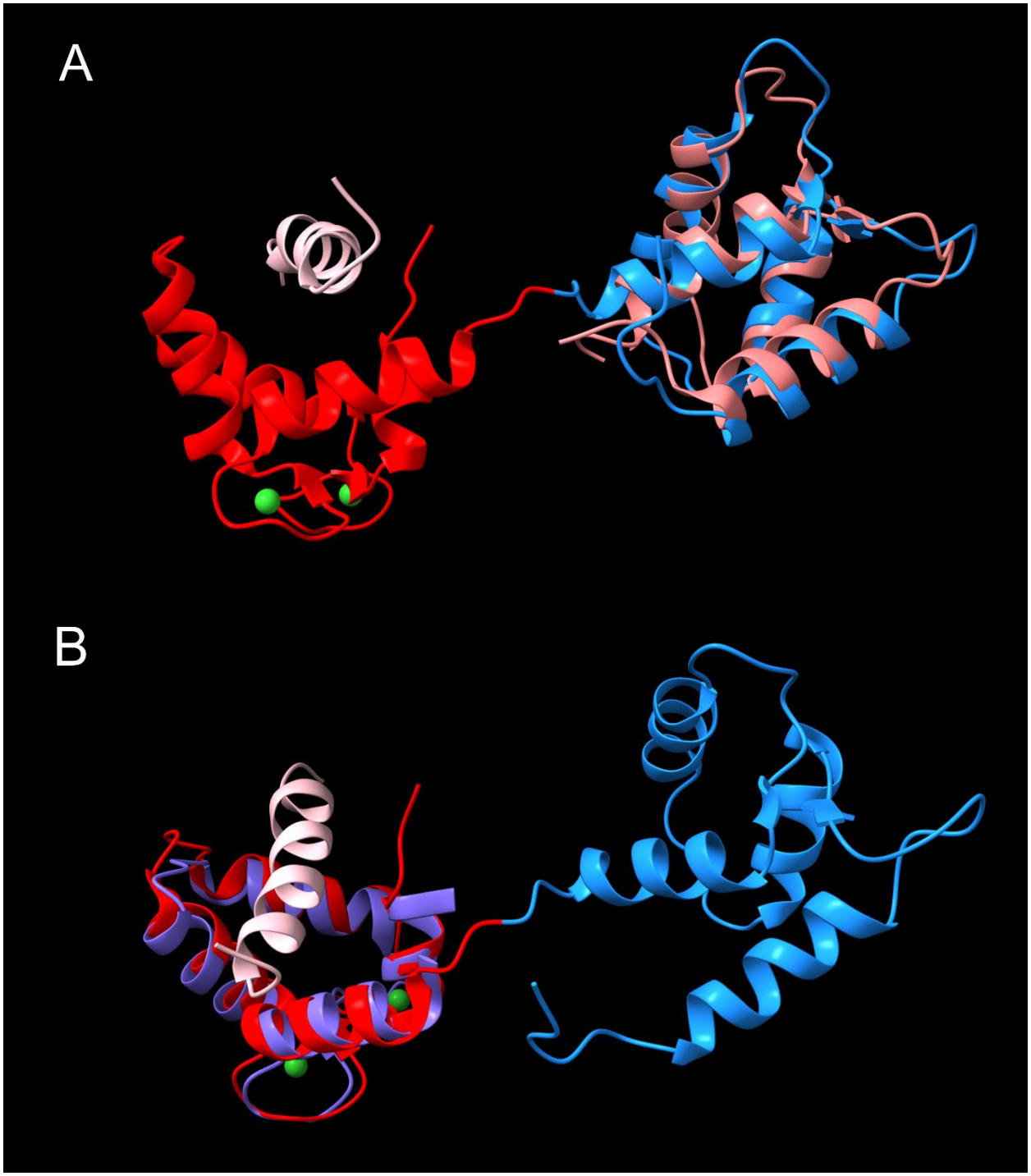

Figure 2.3.4 A: *An overlay of the Ca_2/CaM12-IQ N-lobe (blue) with the apoCaM N-lobe(dark pink).* **B:** *An overlay of the Ca_2/CaM12-IQ C-lobe (red) with the CaM C-lobe of the Ca_4/CaM12-IQ crystal structure (purple). The IQ of the Ca_2/CaM12-IQ structure is shown in pink.*

2.4 Validating the NMR Structure of Half-calcified Calmodulin by Mutagenesis

Both apoCaM and Ca_2/CaM bind to the IQ peptide primarily through the CaM C-lobe. However, the NMR structure of apoCaM bound to the IQ indicates an important salt bridge between E85 and E88 on apoCaM and K1662 of the IQ.[43] Conversely, in the Ca_2/CaM_{12}-IQ structure, K1662 is solvent exposed, pointing away from CaM. From these structures, it is predicted that mutating K1662 to a negatively charge residue, such as glutamate, should have a large impact on the binding of apoCaM to the peptide, while the K1662E mutation should have little effect on Ca_2/CaM binding. Solubility issues with the K1662E peptide (IQ^{K1662E}) precluded ITC studies with this mutant. Instead, Fluorescence Polarization (FP) was used to measure this binding of Ca_2/CaM to the IQ peptide. The FP binding curves of both the apoCaM and Ca_2/CaM12 binding to IQ^{K1662E} as well as Ca_2/CaM_{12} binding to the wild-type IQ (IQ^{WT}) are shown in **Figure 2.4.1**. As predicted, the titration of the IQ peptides with Ca_2/CaM_{12} reached full saturation at 100 nM Ca_2/CaM12. This indicates a K_D < 100 nM, similar to the IQ^{WT} affinity measured with ITC.

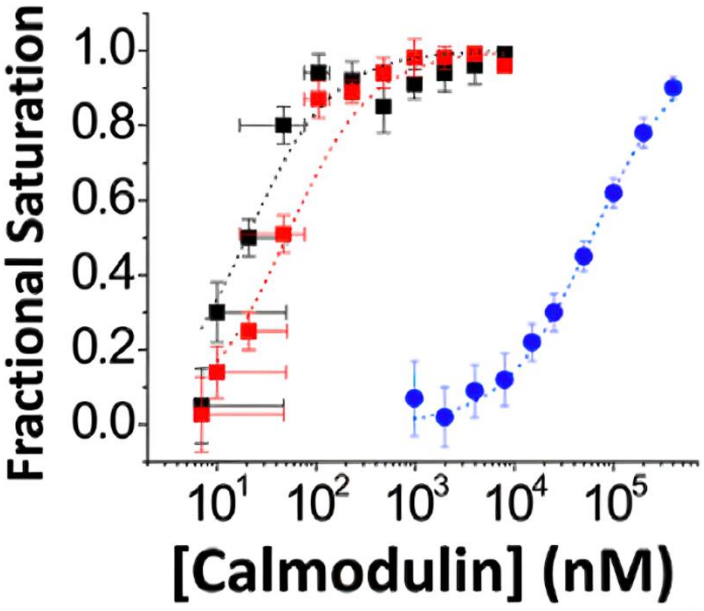

Figure 2.4.1 *Fluorescence polarization binding curves for CaM_{12} binding to IQ^{WT} (black), IQ^{K1662E} (red), and IQ^{Y1657D}(blue).*

Unfortunately, more accurate determination of the Ca_2/CaM_{12}-IQ^{K1662E} binding affinity could not be measured. Limited detection sensitivity required a minimum of 100nM peptide concentration, which is much greater than the K_D of 16nM measured with ITC. However, as the binding curves for Ca_2/CaM_{12} binding to both IQ^{K1662E} and IQ^{WT} peptides are saturated at 100nM, the upper limit of this binding is set at 100nM for both peptides, which is consistent with the measurements done by ITC of the IQ^{WT} binding. In contrast, apoCaM is shown to bind to IQ^{K1662} peptide with a K_D of 60μM, putting this interaction outside the range of its physiological concentrations.[49] Collectively, these results identify as the K1662E mutation as a method of selectively disabling apoCaM binding to the IQ motif of the $Ca_V1.2$, while retaining nanomolar binding of Ca_2/CaM_{12} to the channel.

The hydrophobic residues on the channel that are important for Ca_2/CaM_{12} binding (Y1649, I1654, Y1657, and F1658) occupy the same side of the IQ helix. These residues point down into the hydrophobic pocket formed by the open EF-hands of the Ca^{2+}-bound CaM C-lobe. The NMR structure of the Ca_2/CaM_{12}-IQ complex would predict that the mutations to these residues should weaken this binding interaction. ITC was used to test the affinity of Ca_2/CaM_{12} binding to these peptide mutants at 27ºC. These isotherms are shown in **Figure 2.4.2**. The results of these experiments are summarized in **Table 2.4.1**.

Table 2.4.1

$Ca_2/CaM12$-IQ Mutant	K_D (nM)
$Ca_2/CaM12$-IQ WT	16 ± 5
$Ca_2/CaM12$-IQ ^{I1654A}	60 ± 10
$Ca_2/CaM12$-IQ^{Y1657D}	8000 ± 10
$Ca_2/CaM12$-IQ^{F1658D}	4000 ± 10
$Ca_2/CaM12$-IQ^{Y1649A}	26 ± 5

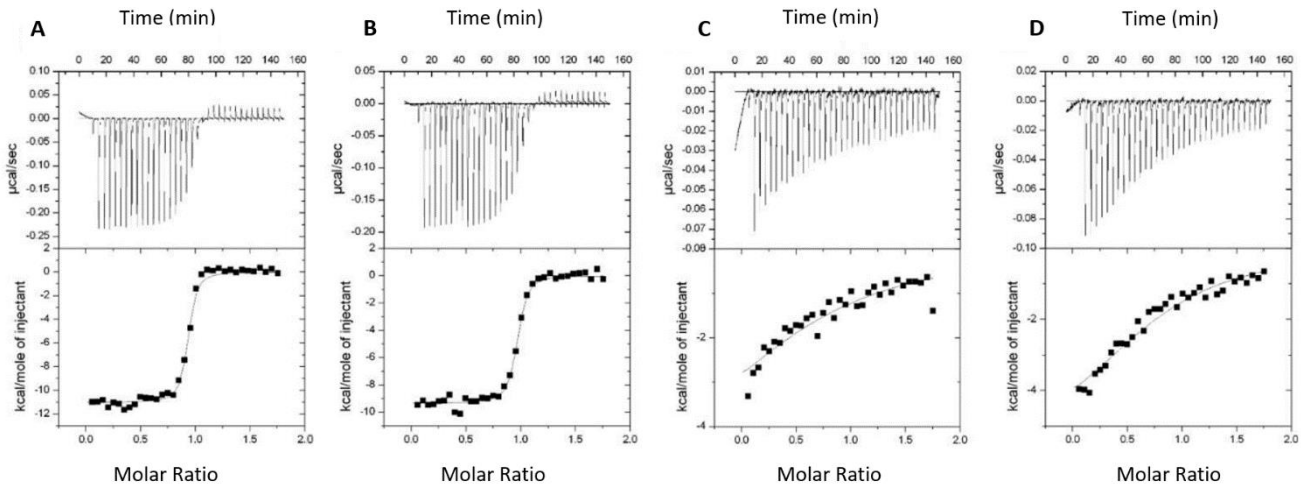

Figure 2.4.2 A-D *ITC measurement at 27ºC of Ca_2/CaM_{12} binding to (**A**) IQ^{Y1649A}, (**B**) IQ^{I1654A}, (**C**) IQ^{Y1657D}, and (**D**) IQ^{F1658D}. The IQ peptide concentrations for IQ^{Y1649A} (**A**), and IQ^{I1654A} (**B**) were each 10µM in 1.5 ml in the sample cell for titration with 100 µM Ca_2/CaM_{12}. The IQ peptide concentrations for IQ^{Y1657D} (**C**) and IQ^{F1658D} (**D**) were each 50µM in 1.5ml in the sample cell for titration with 500µM Ca_2/CaM_{12}. All titrations used 35 injections of 10µl of Ca_2/CaM_{12}.*

The Y1649A and I1654A showed smaller perturbation from the IQ^{WT} affinity of 16 ± 5nM with affinities of 26 ± 5nM and 60 ± 10nM, respectively. In contrast, the mutations Y1657D and F1658D have a much greater effect, with affinities of 8000 ± 10nM and 4000 ± 10nM. There is a marked difference between the alanine and aspartate mutants. This is consistent with the structure which shows these key residues pointing towards a hydrophobic pocket formed by the CaM C-lobe. Charged side chain mutations, such as aspartate, would severely disrupt this interaction while a nonpolar side chain from Ala would have a much smaller effect on the binding. Demonstrating this concept, when the F1658D mutation was replaced with the mutation F1658A, we recorded a K_D of 32 ± 5nM, rescuing the affinity significantly.

The exothermic nature of the Ca_2/CaM_{12}-IQ binding shown in the ITC isotherms would indicate that raising the temperature from 27ºC to 37ºC should increase the K_D. As predicted, the K_D for IQ binding to Ca_2/CaM_{12} increased from 16 ± 5 nM (at 27ºC) to 37 ± 10 nM (at 37ºC). The

measurement at 37ºC also showed an increase in ΔH from -10 kcal/mol at 27ºC to -15 kcal/mol. This would indicate a negative ΔC_p which is consistent with the large change in solvent exposed hydrophobic surface area upon binding of the IQ peptide to Ca_2/CaM_{12}.

2.5 Mutations in the IQ motif and their Effects on $Ca_V1.2$ Channel Electrophysiology

The NMR structures of the Ca_2/CaM_{12}-IQ and apoCaM-IQ complexes combined with the findings from my binding studies suggests IQ residues that are important for CaM binding to $Ca_V1.2$. The K1662E mutation of the IQ motif was shown to have a dramatic weakening effect on the binding of apoCaM to the channel under physiological conditions. This same mutation does not appear to impact the binding of Ca_2/CaM_{12}. As a result, mutation of this key salt bridge would selectively disable apoCaM binding while retaining the high affinity binding of Ca_2/CaM_{12}. Previous studies have found that the K1662E mutation does not have any impact on the open probability (P_o) of the $Ca_V1.2$ channel.[43] In contrast, the I1654A mutation, which affects both the Ca_2/CaM_{12} and the apoCaM binding, has been shown to decrease the P_o of the channel by 6-fold.[43] This would suggest that it is the half-saturated Ca_2/CaM, with two Ca^{2+} bound to the C-lobe, that preassociates with and boosts the P_o of the channel and not apoCaM as has been previously proposed.[37]

In addition to pre-associating with the channel and increasing channel activity under basal conditions, CaM deactivates the channel rapidly upon channel opening. In order to test the hypothesis that $Ca_V1.2$ is preassociated with Ca_2/CaM, Dr. Johannes Hell's lab recorded the effect of the K1662E mutation on channel CDI. Whole-cell patch clamp recordings of Ca^{2+} and Ba^{2+} currents showed no significant perturbation to CDI with the mutation of K1662E, when compared to IQ^{WT}. This is easily visible when compared to the I1654A mutation which is known to decrease

CDI.[37,39,41] This is in agreement with the effects of these mutations on P_o and suggests the preassociation of Ca_2/CaM under basal conditions promotes channel activity and prepares the channel for rapid CDI.

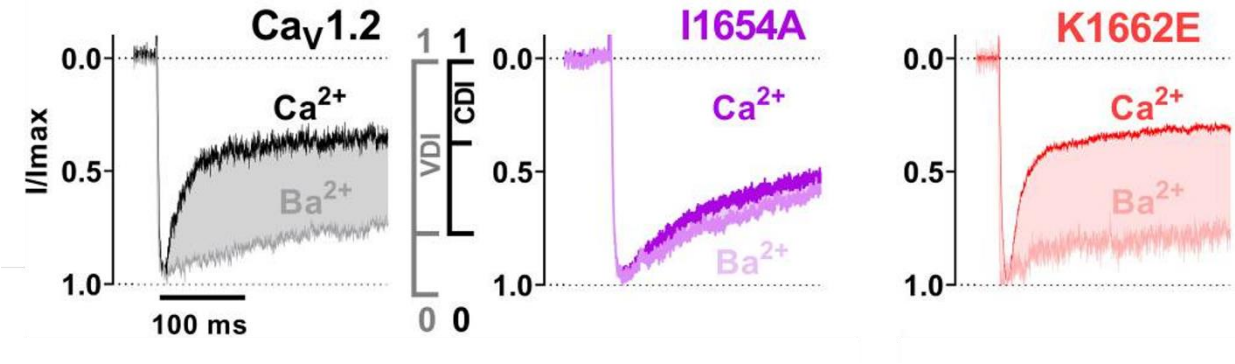

Figure 2.5.1 *Representative whole-cell patch clamp Ca^{2+} and Ba^{2+} current recordings of WT (black), I1654A (purple), K1662E (red).*

The structure of Ca_2/CaM_{12} bound to the IQ motif indicates several important hydrophobic residues on the peptide that are important for binding. Y1657 makes significant contact with the protein and mutation of this residue showed the greatest decrease in affinity in our binding studies. Prof Johannes Hell's lab showed that this mutation decreased whole-cell Ca^{2+} and Ba^{2+} currents as well as CDI. Single channel measurements show an 80% decrease in P_o for Y1657D when compared to the WT channel. This decrease in P_o and CDI are comparable to those seen with the I1654A mutation. Conversely, the K1662 mutation which affects apoCaM binding, but not Ca_2/CaM_{12} binding, has little effect on P_o and CDI. This decrease in P_o is clearly visible in an ensemble average of single-channel currents (**Figure 2.5.2**). Surface biotinylation experiments (done by Andrea Coleman in collaboration with Dr. Horne and Dr. Hell) were used to determine the effect of the mutation on surface expression of the channel and determined a nearly 50% decrease in surface expression (**Figure 2.5.3)**. This decrease in surface expression impacts the P_o of the channel, however, it cannot account entirely for the loss in P_o.

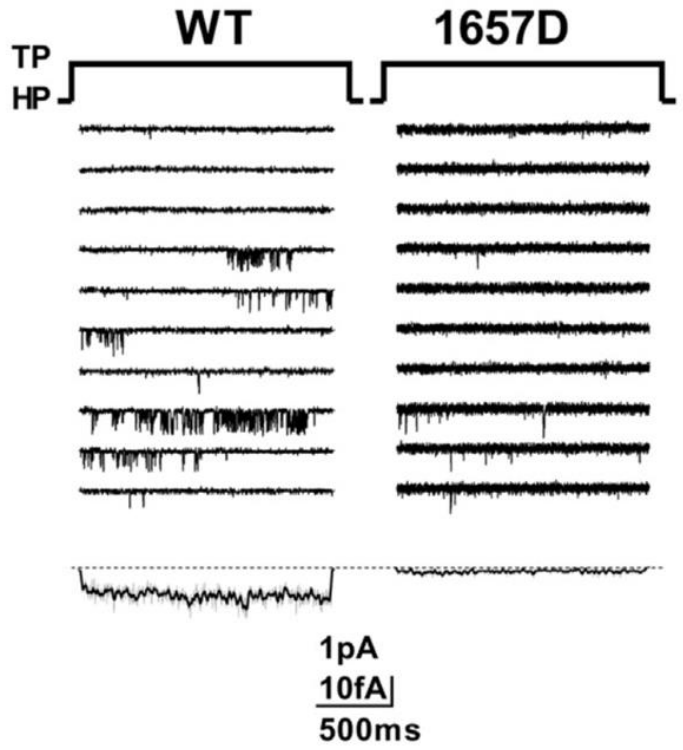

Figure 2.5.2 *10 consecutive, representative single-channel traces for each WT and Y1657D channel. A mean ensemble average current of 857 superimposed traces is shown below).*

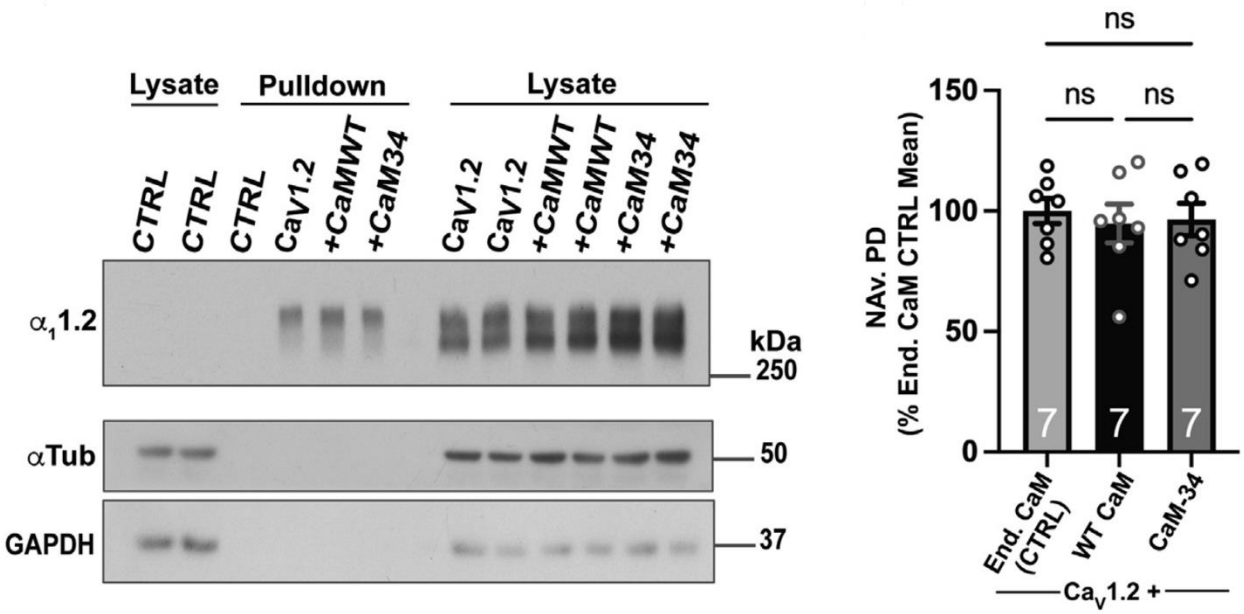

Figure 2.5.3 A *Surface biotinylation of CaV1.2 was followed by Neutravidin pull downs and immunoblotting (right panels) with antibodies against the proteins indicated at the left. The left panels show immunoblots of total lysate. Tubulin (α-Tub) and GAPDH were used as loading controls for lysate samples (left) and assessment of membrane integrity (right; all left and right panels were from same gels and exposures). Absence of tubulin and GAPDH immunoreactivity indicates that the biotin reagent did not leak into cells ruling out biotinylation of intracellular proteins.* **B** *Quantification of α11.2 immunosignals in Neutravidin pull downs (NAv.PD) normalized to WT α11.2 (set to 100%)*

2.6 CaM Expression Effects on Channel Activity

The effects of overexpressing exogenous CaM have been recorded to strongly increase the open probability of the $Ca_V1.3$ channel.[37] However, the levels of overexpressed exogenous CaM relative to endogenous CaM were unknown. In order to determine the effects of ectopically expressed CaM, it would be necessary for exogenous CaM to be expressed to a much larger degree than endogenous CaM. Thus, Andrea Coleman in collaboration with Dr. Horne investigated the levels of CaM expression by immunoblotting extracts from HEK 293T cells transfected with $Ca_V1.2$ expression constructs as well as either WT CaM or CaM_{34} (D94A/D130A) which disables Ca^{2+}-binding to the C-lobe. The level of overexpressed WT CaM was ~10 fold greater than that of

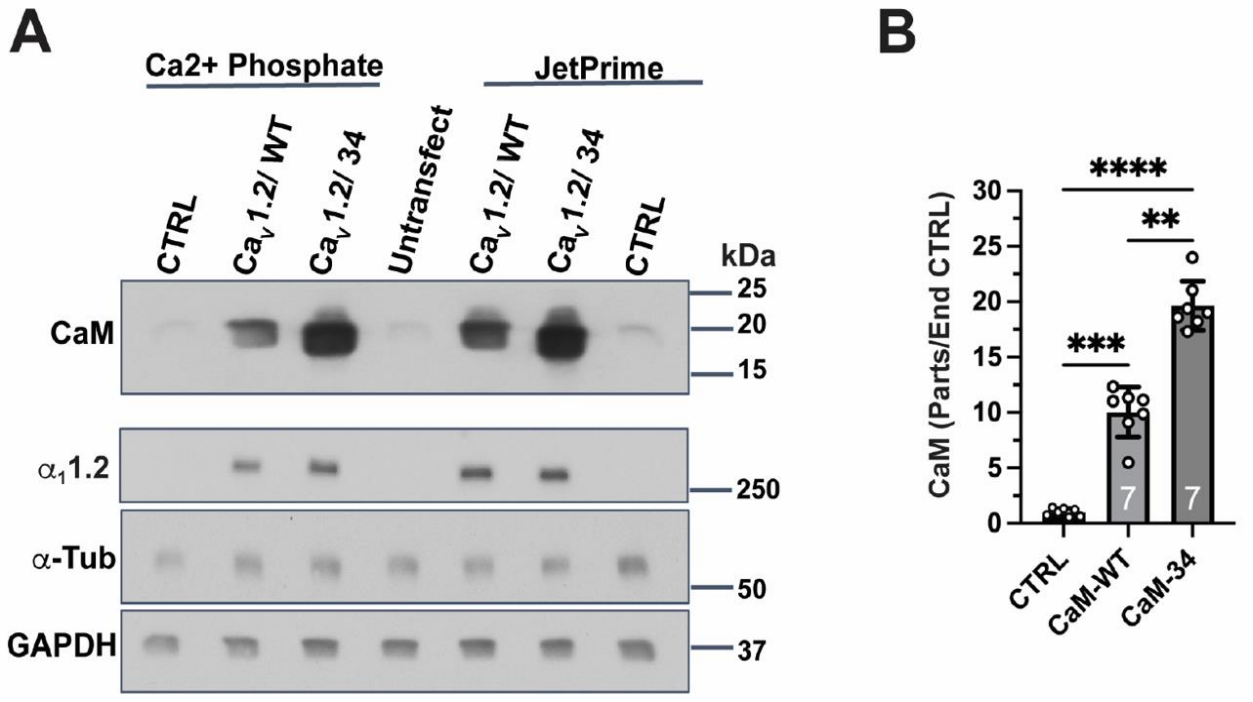

Figure 2.6.1 *Immunoblots of total lysates of HEK 293T/17 cells transfected with $\alpha_1$1.2, $\alpha_2\delta$1, and β_{2A} plus untagged (pJPA7) WT CaM or CaM34 using calcium phosphate versus JetPrime or mock-transfected (CTRL) or untransfected HEK 293T/17 cells. Tubulin (α-Tub) and GAPDH were used as internal loading controls. (**B**) Quantification of CaM immunosignals normalized to endogenous CaM (set to value of 1) as detected in mock-transfected CTRL cells (n=7 independent experiments; one-way ANOVA (F=174.8, p<0.0001), Tukey post-hoc test, **p<0.01, ***p<0.001, and ****p<0.0001).*

the endogenous CaM and the level of CaM_{34} overexpression was ~20 fold greater than that of endogenous CaM, shown in **Figure 2.6.1**.

To investigate the effects of ectopic CaM expression on endogenous CaM levels, Dr. Horne's and Dr. Hell's group expressed YFP-tagged WT-CaM and CaM_{34} (MW≈45kDa). Comparison of the 17 kDa endogenous CaM bands from cells transfected with WT CaM or CaM_{34} and the 17kDa bands shows no significant change in endogenous CaM levels when CaM is ectopically expressed.

Overexpression of the WT CaM showed a 300% increase in P_o when compared to $Ca_V1.2$ expression alone. This is consistent with previous studies.[37] However, at basal Ca^{2+} concentrations, CaM exists in both apoCaM and half-saturated Ca_2/CaM states. In order to test the importance of CaM C-lobe calcium-binding for channel activation, CaM_{34} was ectopically expressed, and the measured P_o showed no significant increase when compared to $Ca_V1.2$ alone. This suggests that Ca^{2+}-binding to the C-lobe of CaM is required for increasing the channel P_o, which would imply

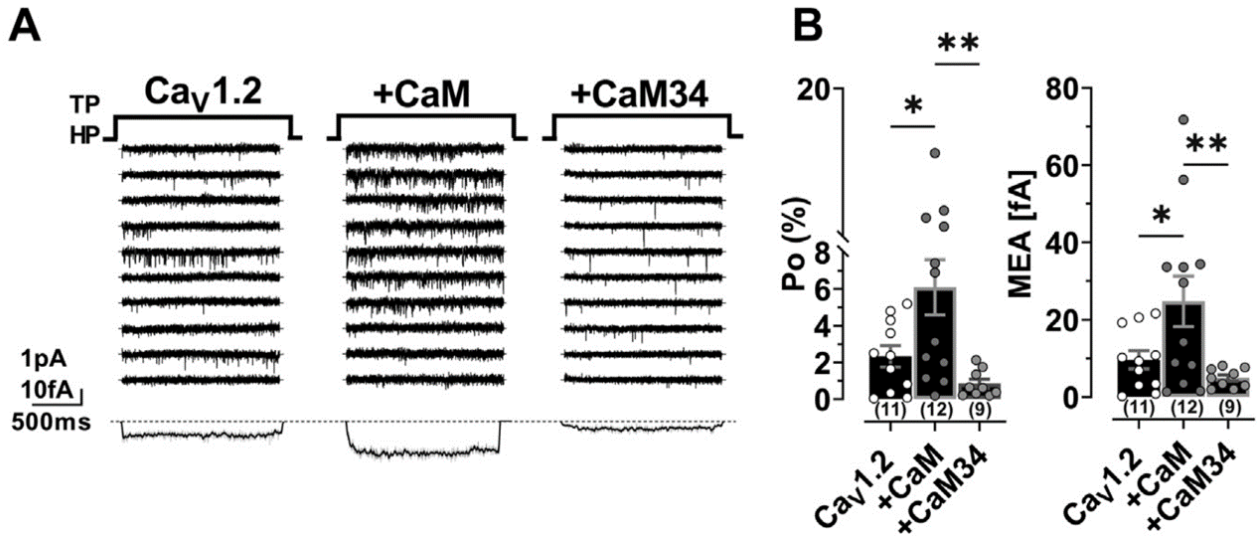

Figure 2.6.2 A *10 consecutive representative single-channel traces of WT $Ca_V1.2$ expressed alone (left) or together with WT CaM (middle) or CaM34 (right). Bottom: mean ensemble average calculated from a total of 2009 superimposed traces for $Ca_V1.2$ expressed without CaM (n = 11 cells), 2327 traces for CaV1.2 expressed with WT CaM (n = 12 cells), and 1655 traces for CaV1.2 expressed with CaM_{34} (n = 9 cells).* **B** *Quantification of P_o (left) and MEA (right).*

that it is Ca_2/CaM (and not apoCaM) that activates the channel under basal, low-Ca^{2+} conditions. Representative single traces and mean average ensemble (MEA) current for ectopically expressed $Ca_V1.2$ alone, with WT CaM, and CaM_{34} are shown in **Figure 2.6.2**. Neither WT CaM nor CaM_{34} expression were shown to have any effect on surface expression of $Ca_V1.2$ (**Figure 2.6.3)**.

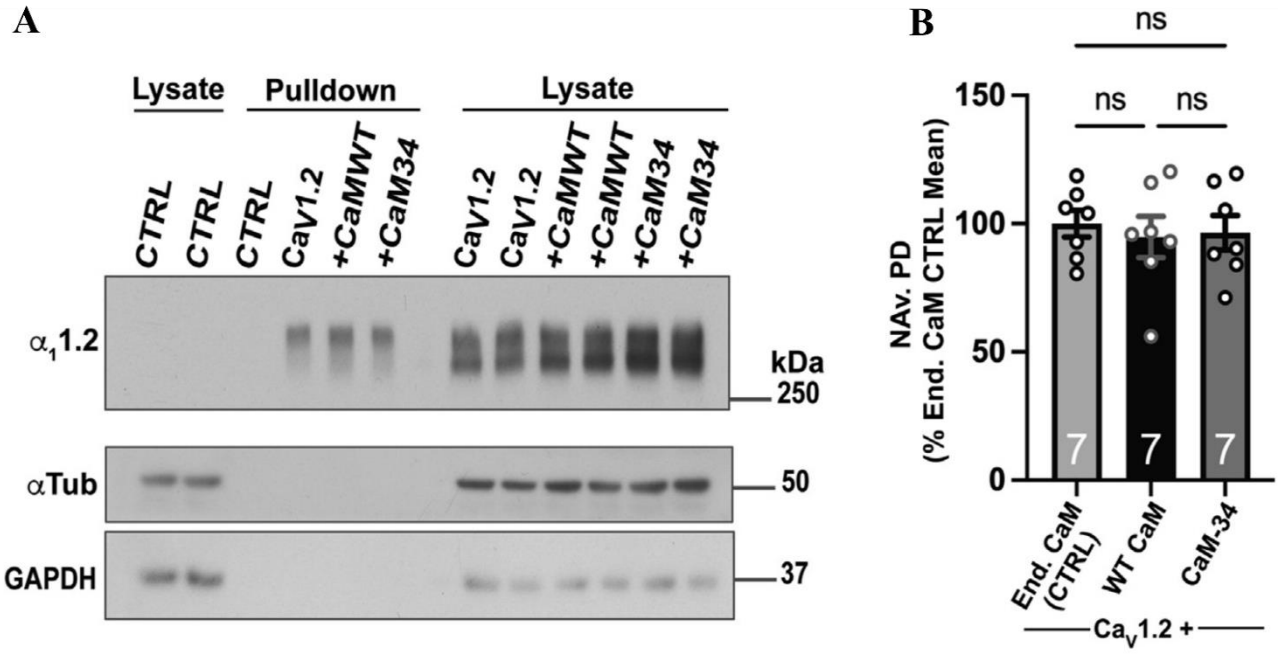

Figure 2.6.3 *surface biotinylation of $Ca_V1.2$ was followed by Neutravidin pull downs (middle of blot) and immunoblotting with antibodies against the proteins indicated at the left. Right side shows respective total lysate samples in duplicate and left side total lysate samples from mock-transfected cells. Cells expressing CaV1.2 only or CFP-tag empty vector only were used as controls (CTRL). Tubulin (α-Tub) and GAPDH were used as loading controls for lysate samples and assessment of membrane integrity for pull-down samples. Absence of tubulin and GAPDH immunoreactivity ruled out biotinylation of intracellular proteins.* **B** *quantification of α11.2 immunosignals in Neutravidin pull downs (NAv.PD) normalized to mean (set to 100%) of the signal in CaV1.2 only samples (control, only endogenous CaM); n = 7; one-way ANOVA (F = 0.1547, p = 0.8578), followed by Tukey's post-hoc test, ns = p > 0.05). CaM, calmodulin; MEA, mean ensemble average.*

2.7 Discussion

CaM has been shown to preassociate with $Ca_V1.2$ and analogous L-type channels under basal conditions ($[Ca^{2+}]$ = 100 nM),[42] which is believed to both elevate channel activity at low Ca^{2+} levels and promote rapid channel inactivation at high Ca^{2+} levels. The CaM-dependent channel activity has previously been explained by channel preassociation with Ca^{2+}-free apoCaM, similar to that seen in sodium channels.[37] However, overexpression of the CaM_{34} mutant failed to activate the channel and largely prevents channel inactivation (**Fig. 2.6.2**). This would imply that Ca^{2+}-binding to the C-lobe of CaM is necessary for modulation of $Ca_V1.2$ channel function. Ca^{2+} binding studies showed that CaM binding to $Ca_V1.2$ increases the apparent Ca^{2+}-affinity of CaM into the nanomolar range (**Fig. 2.1.3**). This is consistent with previous binding studies[47,50] and indicates that under basal Ca^{2+} concentrations over 50% of CaM C-lobe has $2Ca^{2+}$ bound when CaM is saturated with the IQ peptide. With estimated free endogenous CaM levels of 50-100nM, the K_D of 16nM for Ca_2/CaM binding to the IQ motif would imply that ~50% of $Ca_V1.2$ is bound to Ca_2/CaM under basal conditions. This binding of Ca_2/CaM to $Ca_V1.2$ under basal conditions may have implications for cardiac disease because mutations in CaM (D96V, N98I, D130S, D134H in **Fig. 1.2.1**) that disable Ca^{2+} binding to EF3 and EF4 abolish CDI and cause cardiac arrhythmias.[13]

The NMR structure of Ca_2/CaM_{12}-IQ is comprised of a Ca^{2+}-free CaM N-lobe in a closed conformation, a flexible linker, and an open-conformation, Ca^{2+}-saturated C-lobe binding to the IQ peptide. The two lobes appear independently folded, with no observed inter-lobe contacts, similar to apoCaM. Only the Ca^{2+}-bound C-lobe contacts the IQ-motif. The structure and IQ interaction surface of the Ca_2/CaM_{12} C-lobe are similar to the C-lobe of the Ca_4/CaM-IQ crystal structure. The IQ motif binds to apoCaM with a 180º rotated orientation compared to Ca_2/CaM_{12}

and Ca_4/CaM. This reversed orientation may explain the 100-fold greater affinity of Ca_2/CaM for the IQ. Having the same IQ binding orientation for both Ca_2/CaM and Ca_4/CaM supports Ca_2/CaM as the basal, preassociating CaM species responsible for channel activation. Additionally, this preassociation allows for rapid inactivation of the channel with CaM in the Ca^{2+}-saturated Ca_4/CaM state, seen in the Ca_4/CaM-IQ crystal structure. Preassociation of apoCaM to the channel would require CaM to unbind from the channel to allow for reorientation of the IQ and rebinding into the position seen in the Ca_4/CaM-IQ crystal structure to engage CDI. This process of unbinding and rebinding would be slowed by molecular diffusion and contradict the point of having CaM preassociation for rapid channel deactivation. Conversely, the Ca_2/CaM C-lobe binds to the channel in the same manner as the Ca_4/CaM C-lobe which would allow CaM to remain bound to the channel upon influx of Ca^{2+} and facilitate rapid CDI.

The functional analysis of $Ca_V1.2$ performed by the Hell lab (**Figs. 2.5.1-3**) agrees with my binding studies and analysis of the available CaM-IQ structures (**Fig. 2.3.3**). The K1662E mutation, which targets a salt bridge specifically vital for apoCaM binding to the channel, did not have an appreciable effect on channel P_o, CDI, I_{Ba}, or I_{Ca}. Notably, the K1662E mutation has no effect on Ca_2/CaM binding. The Y1657D mutation impairs the binding of apoCaM by 6-fold and Ca_2/CaM by 500-fold. This mutation decreases channel P_o, CDI, I_{Ba}, and I_{Ca}. These results indicate that the binding of Ca_2/CaM, specifically, is important for facilitation and deactivation of channel activity.

Previous work has shown that overexpression of WT CaM strongly boosted the P_o of the channel.[37] It was also shown that the I1654M mutation reduced P_o, and overexpression of WT CaM rescued this loss. Also, I1654 had been shown to be important for apoCaM binding. This led to the natural conclusion that apoCaM binding is important for boosting the P_o under basal

conditions. However, the functional and binding studies in this thesis have shown that I1654 is also important for Ca_2/CaM binding and that both species of CaM should be present under basal conditions. To more directly test the effects of apoCaM overexpression on channel activity, the Hell lab ectopically expressed CaM_{1234} (D21A/D57A/D94A/D130A) to disable Ca^{2+}-binding to all four EF-hands, ensuring the apoCaM as the dominant CaM species. Additionally, CaM_{34} was expressed to target CaM C-lobe EF-hands which my binding studies demonstrated would bind Ca^{2+} under basal conditions. Neither overexpression of CaM_{1234} nor CaM_{34} increased P_o. The inability of the overexpressed, constitutively Ca^{2+}-free CaM_{1234} to boost the P_o of the channel, even when expressed to levels 20-fold higher than those of endogenous CaM, suggests that apoCaM does not augment channel acvtivity. Furthermore, the inability of CaM_{34} to boost P_o, indicates that Ca^{2+}-binding to the CaM C-lobe is necessary to enhance basal channel activity.

The binding studies above suggest that ~50% of $Ca_V1.2$ channels are occupied and activated by Ca_2/CaM under basal conditions. The low cytosolic Ca^{2+} concentration (50-100 nM) and low affinity binding of apoCaM for the channel IQ motif indicates that half of $Ca_V1.2$ channels are not bound to CaM under basal conditions. α-Actinin has been shown to bind to the IQ motif and to increase the activity of $Ca_V1.2$,[43] while also anchoring the channel to the cell surface, augmenting the surface expression of the channel. Thus, I propose a model in which $Ca_V1.2$ is either occupied by α-actinin, which anchors $Ca_V1.2$ at the cell surface (especially in dendritic spines where α-actinin is concentrated) or by Ca_2/CaM. Accordingly, in addition to strongly promoting Po, α-actinin also augments the $Ca_V1.2$ surface expression, perhaps by connecting to F-actin. On the other hand, Ca_2/CaM augments Po with apparently little if any effect on surface expression. Channel occupancy by Ca_2/CaM could be increased upon modest increases of basal Ca^{2+} influx potentially in a positive feedback loop at low Ca^{2+} levels and low channel activity.

However, prolonged displacement of α-actinin by Ca_4/CaM would triggers endocytosis of $Ca_V1.2$ as a negative feedback mechanism.[61] At this point, it is not certain how α-actinin and CaM intersect at the IQ motif to govern $Ca_V1.2$ activity. Future research is needed to learn the exact function of these interactions.

Combining the NMR structure of Ca_2/CaM-IQ (**Fig. 2.3.3**) with the known cryoEM structures of $Ca_V1.2$,[11] I propose a new structural mechanism for Ca^{2+}-dependent inactivation (CDI) for $Ca_V1.2$ (**Fig. 2.7.1**). $Ca_V1.2$ is proposed to occupy three possible channel states: the closed state (**Figs. 2.7.1A**) in which the IQ may be unbound or bound to Ca_2/CaM, open & activated bound to Ca_2/CaM (**Figs. 2.7.1B-C**), and open & inactivated bound to Ca_4/CaM (**Figs. 2.7.1E-F**). Under basal conditions ($[Ca^{2+}]$ = 50-100 nM), 50% of $Ca_V1.2$ channels are estimated to be bound to Ca_2/CaM (**Figs. 2.7.1A-B**) and the remaining channels are likely not bound to apoCaM (**Fig. 2.7.1B**), because apoCaM binds to $Ca_V1.2$ in the micromolar range that is significantly higher than physiological apoCaM levels.[36] Neuronal stimulation produces membrane depolarization that switches the channel from closed (**Figs. 2.7.1A**) to open (**Fig. 2.7.1B**). When the channel first opens, the cytosolic Ca^{2+} concentration is transiently still low (< 100 nM) with about half of the channels still bound to Ca_2/CaM (at $[Ca^{2+}]$ = 50-100 nM). The remainder of the open channels are either not bound to CaM or are bound to Ca_4/CaM (**Fig. 2.7.1E**). I propose that the binding of Ca_2/CaM to $Ca_V1.2$ switches the channel into an active conformation in which the IQ motif folds back to interact with the channel EF-hand on one side, while Ca_2/CaM is bound to the opposite side of the IQ helix as seen in the NMR structure of Ca_2/CaM-IQ (**Fig. 2.3.3**). The structure of the inactive channel bound to Ca_4/CaM (**Figs. 2.7.1E-F**) is proposed to have the channel EF-hand interact with the III-IV linker as seen in the cryoEM structure of CaV1.1 in the inactive state.[10] I propose that the inactive channel also has an exposed

IQ-motif that is bound to Ca_4/CaM (**Figs. 2.7.1E-F**). Both lobes of Ca_4/CaM are proposed to wrap around the IQ helix as seen in the crystal structure of Ca_4/CaM-IQ[44]. Prolonged voltage-induced channel opening causes a Ca^{2+} influx in which the cytosolic Ca^{2+} concentration increases to about 1 micromolar (**Figs. 2.7.1C & 2.7.1F**). This rise in Ca^{2+} concentration promotes formation of Ca_4/CaM, which binds tightly to the inactivated channel and switches all channels into the inactivated state (**Fig. 2.7.1F**) to produce CDI. By contrast, $Ca_V1.2$ switches back to the high open probability active channel state when Ca^{2+} dissociates from the CaM N-lobe at low Ca^{2+} levels (**Fig. 2.7.1B**). This explains why the channel has highest open probability at basal Ca^{2+} levels in which Ca^{2+} is bound to the CaM C-lobe but not bound to the CaM N-lobe.

An important prediction of the model in Fig. 2.7.1 is that Ca^{2+} binding to the CaM C-lobe should be essential for producing high channel Po under basal conditions. Also, Ca^{2+} binding to the CaM N-lobe should be essential for channel inactivation at high Ca^{2+} levels. Indeed, electrophysiology experiments on the CaM_{34} mutant confirm that Ca^{2+} binding to EF3 and EF4 is essential for producing high channel Po under basal conditions (**Fig. 2.6.2**). However, electrophysiology experiments on $Ca_V1.2$ in the presence of CaM_{12} indicate a detectable amount of CDI that still persists in the presence of CaM_{12}.[39] This residual CDI in the presence of CaM_{12} might be caused by artificial binding of two CaM_{12} molecules to a single $Ca_V1.2$. NMR titrations suggest that a second molecule of CaM_{12} bound to the IQ (with high micromolar K_D) might mimic the binding of the Ca^{2+}-bound CaM N-lobe, and artificially stabilize the inactive channel state. HSQC spectra of ^{15}N-labeled CaM_{12} bound to unlabeled IQ peptide reveal two NMR peaks for each residue that may represent two separate CaM_{12} bound to a single IQ [**Fig. 2.8.1**]. The spectral heterogeneity disappears and a 1:1 complex is formed when [IQ] is raised more than 2-fold higher than [Ca_2/CaM_{12}]. However, in HEK293 cells, the overexpressed CaM_{12} concentration could be

high enough (>10 μM)[39] to generate a significant fraction of the 2:1 complex, which I propose could cause the residual and artificial amount of CDI that is observed when overexpressing CaM_{12} in HEK cells. Future cryoEM studies are needed to solve the structures of $Ca_V1.2$ bound to CaM

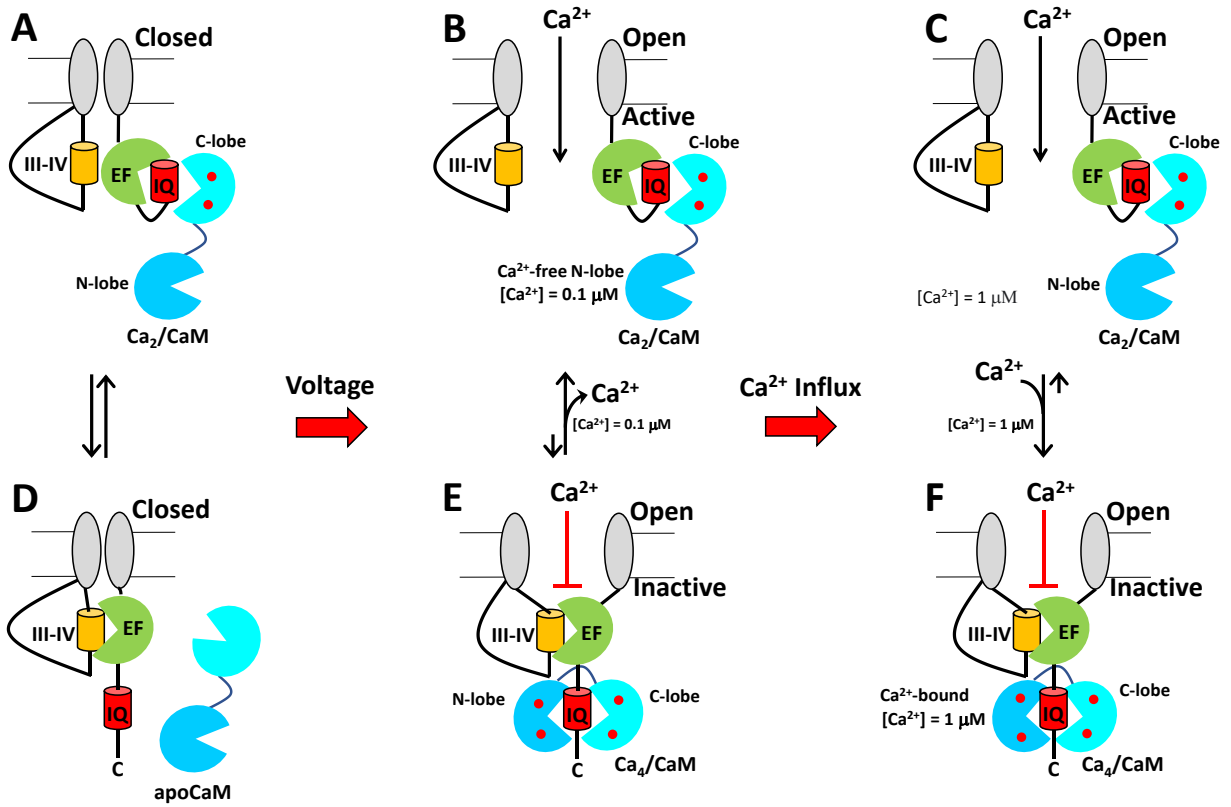

in both the half-calcified and fully calcified states to test the structural predictions of the model in **Fig. 2.7.1**.

Figure 2.7.1 Structural Mechanism of Ca^{2+}-dependent inactivation of $Ca_V1.2$ promoted by CaM. **A** Closed channel bound to Ca_2/CaM. **B** Open/activated channel bound to Ca_2/CaM at low Ca^{2+} ($[Ca^{2+}] < 100$ nM). **C** Open/activated channel at high Ca^{2+} ($[Ca^{2+}] = 1$ μM). **D** Closed channel not bound to CaM. **E** Open/inactivated channel bound to Ca_4/CaM at low Ca^{2+}. **F** Open/inactivated channel bound to Ca_4/CaM at high Ca^{2+} ($[Ca^{2+}] = 1$ μM). Half-calcified CaM (Ca_2/CaM) drives formation of the open/active channel at low Ca^{2+} levels (reverse arrow between B and E). Fully calcified CaM (Ca_4/CaM) drives formation of the open/inactive channel at high Ca^{2+} levels (forward arrow between C and F). In the inactive channel, the exposed IQ-motif is surrounded by both CaM lobes as seen in the crystal structure.[44] Bound Ca^{2+} (red circles), channel EF-hand (green), IQ-motif (red cylinder), III-IV linker (orange cylinder).

2.8 Experimental Procedures

$CaM_{12'}$ mutagenesis and purification and IQ peptide for NMR: The $CaM_{12'}$ mutation ((D21A/D23A/D25A/E32Q/D57A/D59A/N61A/E68Q) was introduced into *Xenopus* CaM complementary DNA by PCR QuickChange procedure.[62] The mutated complementary DNA was inserted into the NcoI/ BamHI sites of a pET11d vector and verified by automated Sanger sequencing. The recombinant $CaM_{12'}$ protein was expressed from a pET11d vector in a BL21(DE3) Codon Plus *Escherichia coli* strain (Stratagene) and purified as described previously.[27] The $Ca_V1.2$ IQ peptide ($Ca_V1.2$ residues 1644–1664) was purchased from ChinaPeptides. The peptide was dissolved in d_6-dimethyl sulfoxide to give a peptide concentration of 7.8 mM. The peptide concentration was determined by measuring absorbance at 280 nm with ε_{280} = 2980 M^{-1} cm^{-1}. An aliquot of peptide (1.5 equivalents) was added to a dilute solution of CaM_{12} (50 μM protein dissolved in 20 mM 2-amino−2−hydroxymethyl-propane-1,3-diol-d11 [Tris-d_{11}] with 95% H_2O/5% D_2O). The complex was then concentrated to a final concentration of 500 μM in a final volume of 500 μL for NMR experiments. The 1.5-fold excess of IQ peptide in the NMR sample of Ca_2/$CaM_{12'}$-IQ was necessary to minimize the formation of a 2:1 complex, in which two molecules of $CaM_{12'}$ were bound to one IQ. **Figure 2.6.1** shows a HSQC spectrum with equal concentrations of $CaM_{12'}$ and IQ peptide. This spectrum includes two distinct peaks for many C-lobe residues of $CaM_{12'}$. The most intense peak represented a 1:1 complex (~90% occupancy) and a weaker second peak, which we believe to represent a second CaM_{12} molecule bound to opposite side of the IQ-motif in a 2:1 complex (~10% occupancy). Under conditions where the CaM_{12} concentration is more than 10-fold greater than that of $Ca_V1.2$, like what exists inside HEK293 cells used in the CaV1.2 electrophysiological experiment, channel occupation by the 2 separate $CaM_{12'}$ proteins could reach nearly 100%. The 2:1 complex likely consists of a single IQ

peptide that binds tightly to a Ca^{2+}-bound C-lobe on one side of the IQ helix (CaM_{12}, C-lobe contacting I1654 and Y1657) as well as a second CaM_{12}, C-lobe that binds with lower affinity to the opposite side of the IQ helix (CaM_{12}, C-lobe contacting F1648 and F1652). The binding of a second C-lobe from CaM_{12}, mimics the binding of a Ca^{2+}-bound CaM N-lobe, as would be seen with WT CaM. Therefore, we suggest that the remaining CDI observed for $Ca_V1.2$ in the presence of CaM_{12}, is an artifact of the formation of a 2:1 complex in HEK293 cells, involving two of the overexpressed CaM_{12} molecules bound to a single channel.

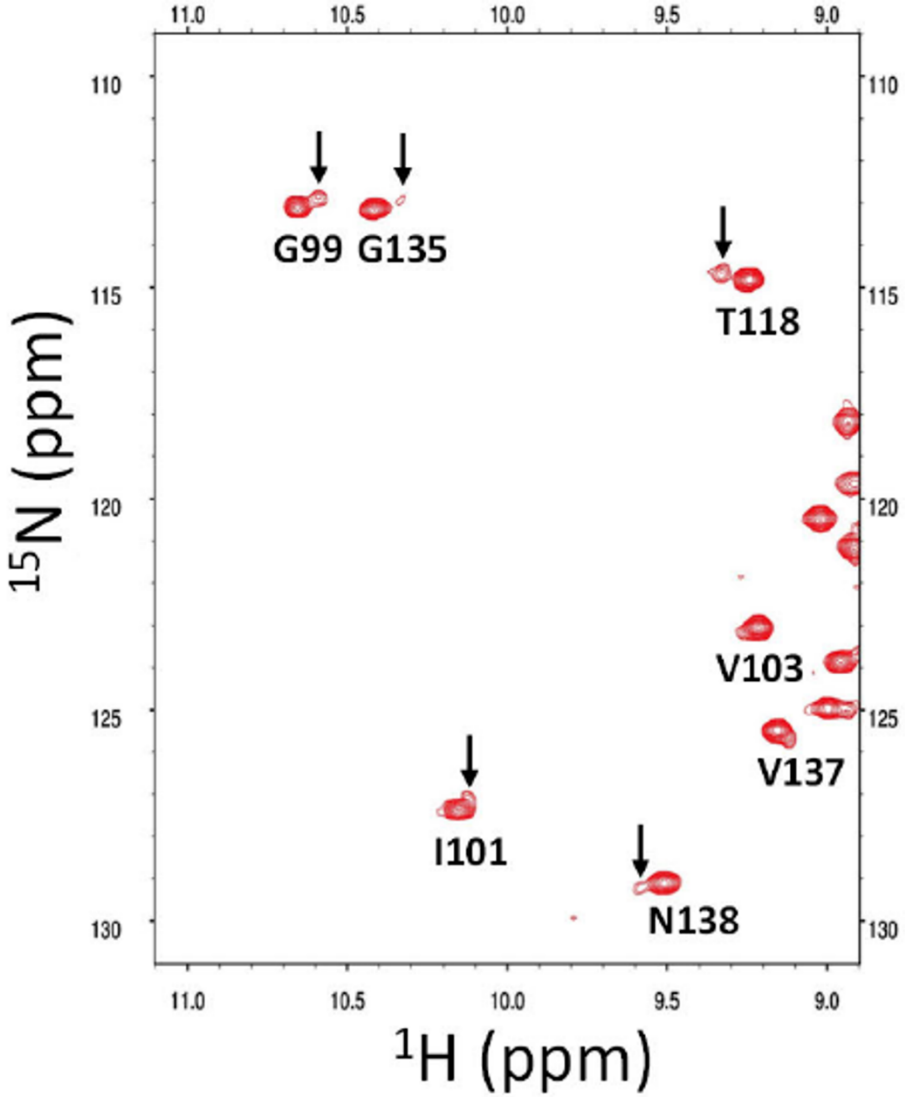

Figure 2.8.1 *HSQC spectrum of ^{15}N-labeled Ca_2/CaM_{12}, (100 μM) bound to unlabeled IQ peptide (100 μM) shows sample heterogeneity. Lower occupancy 2:1 complex C-lobe residues indicated by arrows.*

Isothermal Titration Calorimetry: ITC experiments were performed using a VP-ITC calorimeter (Micro-Cal) at 27º C and 37º C. The data were acquired and processed with MicroCal software (https://www. originlab.com) as described previously.[33] The first data point from each ITC isotherm was deleted because the amount of $Ca_V1.2$ channel regulation by half-calcified CaM of injectant delivered during the first injection has significant error caused by a dead volume void in the injection syringe. For ITC experiments in **Figure 2.1.3**, samples of Ca^{2+} (injectant) and CaM_{12}–IQ complex (titrant) were prepared by exchanging each into buffer containing 20 mM Tris, pH 7.4, and 100 mM KCl. The CaM_{12}–IQ complex in the sample cell (10 μM at 27º C or 8.0 μM at 37º C in 1.5 ml) was titrated with aqueous $CaCl_2$ (0.23 mM at 27º C or 0.3 mM at 37º C) using 35 injections of 10 μl each. For the ITC experiments in **Figure 2.4.2,** samples of Ca_2/CaM_{12} (injectant) and IQ peptide (titrant) were prepared by exchanging each into buffer containing 20 mM Tris, pH 7.4, 100 mM KCl, and 1 mM $CaCl_2$. The concentrations of the IQ peptides (WT, Y1649A, I1654A, or F1658A) were each 10 μM in 1.5 ml in the sample cell for titration with 0.1 mM Ca_2/CaM_{12}, and the concentrations of Y1657D and F1658D were each 50 μM in 1.5 ml for titration with 0.5 mM Ca_2/CaM_{12}. Titrations consisted of 35 injections of 10 μl each.

NMR spectroscopy: All NMR measurements were performed at 303 K using a Bruker Avance III 600 MHz spectrometer equipped with a four-channel interface and triple-resonance cryoprobe. Two-dimensional NMR experiments (heteronuclear single quantum coherence [HSQC] and HSQC-IPAP) were recorded on samples of 15N-labeled Ca_2/CaM_{12} (0.5 mM) bound to unlabeled IQ-peptide (0.75 mM). Each sample was dissolved in 20 mM 2-Amino−2−hydroxymethyl-propane-1,3-diol-d11 (Tris-d_{11} at pH 7.5), 1.0 mM $CaCl_2$, and 95% H_2O/5% D_2O. Three-dimensional NMR experiments for assigning backbone and side-chain resonances, and NOESY-derived distance restraints were analyzed as described previously.[63]

NMR data were processed using NMRPipe[64] and analyzed with SPARKY.[65] To measure RDCs of Ca_2/CaM_{12} bound to the IQ peptide, the filamentous bacteriophage Pf1 (Asla Biotech Ltd) was used as an orienting medium.[54] Pf1 (120 mg/ml) was added to an NMR sample that contained either ^{15}N-labeled Ca_2/CaM_{12} bound to unlabeled IQ. 1H-15N residual dipolar coupling constants (DNH) were measured using a 2D IPAP (in-phase/antiphase) ^{1}H-^{15}N HSQC experiment as previously described.[66] Briefly, the backbone N-H RDCs were calculated by measuring the difference in ^{15}N splitting for each amide resonance, both in the presence and absence of the orienting medium. The RDC Q-factor and analysis of RDC data were calculated by PALES.[67] The Q-factor is calculated as $Q = RMS(D_{meas}-D_{calc})/RMS(D_{meas})$, where D_{meas} is the measured RDC, D_{calc} is the calculated RDC, and RMS is the root mean square difference. A Q-factor of 30% corresponds to 2 Å resolution.

NMR structure calculation: NMR-derived structures of Ca_2/CaM_{12} bound to the IQ peptide were calculated using restrained molecular dynamics simulations within Xplor-NIH.[56] RDCs, NOE distances, dihedral angles from TALOS+[55], and backbone hydrogen bonds were used as structural restraints. NOEs were obtained from 15N-edited NOESY-HSQC, ^{13}C-edited NOESY-HSQC (aliphatic), and ^{13}C-filtered NOESY-HSQC as previously described.[68] Backbone dihedral angles were calculated by TALOS+[55] using backbone chemical shifts (H_α, C_α, C_β, CO, ^{15}N, and HN) as input. Hydrogen bond restraints in helices and β-sheets were verified by measuring amide hydrogen-deuterium exchange rates as previously described.[68] The XplorNIH structure calculation was performed in three stages: annealing, refinement, and water refinement.[69] Annealing started from an extended random structure. A total of 200 structures were calculated and the one with lowest energy was used as a starting structure during the refinement. The lowest

energy structure was refined in an explicit water environment. A Ramachandran plot was generated by PROCHECK-NMR[60] and structure quality was assessed by MolProbity.[70]

Fluorescence Polarization Assays: Fluorescein-labeled peptides (100 nM; ChinaPeptides) were titrated with increasing concentrations of purified Ca_2/CaM_{12} in FP buffer (20 mM Tris, pH 7.4, 100 mM KCl, 1 mM $MgCl_2$, 1.0 mM $CaCl_2$) or apoCaM in Ca^{2+}-free buffer (20 mM Tris, pH 7.4, 100 mM KCl, 1 mM $MgCl_2$, 2.0 mM EGTA). FP was measured with a Synergy 2 plate reader (BioTek) as described.[71] FP was calculated as $P = (I_v - g*I_h)/(I_v + g*I_h)$; I_v and I_h are vertical and horizontal fluorescence intensity, respectively, and g is the correction factor for fluorescein. To obtain binding curves and K_D values, data were fitted in GraphPad Prism 5 (GraphPad Software Inc) to the equation $Y = B*X/(K_d + X)$; B is maximal FP value that would be reached at saturation as determined by extrapolation of the fitted curve.

Concentration profiles of CaM species versus [Ca^{2+}]: The concentration profiles of apoCaM-IQ, Ca2/CaM-IQ, and Ca4/CaM-IQ as a function of the free Ca^{2+} concentration werecalculated according to the following scheme in **Figure 2.8.2**.

$$apoCaM - IQ + 2Ca^{2+} \xrightarrow{K_1=10^{14}\ M^{-2}} Ca_2/CaM - IQ$$

$$Ca_2/CaM - IQ + 2Ca^{2+} \xrightarrow{K_2=10^{12}\ M^{-2}} Ca_4/CaM - IQ$$

$$where\ K_1 = \frac{[Ca_2/CaM - IQ]}{[apoCaM - IQ][Ca^{2+}]^2} = 10^{14}\ M^{-2}\ \&\ K_2 = \frac{[Ca_4/CaM - IQ]}{[Ca_2/CaM - IQ][Ca^{2+}]^2} = 10^{12}\ M^{-2}$$

Figure 2.8.2 Kinetic scheme for sequential binding of Ca^{2+} to the CaM C-lobe (K_1) and CaM N-lobe (K_2).

Expression of $Ca_V1.2$ IQ domain mutants and CaM species in HEK 293T/17 cells: HEK 293T/17 cells (ATCC) were maintained as previously described.[43,72] For electrophysiology, Lipofectamine 2000 (Invitrogene) or JetPrime (Polyplus Transfection) was used to transiently transfect cells with indicated plasmid DNAs in 35 mm dishes. For biochemistry experiments, transient transfection of HEK 293T/17 cells in 100 mM dishes was achieved using either JetPrime or, as previously described,[43,72] the calcium phosphate method. Cells were cotransfected with plasmids encoding the pore-forming $\alpha_1$1.2 subunit N-terminally tagged with eCFP[43,72] or mCherry[73]plus pGWIH-based plasmids encoding the auxiliary subunits rat β2A[74] and rabbit α2δ-1[75] as previously described.[43,72] For all transfections, equimolar ratio of 1:1:1 was used for $Ca_V1.2$ channel subunits and later further optimized (JetPrime) for CaM (at ratio of 1:1:1:0.5 for α11.2:β2A:α2δ−1:CaM). Rat brain α11.2 (GenBank ID: M67515.1) N-terminally fused to eCFP was utilized as previously described.[43] The point mutations in plasmids encoding single-residue I1654A, Y1657D (this report), and K1662E exchanges in α11.2 were generated via QuikChange II as previously described using N-terminally eCFP[43,72] or mCherry tagged[73] rat brain α11.2 plasmid template DNAs. We studied CDI using mCherry-tagged α11.2 subunit coexpressed with the other, untagged $Ca_V1.2$ subunits and WT CaM or the calmodulin mutant CaM[34] (kindly provided by JP Adelman)[41]. For some biochemical experiments shown in Fig. S2, YFP-tagged CaM was used.[76]

Whole-cell patch clamp recording: Macroscopic Ba^{2+}-(I_{Ba}) and Ca^{2+} currents (I_{Ca})of $Ca_V1.2$ L-type Ca^{2+} channels were obtained in the whole-cell configuration using external bath solution containing 134 mM N-methyl-D-glucamine, 10 mM $BaCl_2$ (for CDI, 10 mM $CaCl_2$), 1 mM $MgCl_2$, 10 mM Hepes, and 10 mM glucose with an adjusted pH of 7.4 (Cs-OH) and an

osmolarity of 300 to 310 mOsm (sucrose). Intracellular pipette solution contained (in mM) 125 $CsMeSO_3$, 5 CsCl, 10 EGTA, 10 Hepes, 1 $MgCl_2$, 4 Mg-ATP, and pH 7.3 (CsOH), mOsm 290 to 300 (sucrose). Cells were clamped at a holding potential of -80 mV and depolarized for 900 ms to a series of activating potentials, from −60 mV to +50 mV (or +80 mV for Ca^{2+} currents), in increments of 10 mV at an interval of 0.033 Hz. The series resistance and the cell capacitance were directly taken from the Amplifier (Axopatch 200B, Molecular Device) and compensated to ~40%. Data were sampled at 10 kHz and lowpass filtered at 2 kHz. Leak subtracted raw data were analyzed with Pclamp10 and GraphPad Prism IX software. All recordings were performed at room temperature (RT).

Cell-attached patch clamp recording: Single-channel recordings were performed as described previously.[43,77] In brief, low noise raw data were recorded with an Axopatch 200B amplifier and data were sampled at 10 kHz with a low-pass filter at 2 kHz (3 dB, four pole Bessel) and digitalized with a Digidata 1440 digitizer. Recording electrodes were pulled from borosilicate capillary glass (0.86 OD/1.25 ID) with a Flaming/Brown micropipette puller (Model P-97, Sutter Instruments), heat polished, and coated with Sylgard (Sylgard 289) until close to the electrode tip. Electrode resistance in solution was usually 5 to 10 MΩ.To keep the membrane potential close to 0 mV the extracellular bath solution contained 120 mM K-Glutamate, 25 mM KCl, 2 mM $MgCl_2$, 1 mM $CaCl_2$, 10 mM EGTA, 10 mM Hepes, and 2 mM Na_2-ATP pH 7.4 (KOH). The intracellular pipette solution contained (in mM) 110 $BaCl_2$ and 10 Hepes, adjusted to pH 7.4 (TEA-OH). Cells were depolarized for 2 s from a holding potential of -80 mV to 0 mV every 7 s. Event lists were created from raw Ba^{2+} currents after leak and capacity transients were digitally subtracted by pClamp 10. Unitary current events were then analyzed based on the half-height criterium[78] using the single-channel software provided by pClamp 10. For statistical analysis, single-channel

parameters were corrected by the channel number (k), respectively, the maximum of simultaneously open channels (PMAX). The number of channels in the patch was estimated based on the observed simultaneous openings and is a precise parameter for $k < 4$, as included in this article and originally described by R. Horn.[79] On average, 100 to 200 Ba^{2+} current traces were recorded for each cell for each experimental condition for an appropriate statistical analysis.

Surface biotinylation, NeutrAvidin pull downs, and immunoblotting: Surface biotinylation and analysis of $Ca_V1.2$ surface expression was carried out essentially as previously described[43,72] with the following modifications. Twenty-two to twenty-four hours post transfection, HEK 293T/17 cells plated in 100 mm diameter dishes were rinsed with RT PBS-CM (PBS supplemented with 1 mM Ca^{2+} and 0.5 mM Mg^{2+}) and placed on ice. Cell were incubated with freshly prepared 0.4 mg/ml of EZ-Link-Sulfo-NHS-LC-biotin (Thermo Fisher Scientific) in PBS-CM for 30 min, followed by quenching of remaining NHS reactive groups with ice-cold 100 mM glycine in PBS-CM, four separate washes with quenching buffer, and a final rinse with PBS alone. Labeled and quenched cells were dislodged by scrapping and directly lysed into ice-cold radioimmunoprecipitation assay buffer (50 mM Tris-HCl, pH 7.4, 150 mM NaCl, 5 mM EGTA, 10 mM EDTA, 1% NP−40, 0.05% SDS, 0.4% DOC, and 10% glycerol) supplemented with protease inhibitors: 1 μg/ml leupeptin (Merck Millipore), 2 μg/ml aprotinin (Merck Millipore), 1 μg/ml pepstatin A (Merck Millipore), and 34 μg/ml PMSF (Sigma). Lysates were cleared of insoluble material via centrifugation at 200,000g for 30 min at 4º C. The protein concentration of the solubilized material in the cleared lysate was determined by a standard bicinchoninic acid assay (Thermo Fisher Scientific). Biotinylated constituents in equal amount protein lysates (e.g., 400 μg/sample) were affinity purified by incubation with 30 μl of NeutrAvidin-conjugated Sepharose beads (Thermo Fisher Scientific) for 2 h at 4º C. Bead-bound material was sedimented by

centrifugation, washed several times with ice-cold buffer, and bound proteins extracted in SDS sample buffer (with shaking at 65º C for 15 min). Proteins from pull downs as well as directly loaded lysates were fractionated by 7.5% acrylamide SDS–PAGE and transferred onto polyvinylidene difluoride (PVDF; Bio-Rad) membranes. For experiments used for analysis of CaM expression levels in directly loaded lysates, 12% acrylamide gels were used. PVDF membranes were stained with Ponceau S, imaged, washed, and then incubated in blocking buffer (150 mM NaCl, 10 mM Tris–HCl, pH 7.4 (TBS) with 0.1% Tween (TBST) and 2% bovine serum albumin (RPI Corp.)) for 1 h at RT and then incubated with primary antibodies in blocking buffer for 3 h at RT. For analysis of surface expressed $Ca_V1.2$, α11.2 was detected using rabbit antibodies against epitopes in the intracellular loop II/III (FP1 or CNC1) and the CNC2 epitope near the C terminus of α11.2.[80] When CaM expression in directly loaded lysates was assessed, the membranes were probed with a mouse anti-CaM monoclonal primary antibody (made against a synthetic peptide corresponding to the 21 carboxy terminal amino acids (128–148) of bovine calmodulin) obtained from from Sigma Millipore (catalog no.: # 05-173, Lot # 2717626). YFP-tagged CaM signals were further verified by the NeuroMab mouse anti-GFP monoclonal antibody N86/8 (UC Davis). Signals obtained from probing with antibodies against the cytosolic proteins GAPDH (mouse monoclonal, Sigma/Millipore 214592) and α-tubulin (DM1A mouse monoclonal, Santa Cruz Biotechnology SC32293) were used (along with Ponceau S-stained bands) as loading controls for correction of variation in protein content between lysate samples. The absence of GAPDH and α-tubulin antibody signals in NeutrAvidin-pull down samples also served as intracellular protein controls for assurance of plasma membrane integrity during the biotinylation of plated cells. PVDF membranes were washed for 40 min with at least five exchanges of TBST, incubated with horseradish peroxidase–conjugated secondary goat antimouse antibodies (Jackson)

or mouse anti-rabbit antibodies (Jackson) for 1 h at RT, and washed again with TBST with at least five exchanges for 1.5 h. Immunosignals were detected using the horseradish peroxidase substrates Luminata Classico or Crescendo (Merck Millipore) or Femto (Thermo Fisher Scientific) by X-ray film (Denville Scientific Inc). Multiple exposures over increasing time periods were taken to ensure that all signals were in the linear range.[81,82]

Analysis of immunoblots: Signal intensity for each band in scanned film images of immunoblots were assessed using ImageJ (https://imagej.nih.gov). Background signals in individual lanes were subtracted from the band signal prior to quantitative analysis. Differences in immunosignal strengths were corrected for potential immunoblotting and film exposures differences between experiments, as described.[43,72] Loading control (e.g., GAPDH, α-tubulin) lysate immunosignals were used to correct for minor differences in protein amounts loaded in individual sample lanes. To correct for variation in test immunosignals (e.g., α11.2, CaM) between experimental replicates, normalization was done according to the 'sum of the replicates' method as described.[83] Each immunosignal for a protein (e.g., α11.2, CaM) on one blot was divided by the sum of all immunosignals from the same immunoblot exposure for that experimental run to obtain the relative signal fraction for each band.[83] The means of these signal intensity fractions were calculated for each condition (e.g., α11.2 WT, Y1657D) from all experiments (e.g., α11.2 WT, Y1657D) and these means then divided by the mean value of the test control (e.g., α11.2 WT, which is now equal to 1% or 100%). All data were statistically analyzed (GraphPad Prism IX software) applying either a Student's t test (two-sample comparison) or ANOVA with Tukey post hoc test.

Chapter 3

Structural Insights into $Ca_V1.2$ Channel Activation by CaBP1

3.0 CaBP1 is a Homolog of CaM that Activates $Ca_V1.2$

Calcium binding protein 1 (CaBP1), an 18.7 kDa homolog of CaM, belongs to a family of neuronal Ca^{2+} sensors (CaBP1-5)[84] that regulate a variety of Ca^{2+} channel targets. Multiple splice-variants and various isoforms of CaBPs have been identified and localized in different retinal and neuronal cell types.[85] The abundance and multiplicity of CaBPs in the central nervous system first suggested a role in signal transduction. Indeed, CaBP1, also termed caldendrin,[86] has been shown to modulate the Ca^{2+}-sensitive activity of L-type channel,[31] inositol 1,4,5-trisphosphate receptors,[87,88] and the transient receptor potential channel, TRPC5.[32] My particular focus is to understand how CaBP1 regulates $Ca_V1.2$ channel function. CaBP1 has been shown to abolish CDI in $Ca_V1.2$[9], perhaps by blocking $Ca_V1.2$ binding to CaM.[35,36] CaBP1 also mediates the Ca^{2+}-dependent activation of $Ca_V1.2$ channel activity, in a process known as Ca^{2+}-dependent facilitation (CDF).[9] The goal of this chapter is to determine the atomic-resolution structure of CaBP1 bound to the IQ-motif from $Ca_V1.2$ to help elucidate how CaBP1 activates $Ca_V1.2$ channel activity.

3.1 Structural comparison of CaBP1 and CaM

CaBP1 shares 56% sequence homology with CaM and the two proteins have nearly identical secondary structure (**Fig. 1.3.1A**). Both proteins have two independently folded lobes connected by an interdomain linker, and each of these lobes contains two EF-hand motifs (**Fig. 3.1.2**). EF1 and EF2 form the N-lobe, whereas EF3 and EF4 form the C-lobe. CaM and CaBP1 are proposed to competitively bind to the IQ domain in $Ca_V1.2$ and mutations to the IQ disrupt binding of both proteins.[9,89] In CaM, all four EF-hands bind Ca^{2+} under physiological conditions.[16] By contrast, CaBP1 only binds to Ca^{2+} with high affinity in the C-lobe at EF3 and EF4 (called Ca_2/CaBP1),[9,33] which constitutively mimics half-calcified CaM (Ca_2/CaM). CaBP1 does not bind to Ca^{2+} at physiological levels at EF1 and EF2 because the conserved Glu at the 12-position of these EF-hand loops is mutated to Asp (**Fig. 1.3.1A**). Also, the conserved Asp at the 5-position in EF2 is mutated to Gly. Ca^{2+}-binding to the C-lobe is essential for the functions of both CaBP1 and CaM.[90] A key structural difference between CaBP1 and CaM is the length of the interdomain linker, which is 4 residues longer in CaBP1 (**Fig. 1.3.1 A**). As a result, CaBP1 forms a partial helix in the linker region near the C-lobe, which is stabilized by hydrophobic contacts between I99 of the partial helix and L104 of the CaBP1 C-lobe. The less flexible CaBP1 linker means the two lobes of CaBP1 are less independent than what is seen with CaM. Removal of the N-lobe of CaBP1 results in a 40-fold weaker affinity for the channel, suggesting that the N-lobe may participate in $Ca_V1.2$ IQ domain binding.[9]

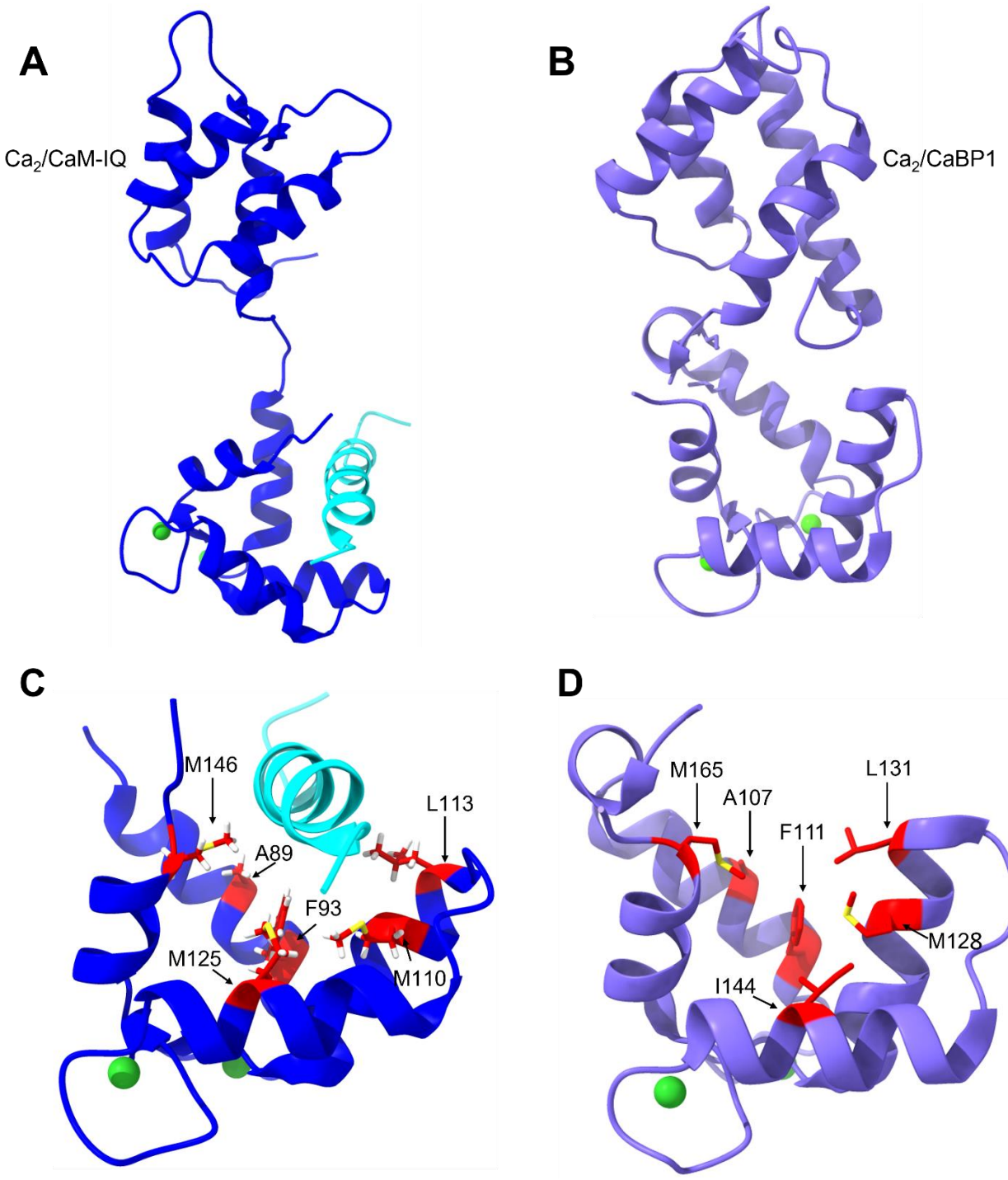

Figure 3.1.2 A *Full Ca_2/CaM_{12}-IQ NMR structure (PDB: 7L8V) showing the longer flexible linker region. The IQ motif is shown in cyan.* **B** *Full Ca_2/CaBP1 crystal structure (PDB: 3OX6) showing shorter linker region and closer relative orientation of CaBP1 lobes.* **C** *Ca_2/CaM_{12}-IQ C-lobe structure with CaM residues important for binding highlighted in red. The IQ motif is shown in cyan.* **D** *Ca_2/CaBP1 C-lobe structure with CaBP1 residues important for binding highlighted in red.*

Comparing the crystal structure of CaBP1 (**Fig. 3.1.2A**) to the NMR structure of the Ca_2/CaM_{12}-IQ complex (**Fig. 3.1.2B**), both structures have a Ca^{2+}-free N-lobe in a closed conformation and a Ca^{2+}-bound C-lobe in the familiar Ca^{2+}-bound open conformation.[18] The open conformation of the Ca_2/CaM C-lobe exposes a pocket of hydrophobic residues that contact the IQ helix (**Figs. 3.1.2 C-D**). The NMR structure of the Ca_2/CaM_{12}-IQ complex indicates that hydrophobic CaM residues (A89, F93, V109, M110, L113, M125, and M146) compose the interaction surface for CaM binding to the $Ca_V1.2$ channel IQ domain. The corresponding residues in the crystal structure of CaBP1[9] form a highly conserved binding surface composed of residues A107, F111, M125, L131, I144, and M165 that may provide hydrophobic contacts for binding to the IQ (**Fig. 3.1.2 D**).

Aromatic IQ-motif residues F1658 and F1661 have been shown to be important for IQ binding to CaBP1.[9] These same residues make significant contact with hydrophobic resides in the CaM_{12} C-lobe seen in the NMR structure of the Ca_2/CaM_{12}-IQ complex (**Fig. 3.1.2**), suggesting that the IQ helix may bind to both CaM and CaBP1 in a similar fashion. However, the location of the CaBP1 N-lobe in the crystal structure sterically blocks the binding of the IQ helix to the C-lobe, in which many CaBP1 N-lobe residues (including R17 and E94) clash with the bound IQ helix. The CaBP1 interdomain linker region is conformationally quite different in the CaBP1 crystal structure[9] versus the NMR solution structures[88], which suggests that the interdomain linker is conformationally flexible and capable of adopting various inter-lobe orientations that could cause the CaBP1 N-lobe to move away from the C-lobe to allow high affinity IQ binding to the C-lobe.

3.2 IQ Binding to CaBP1 Enhances Its Ca^{2+} binding Affinity

The Ca^{2+}-bound CaBP1 was shown previously to bind to the $Ca_V1.2$ IQ peptide in the nanomolar range, in contrast to Ca^{2+}-free CaBP1 that binds to the IQ with micromolar affinity.[36] The 100-fold higher affinity IQ binding to Ca^{2+}-bound CaBP1 (relative to Ca^{2+}-free CaBP1) implies that CaBP1-IQ should bind to Ca^{2+} with 100-fold higher affinity compared to that of free CaBP1 (K_d = 2.5 μM).[33] In other words, the binding of the IQ peptide to CaBP1 should enhance its Ca^{2+}-binding by 100-fold. The apparent dissociation constant (K_D^{app}) for Ca^{2+} binding to CaBP1-IQ can be calculated from previous binding data as follows: $K_D^{app} = \sqrt{\frac{1}{K_1 \times K_2 \times K_3}} = 50 \pm 10\ nM$, where K_1 (10^{12} M^{-2}) describes the binding of two Ca^{2+} to free CaBP1 ($2Ca^{2+} + CaBP1 \xrightarrow{K_1 = 10^{12} M^{-2}} Ca_2/CaBP1$)[33], K_2 (10^8 M^{-1}) describes IQ binding to Ca_2/CaBP1 ($IQ + Ca_2/CaBP1 \xrightarrow{K_2 = 10^8 M^{-1}} Ca_2/CaBP1$)[36], and K_3 (3.8 μM) is the dissociation constant for apoCaBP1-IQ ($CaBP1 - IQ \xrightarrow{K_3 = 4\mu M} CaBP1 + IQ$) (**Fig. 3.2.1**). The calculated Ca^{2+} dissociation constant ($K_D^{app} = 50\ nM$) implies that at least 50% of CaBP1 bound to $Ca_V1.2$ should have 2 Ca^{2+} bound under basal conditions ([Ca^{2+}] = 50-100 nM).[4] To experimentally measure the actual apparent Ca^{2+} binding affinity of CaBP1-IQ, I performed ITC experiments in which increments of Ca^{2+} were added to CaBP1-IQ (**Fig. 3.2.2**). The ITC binding isotherm reveals 2 Ca^{2+} bind to CaBP1-IQ with an apparent Ca^{2+} dissociation constant of 40 ± 5nM that agrees within experimental error with the calculated K_D^{app} value above ($K_D^{app} = 50 \pm 10\ nM$). This result suggests ~50% of CaBP1-IQ would have $2Ca^{2+}$ bound even under basal conditions, similar to that observed above for CaM-IQ in Chapter 2. The existence of Ca^{2+}-bound CaBP1 bound to $Ca_V1.2$ under basal conditions was initially surprising because previous studies suggested that only the Ca^{2+}-free apoCaBP1 is bound to $Ca_V1.2$ under basal conditions.[36] However, the micromolar binding of apoCaBP1 to $Ca_V1.2$ is

too weak to effectively compete with the nanomolar Ca_2/CaM binding to $Ca_V1.2$ that would be needed for CaBP1 to block CDI. It seems more likely that some fraction of Ca_2/CaBP1 must be present under basal conditions to block Ca_2/CaM binding to the channel and prevent CDI.[36]

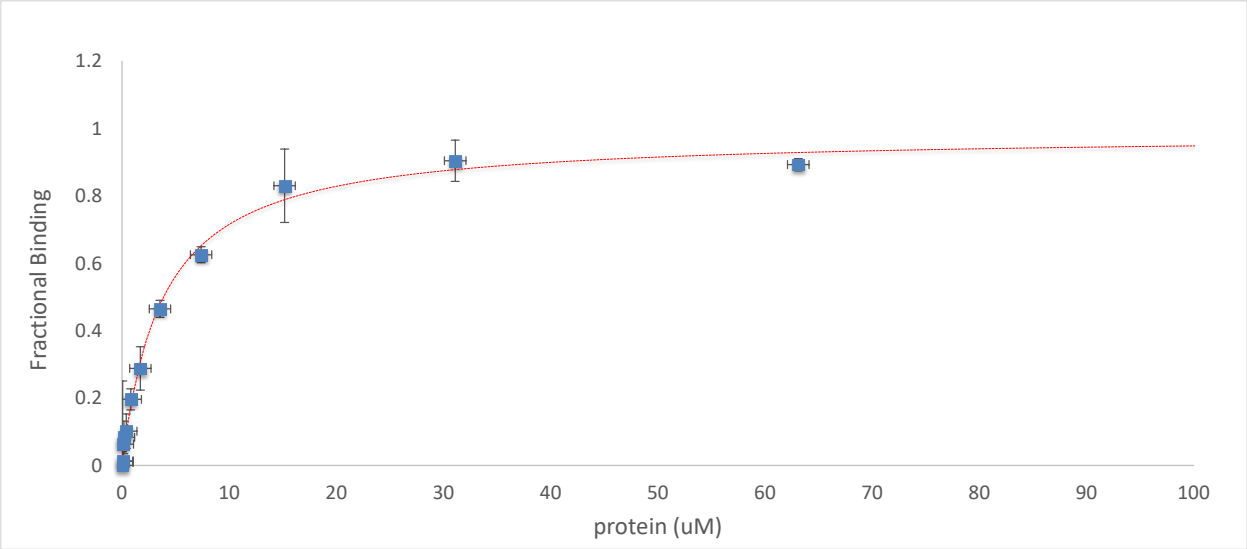

Figure 3.2.1 FP titration of apoCaBP1 binding to fluorescently labeled IQ peptide (Performed by David Anderson and unpublished). The K_d is equal to 3.8 μM.

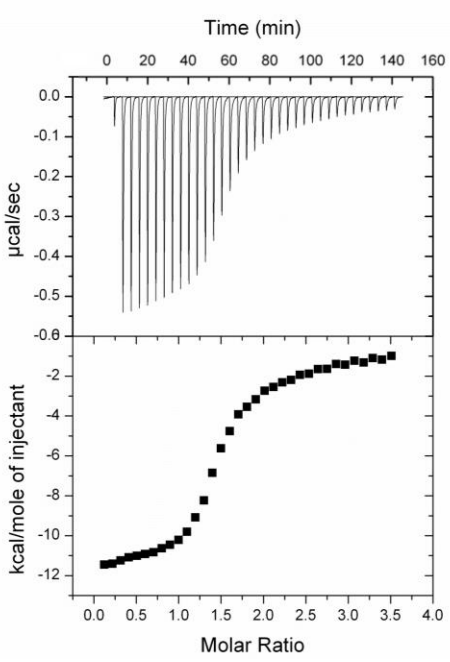

Figure 3.2.2 ITC titration of CaBP1-IQ complex with Ca^{2+} fit to a two-site binding model with a low affinity second Ca^{2+}-binding site representative of CaBP1 EF1 Ca^{2+}-binding.

3.3 Molecular Docking of CaBP1 Binding to IQ using HADDOCK

Before starting NMR structural analysis of CaBP1 bound to the IQ peptide, I first generated a structural model of CaBP1 bound to the IQ helix (based on the known structure of Ca_2/CaM_{12}-IQ) using the HADDOCK 2.4 webserver.[91] HADDOCK (**H**igh **A**mbiguity **D**riven protein-protein **DOCK**ing) is a collection of python scripts from ARIA[92] that uses CNS (Crystallography and NMR System) to calculate the structures of molecular complexes. HADDOCK incorporates experimental data as restraints to guide the docking process, in addition to traditional energetics and shape complementarity. The defining feature of HADDOCK is the use of Ambiguous Interaction Restraints (AIRs). AIRs are residues that have been identified as being important for the interactions using methods such as mutagenesis or NMR chemical shift perturbation and translate this data into distance restraints that are incorporated into the energy function used in calculation. AIRs can define residues as either active or passive. Active residues are of central importance to the binding interaction. These residues will be restrained to be part of the interaction surface throughout the simulation, otherwise incurring a penalty. Solvent accessible residues that are within the 6.5Å of any active residue will be defined as passive residues which will contribute to the interaction surface; however, there is no penalty for a passive residue that is not simulated to be at the interaction surface. Conserved CaBP1 residues M128, L132, I144, and M165 were defined as active residues based on the CaBP1 sequence alignment with CaM (**Fig. 1.3.1**) and the Ca_2/CaM12-IQ NMR structure (**Fig. 2.3.3**). $Ca_V1.2$ IQ residues I1654, Y1657, and F1658 were defined as active residues, because mutation of these residues weakens CaBP1 binding to the IQ peptide (**Table 3.6.1**).

The initial HADDOCK calculation was performed using the crystal structure of CaBP1 (**Fig. 3.3.1A**) docked with the helical IQ peptide structure derived from Ca_2/CaM_{12}-IQ (**Fig. 2.3.3**).

The first stage of the HADDOCK docking simulation randomizes the orientation of the interacting partners (CaBP1 and the IQ peptide). In this stage, both structures are treated as rigid bodies, with all geometrical parameters such as bonds lengths, bond angles, and dihedral angles held constant. The rigid structures are allowed to rotate and translate to optimize the interaction. As previously demonstrated,[9] the position of the CaBP1 N-lobe in the Ca_2/CaBP1 crystal structure prohibits IQ binding to the C-lobe (**Fig. 3.3.1A**). However, the lobes of CaBP1 are expected to adopt a range of inter-lobe orientations. Thus, rotation about the flexible interdomain linker allows the IQ peptide to properly access the CaBP1 binding surface in the C-lobe (**Fig. 3.3.1B**).

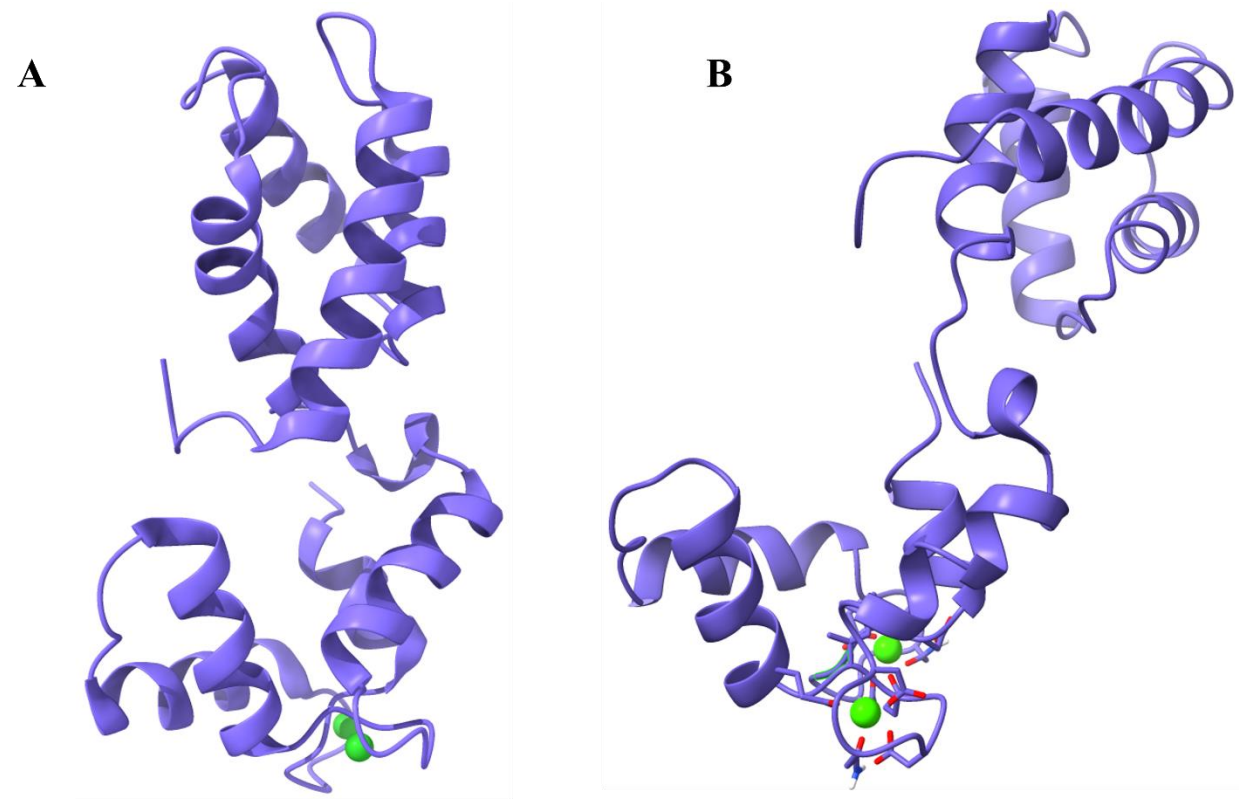

Figure 3.3.1 A *The crystal structure of Ca_2/CaBP1 (PDB: 3OX6).* **B** *The crystal structure of Ca_2/CaBP1 manipulated to allow access to the expected C-lobe binding surface.*

.

HADDOCK then conducts a stage of simulated annealing with the binding partners having freedom in torsion angle space. The bond lengths and bond angles are kept constant at this stage. The orientations are first optimized with rigid bodies. Flexibility is then introduced at the interaction surface which is automatically defined as intermolecular contacts with a 5Å cutoff. Different interaction surfaces defined by unique binding orientations will result in different flexible regions. Backbone and side chains of the flexible region are granted freedom for an additional optimization step.

HADDOCK will then cluster the refined structures based on the Fraction of Common Contacts. The resulting clusters show Ca_2/CaBP1 binding the IQ peptide with two possible

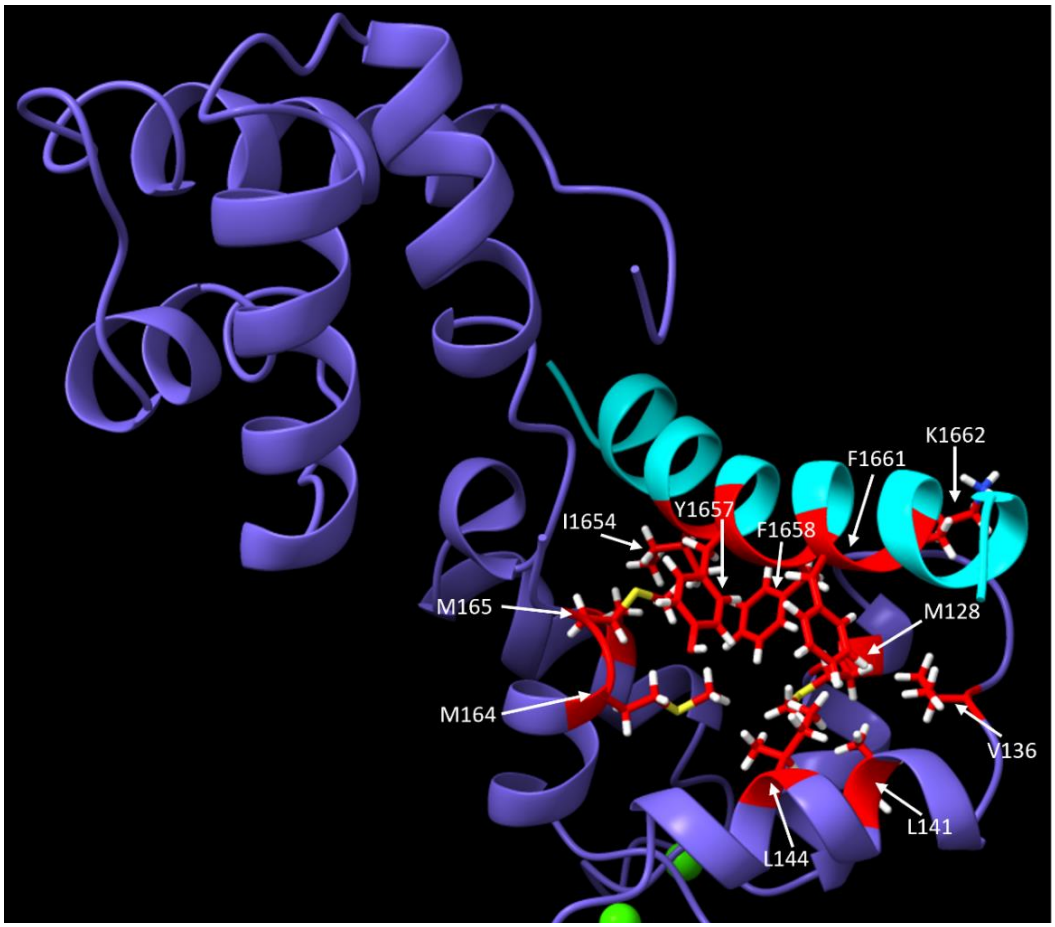

Figure 3.3.2: *The C-lobe of the Ca_2/CaBP1 structure with conserved IQ binding orientation. Key hydrophobic contacts are indicated.*

orientations (**Figs. 3.3.2** & **3.3.3**). In **Fig. 3.3.2**, the orientation of the IQ peptide bound to CaBP1 is the same as that seen in Ca_2/CaM_{12}-IQ (**Fig. 2.3.3**). Many of the hydrophobic contacts of Ca_2/CaM_{12}-IQ structure are conserved in the Ca_2/CaBP1-IQ structure. These include CaBP1 hydrophobic residues M128, L132, I144, and M165 which were designated as active residues. Additional contacts include CaBP1 residues M164, I141, and V136.

Surprisingly, about 50% of the calculated docked structures (**Fig. 3.3.3**) show the bound IQ peptide is rotated 180º degrees relative to the structure in **Fig. 3.3.2**. A key structural feature

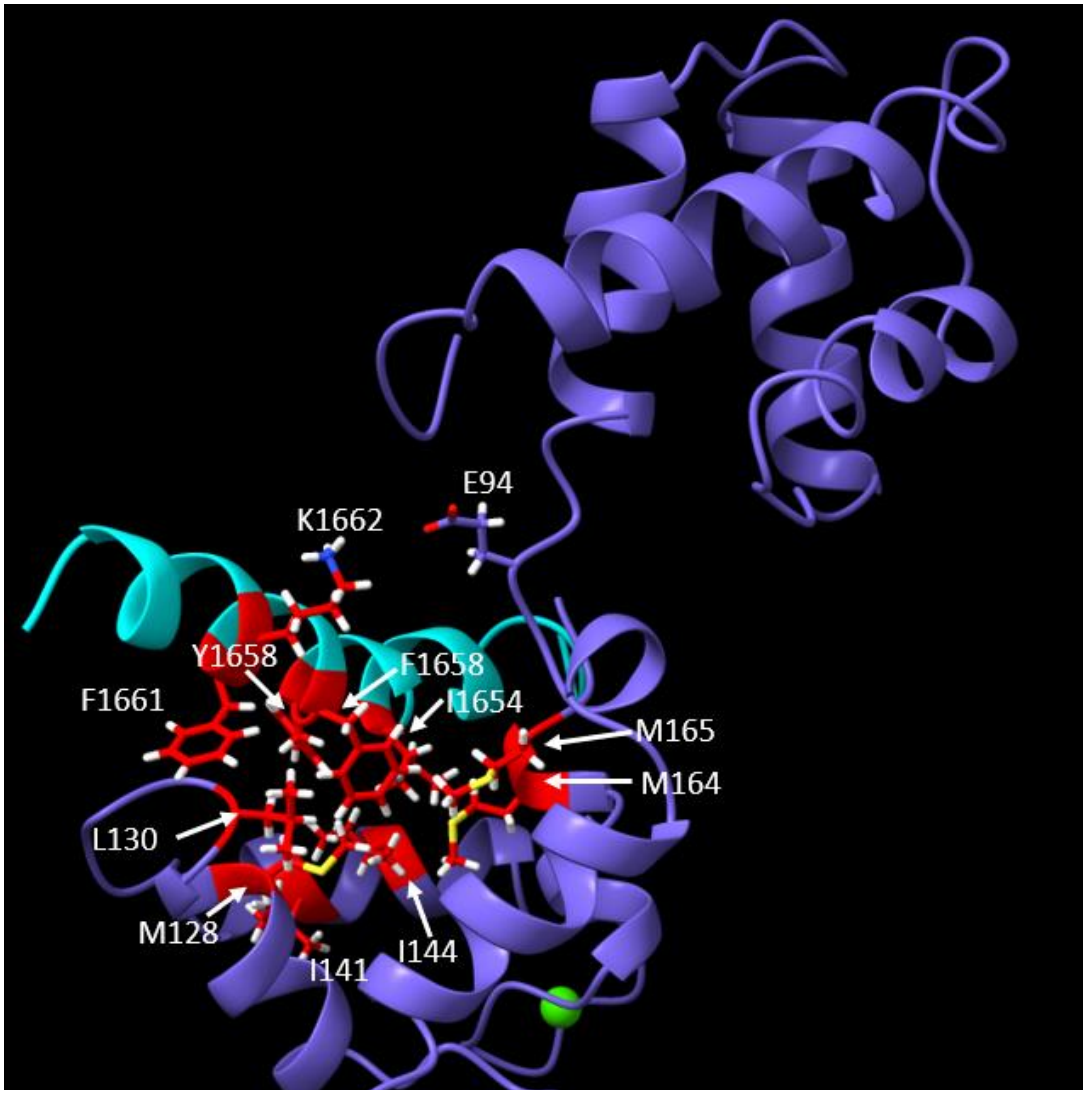

Figure 3.3.3 *The C-lobe of the Ca_2/CaBP1-IQ structure with the 180º IQ peptide rotation. Key contacts, including the K1662/E94 salt bridge, are indicated.*

unique to this opposite binding orientation is the formation of an intermolecular salt bridge between IQ residue K1662 and CaBP1 residue E94. In mutagenesis analysis below (**Section 3.6**), the K1662E mutation causes a 4-fold reduction in binding to CaBP1 (**Table 3.6.1**), consistent with the predicted salt bridge. However, the E94K mutation in CaBP1 has no effect on the binding of the IQ peptide (**Table 3.6.1**), which argues against a salt bridge with K1662. The modeled structure of CaBP1-IQ (**Fig. 3.3.3**) also reveals intermolecular contacts with hydrophobic IQ residues (I1654, Y1657 and F1658) that were observed in Ca_2/CaM_{12}-IQ (**Fig. 2.3.3**).

3.4 NMR Structural Studies of the Ca_2/CaBP1-IQ Complex

The HADDOCK modeling above generates two possible structural models of CaBP1-IQ (**Figs. 3.3.2 & 3.3.3**), but is unable to distinguish between two different IQ binding orientations in which the IQ helix is rotated 180° (**Figs. 3.3.2 & 3.3.3**). In order to determine the correct IQ binding orientation, I performed NMR experiments to probe intermolecular distance restraints between CaBP1 and the bound IQ that can accurately define the correct IQ binding orientation. NMR titrations of ^{15}N-labeled CaBP1 binding to the unlabeled IQ peptide reveal large IQ-induced chemical shift changes for CaBP1 residues in the C-lobe in contrast to no detectable chemical shift change for the N-lobe residues (**Fig. 3.4.3 & 3.4.4**). These NMR chemical shift perturbation data confirm that the IQ peptide is binding to a localized site in the CaBP1 C-lobe and not interacting with the N-lobe. Unfortunately, the solubility of the full-length CaBP1 (200 μM) is not high enough to perform three-dimensional NMR experiments that are needed to make resonance assignments for determining the atomic-resolution structure. Instead, I performed three-dimensional NMR structural analysis on a construct of the CaBP1 C-lobe (residues 99-167) bound to the IQ peptide (called, Ca_2/CaBP1C-IQ) that is much more soluble than the full-length complex and is suitable for three-dimensional NMR. The HSQC spectrum of ^{15}N-labeled CaBP1C bound

to the unlabeled IQ peptide reveals amide chemical shifts of the CaBP1 C-lobe residues that are very similar to those of full-length CaBP1 (**Fig. 3.4.4**). Therefore, the structure of Ca_2/CaBP1C-IQ should accurately mimic the structure of the CaBP1 C-lobe bound to the IQ peptide in the full-length protein.

To solve the NMR structure of Ca_2/CaBP1C-IQ, I first assigned the backbone and side-chain methyl NMR resonances by analyzing triple resonance NMR.[93] These NMR assignments were used to determine NMR structural restraints in the form of NOESY derived interatomic distances.[53] More than 87% of the main chain ^{13}C resonances ($^{13}C\alpha$, $^{13}C\beta$, and ^{13}CO), 85% of backbone amide resonances (^{1}HN, ^{15}N), and 74% of methyl side chain resonances were assigned. These assignments have been deposited in the BMRB (accession number 51518).[93] These backbone amide assignments are shown in **Figure 3.4.1** and the side-chain methyl resonances are shown in **Figure 3.4.2**.

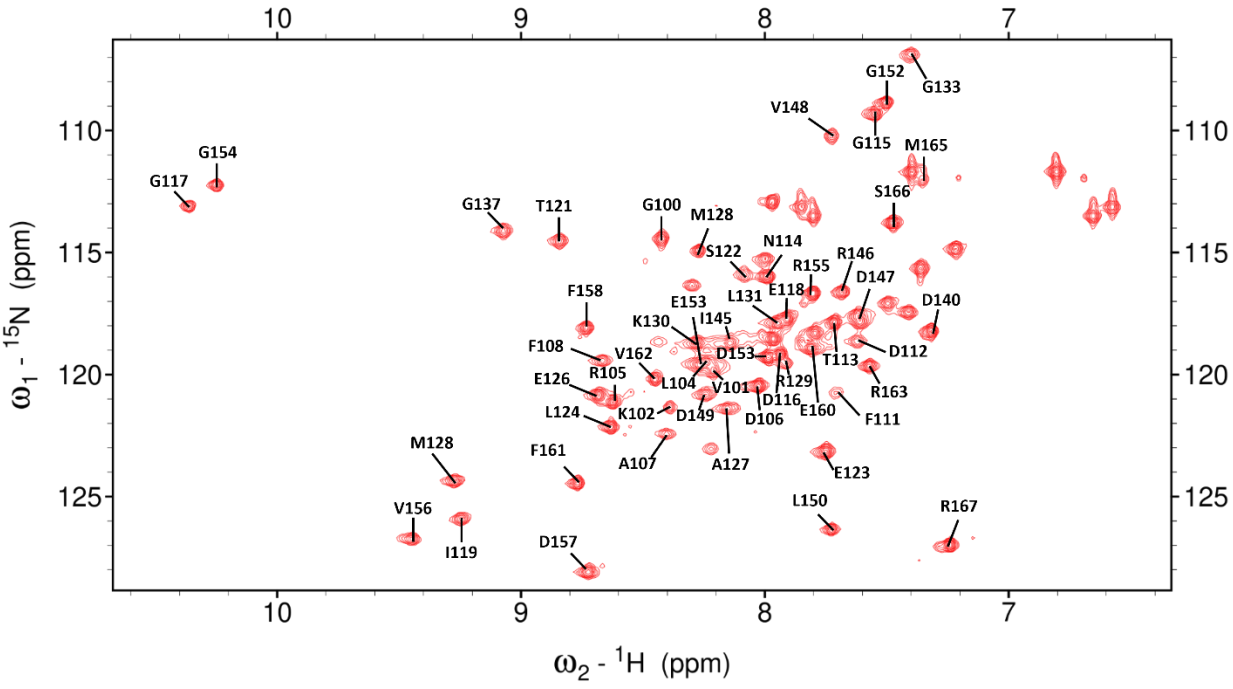

Figure 3.4.1 *^{15}N-HSQC of Ca_2/CaBP1-IQ with backbone amide assignments.*

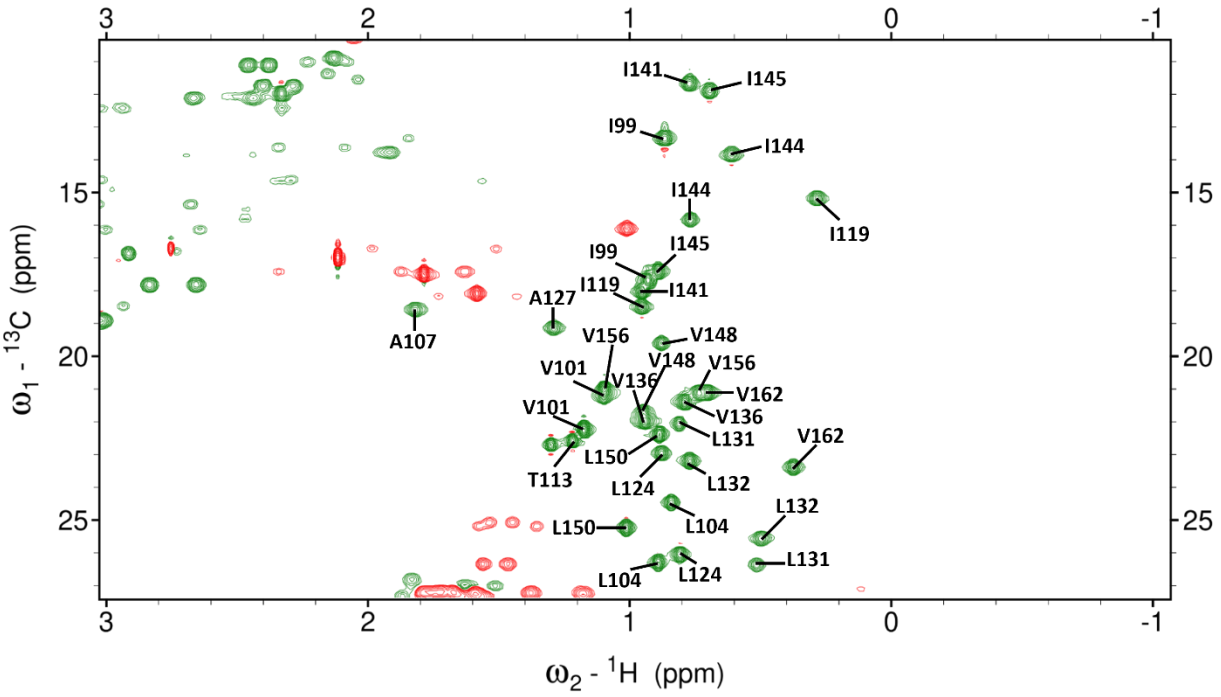

Figure 3.4.2 *Constant-time ^{13}C-HSQC of Ca_2/CaBP1-IQ with side-chain methyl assignments*

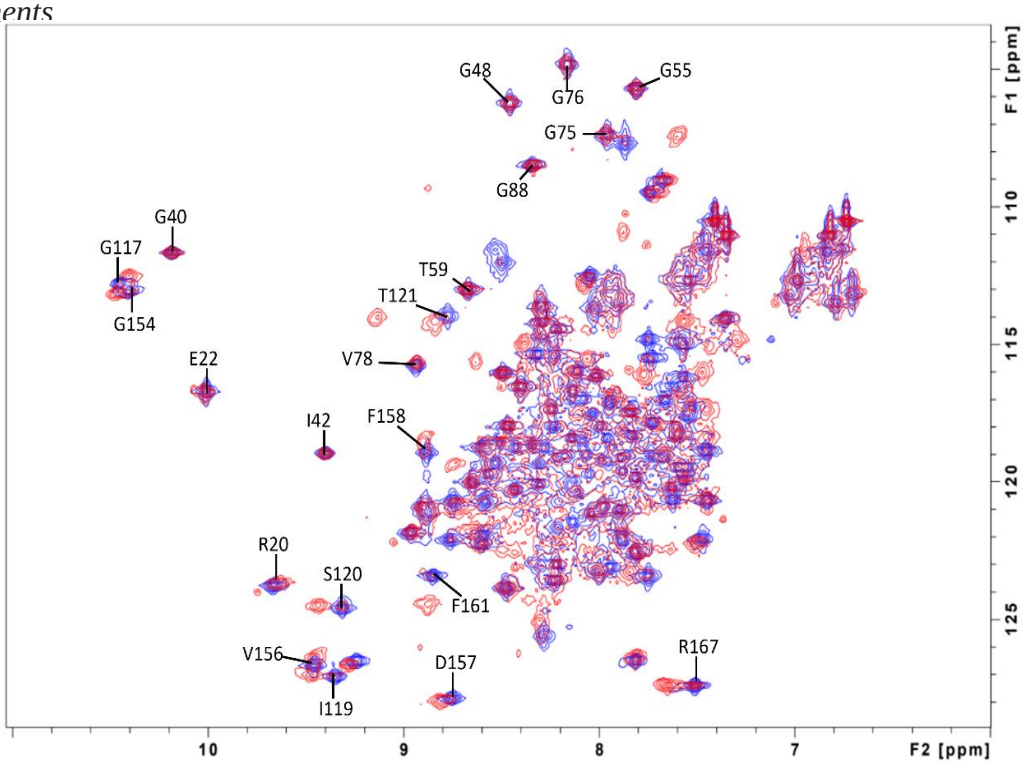

Figure 3.4.3 *^{15}N-HSQC overlay with Ca_2/CaBP1-IQ shown in red and Ca_2/CaBP1 shown in blue. Representative N-lobe residues (residues 15-85) are indicated to show overlapping resonances. Representative C-lobe residues (residues 86-167) are indicated to show perturbed resonances*

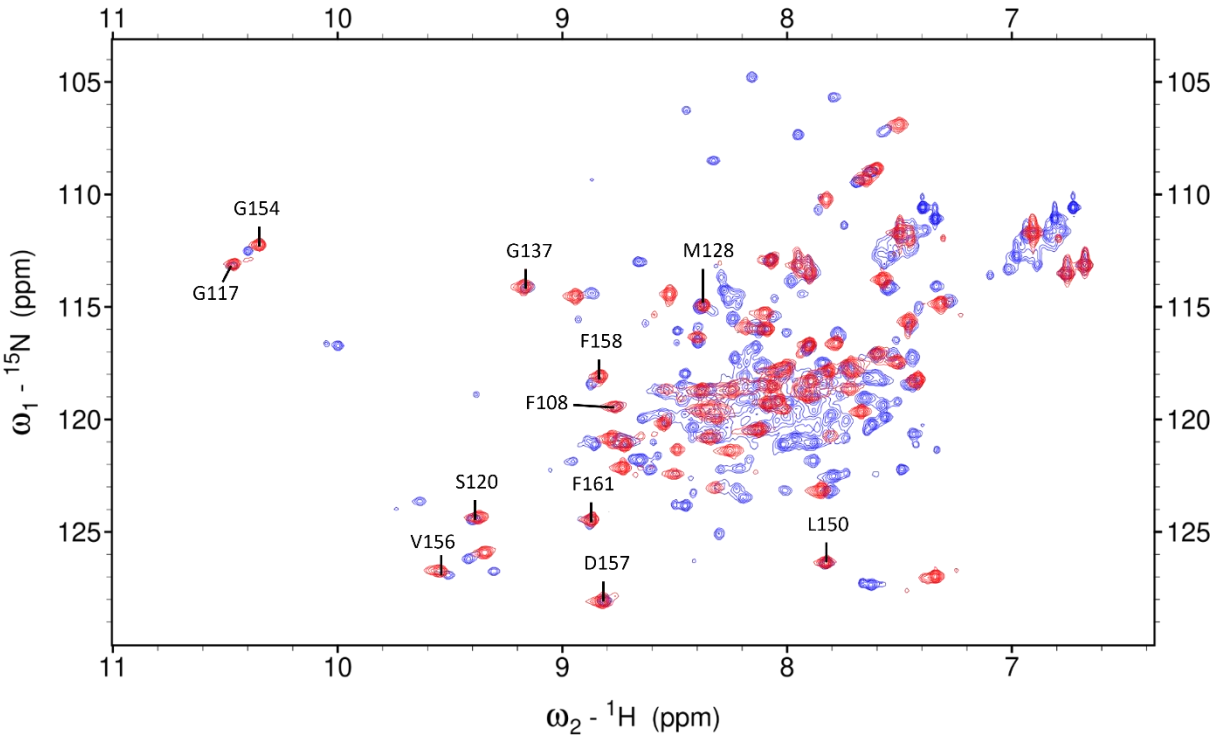

Figure 3.4.4 *^{15}N-HSQC overlay with Ca_2/CaBP1C-IQ shown in red and Ca_2/CaBP1 shown in blue. Representative C-lobe residues (residues 86-167) are indicated to show spectra similarity.*

The backbone and side-chain methyl NMR assignments were used to determine structural restraints (interatomic distances) derived from NOESY spectra (**Fig. 3.4.5**).[53] Intermolecular distance restraints were then used in HADDOCK to increase the accuracy of docking. Representative NOESY data are shown in **Figure 3.4.6**. These intermolecular NOESY crosspeaks represent atoms that are separated by less than 5 Å. CaBP1 residues I144 and V148 both contact IQ residue F1661, towards the C-terminus of the IQ helix. Additionally, CaBP1 residue A107 contacts IQ residue 1654. Visualization of these residues shows clearly (**Figure 3.4.6**) that these NMR restraints are only satisfied when CaBP1 binds to the IQ helix with the same orientation (**Fig. 3.3.2**) as that seen in the structure of Ca_2/CaM_{12}-IQ. This orientation positions CaBP1 residue L132 near IQ residue F1658, which is also detected in the NOESY data. Lastly, this orientation causes K1662 to form a salt bridge with CaBP1 residue D140 (and not E94), which now explains why K1662E causes weaker CaBP1 binding and why CaBP1 mutant E94K has no effect on binding.

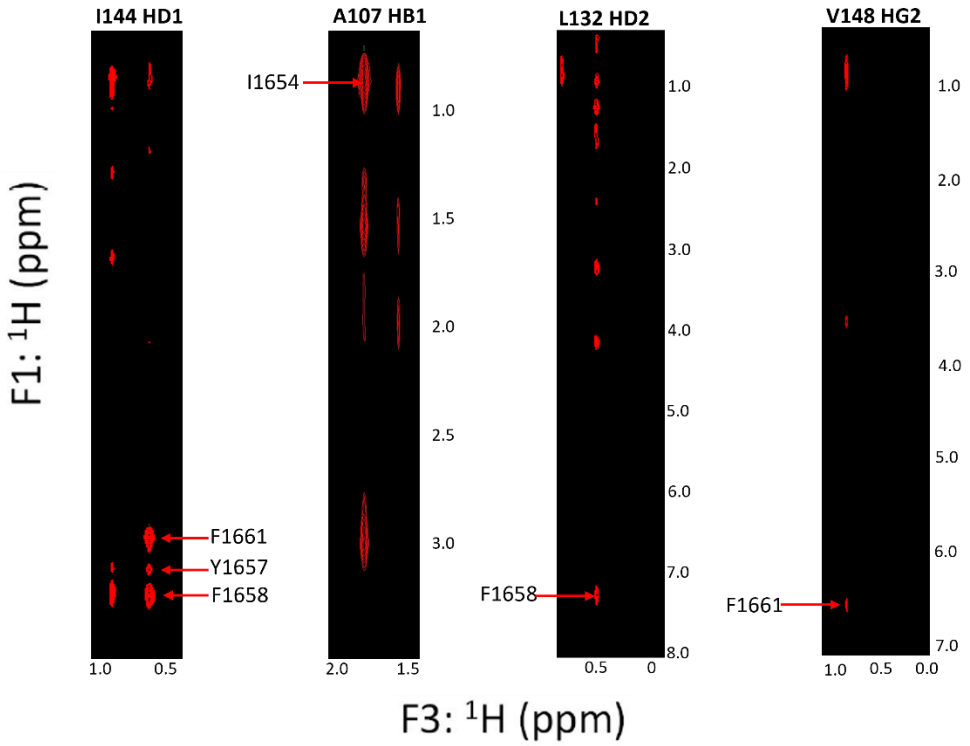

Figure 3.4.5 *Representative ^{13}C-filtered NOESY-HSQC spectra of ^{13}C-labeled Ca_2/CaBP1C bound to unlabeled IQ peptide.*

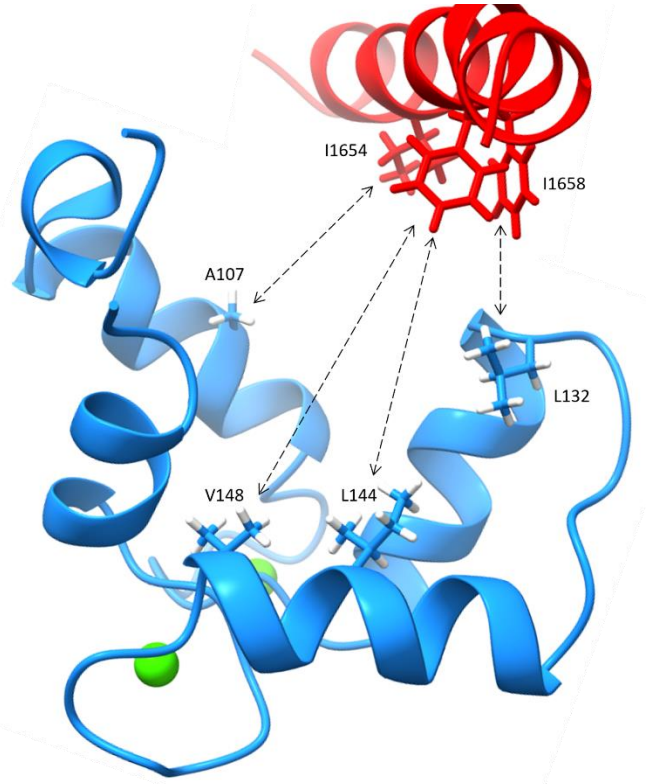

Figure 3.4.6 *Visualization of the intermolecular contacts indicated by NOESY data.*

3.5 NMR Refined HADDOCK Docking Structure Calculation

A total of 19 intermolecular NMR distance restraints (see **Table 3.5.1)** were added to the HADDOCK calculation, and the NMR-derived distance restraints caused the docking calculation to converge conclusively on the IQ-binding orientation (**Fig. 3.5.1**) similar to that seen in the Ca_2/CaM_{12}-IQ structure.[90] The lowest energy cluster included 103 of 200 structures considered for clustering and had a backbone RMSD of 0.9 ± 0.2 Å from the overall lowest-energy structure. **Figure 3.5.1** shows an overlay of the four lowest energy structure of this cluster.

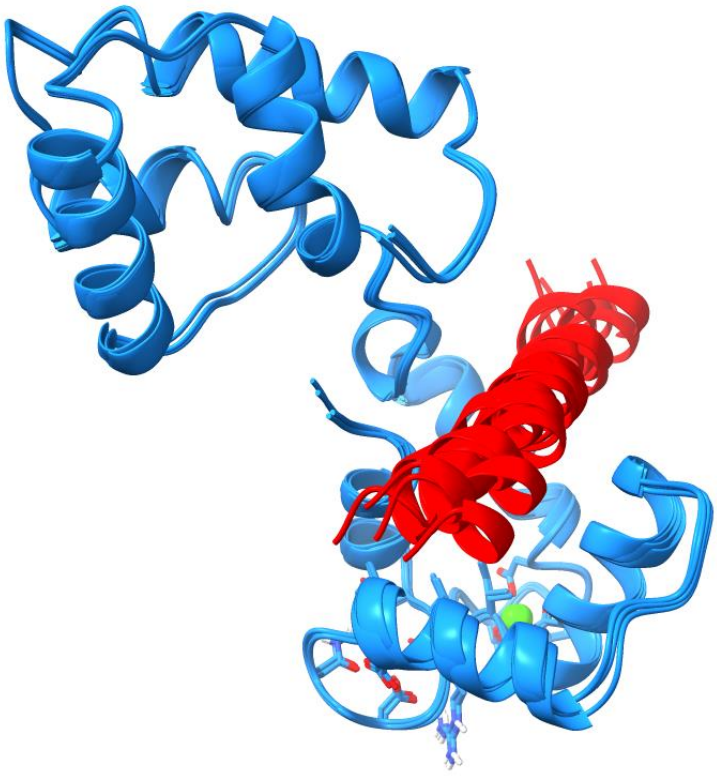

Figure 3.5.1 *Lowest energy HADDOCK docking Ca_2/CaBP1-IQ structure of the top cluster. Ca_2/CaBP1 is shown in blue and the IQ peptide in red.*

Additionally, 46 of the remaining 97 remaining structures considered for clustering formed several smaller clusters (clusters 3, 5, and 6) with similar structure and RMSD. **Figure 3.5.2** shows an overlay of the lowest energy structure of these clusters. The contacts at the center of the

hydrophobic pocket remain largely unperturbed with the additional clusters showing minor rotations of the IQ helix by up to approximately 18º or translational shifts within the pocket up to approximately 4 angstroms. The remaining calculated structures do not exhibit the contacts seen in the NMR structural data and had high relative RMSD from the overall lowest energy structure. This is apparent in the drastically increased restraints violation energy of these clusters. A summary of cluster statistics is shown in **Table 3.5.2.** This includes the HADDOCK score of each cluster, which is a weighted sum of van der Waals, electrostatic, desolvation, and restraint violation energies. This score is calculated at the end of each stage of the calculation and is used to determine which structure will continue to semiflexible annealing and final refinement. The high HADDOCK score of clusters 2 and 4 indicate that the reversed IQ binding orientation (**Fig. 3.3.3**) may be energetically comparable; however, the NMR intermolecular distance restraints are most consistent with the orientation in **Fig. 3.3.2** and inconsistent with the reversed orientation in **Fig. 3.3.3**.

Table 3.5.1
Intermolecular distance pairs

CaBP1 Atom	IQ Peptide Atom
V148HG2	F1661HE
I144HG2	F1661HE
I144HD1	F1661HE
I144HD1	F1658HE
I144HD1	F1658HD
I144HD1	Y1657HE
L132HD2	F1658HD
L132HD2	F1658HE
I99HD1	1657HD
V136HD1	F1658HE
A107HB	I1654HG2
F111HE	I1654HG2
F161HE	I1654HG2
M164HE	F1661HE
M164HE	Y1657HE
M165HE	I1654HD1
M165HE	F1661HE
M165HE	Y1657HE
M128HE	F1658HE

Table 3.5.2
Summary of HADDOCK Cluster Statistics

Cluster	HADDOCK Score	Cluster Size	RMSD From Lowest Energy	Restraints Violation Energy
1	-85.5 ± 1.7	103	0.9 ± 0.2	1.0 ± 0.45
3	-85.3 ± 2.8	20	0.7 ± 0.4	0.7 ± 1.3
2	-85.3 ± 3.5	36	7.2 ± 0.0	91.3 ± 3.04
6	-85.3 ± 4.0	4	1.6 ± 0.1	1.1 ± 0.12
4	-78.7 ± 2.8	18	7.1 ± 0.1	172.8 ± 17.91
5	-67.2 ± 2.6	6	1.4 ± 0.1	1.1 ± 0.36

In addition to intermolecular contacts indicated by NMR, the low restraints violation energies also suggest the formation of a salt bridge between CaBP1 residue D140 and IQ residue K1662. This would explain the decreased affinity of the K1662E mutant. This interaction is shown in **Figure 3.5.3**. Future mutagenesis studies are needed to assess whether the charge reversal mutation (D140K) will weaken CaBP1 binding to the IQ, like what is seen for the K1662E mutant. Also, the D140K mutation should restore CaBP1 binding to the IQ mutant, K1662E.

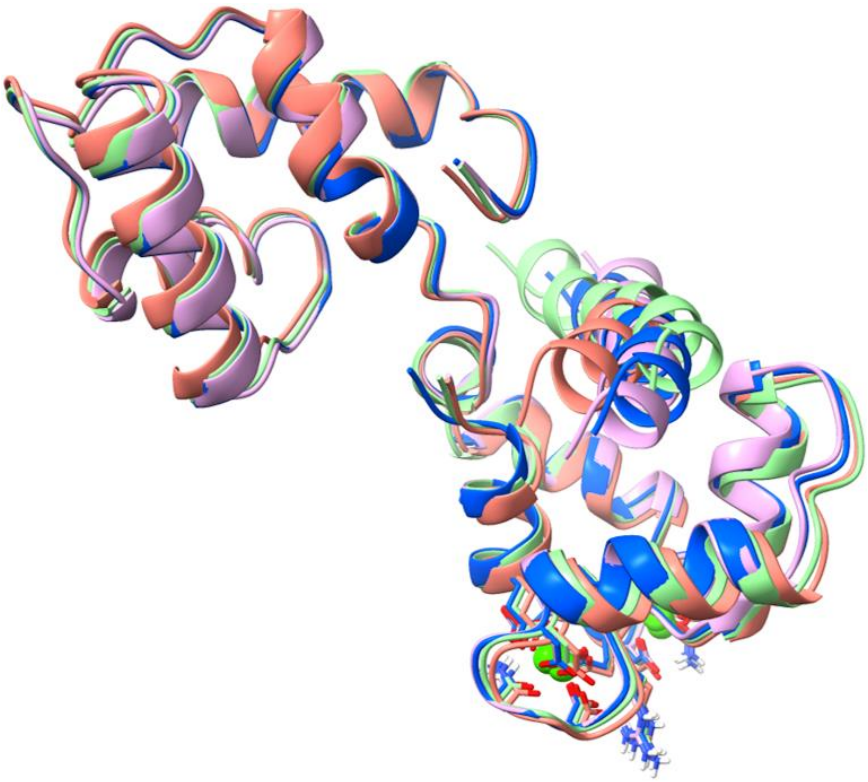

Figure 3.5.2 *Overlay of the lowest energy structures of clusters with the IQ binding orientation similar to the overall lowest energy cluster. The lowest energy cluster 1 is shown in blue, cluster 3 (pink), cluster 5 (peach), and cluster 6 (light green).*

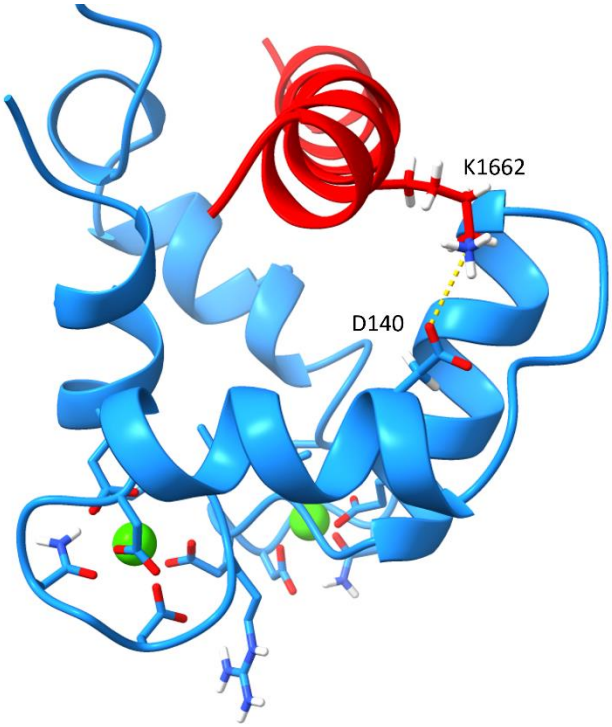

Figure 3.5.3 *Visualization of the D140 ←→ K1662 salt bridge.*

3.6 Mutational Analysis of Binding Contacts in Ca_2/CaBP1-IQ

IQ residues I1654, Y1657, and F1658 in the NMR structure of CaBP1-IQ (Fig. 3.2.2) were identified as key contact points for IQ binding to both CaM and CaBP1.[90] If the IQ binding surface is conserved between the Ca_2/CaM and the Ca_2/CaBP1, then mutation of the interfacial residues (I1654A, Y1657D, and F1658D) should weaken IQ binding to CaBP1 as was seen previously for CaM-IQ.[44,90] The binding Ca_2/CaBP1 to the IQ mutants I1654A, Y1657D, and F1658D were measured using ITC at 27º C. The results of the ITC experiments are shown in **Figure 3.6.1** and are summarized in **Table 3.6.1**.

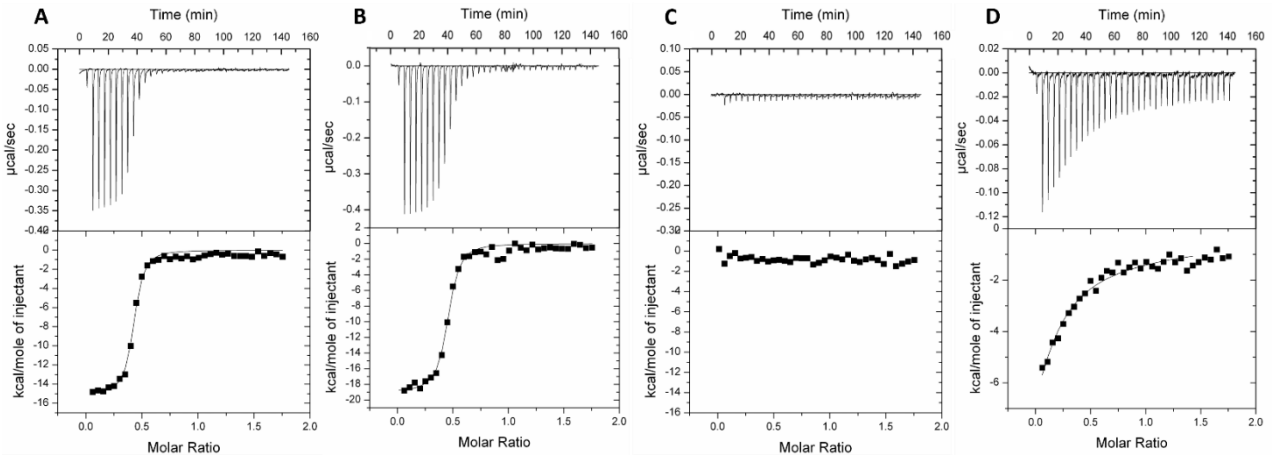

Figure 3.6.1 A-D *ITC measurement at 27ºC of Ca_2/CaBP1 binding to (**A**) IQ^{WT}, (**B**) IQ^{I1654A}, (**C**) IQ^{Y1657D}, and (**D**) IQ^{F1658D}.*

Table 3.6.1
Summary of Ca_2/CaBP1-IQ mutant binding affinities by ITC

Ca_2/CaBP1-IQ Mutant	K_D (nM)
Ca_2/CaBP1-IQ WT	45 ± 9
Ca_2/CaBP1-IQ^{I1654A}	65 ± 10
Ca_2/CaBP1-IQ^{Y1657D}	N/A
Ca_2/CaBP1-IQ^{F1658D}	2300 ± 20
Ca_2/CaBP1-IQ^{K1662E}	200 ± 20
Ca_2/CaBP1^{E94K}-IQ	35 ± 5
Ca_2/CaBP1^{I144E}-IQ	500 ± 40

As expected, the ITC results for CaBP1 binding to the IQ mutants are similar to what was seen with Ca_2/CaM_{12}-IQ binding. The I1654A IQ mutation caused a 30% reduction in Ca_2/CaBP1 binding affinity (K_D^{WT} = 45 ± 9 nM vs K_D^{I1654A} = 65 ± 10 nM). The F1658D IQ mutation caused a more than 50-fold reduction in Ca_2/CaBP1 binding affinity (K_D^{WT} = 45 ± 9 nM vs K_D^{F1658D} = 2300 ± 20 nM). And the Y1657D IQ mutation reducing Ca_2/CaBP1 binding beyond the detectable range. These results together demonstrate the conserved IQ residues (I1654, Y1657 and F1658) serve as hydrophobic anchors that are essential for binding to CaBP1. The NMR structure of Ca_2/CaBP1-IQ also identified residues of CaBP1 at the binding interface. The CaBP1 residue, I144 contacts IQ residues F1657, F1658, and F1661, and CaBP1 residue E94 is predicted to form an intermolecular salt bridge with K1662 in the structure with the reversed IQ binding orientation (**Fig. 3.3.3**). The ITC binding experiments of each mutant are shown in **Figure 3.6.2** and summarized in **Table 3.6.1**.

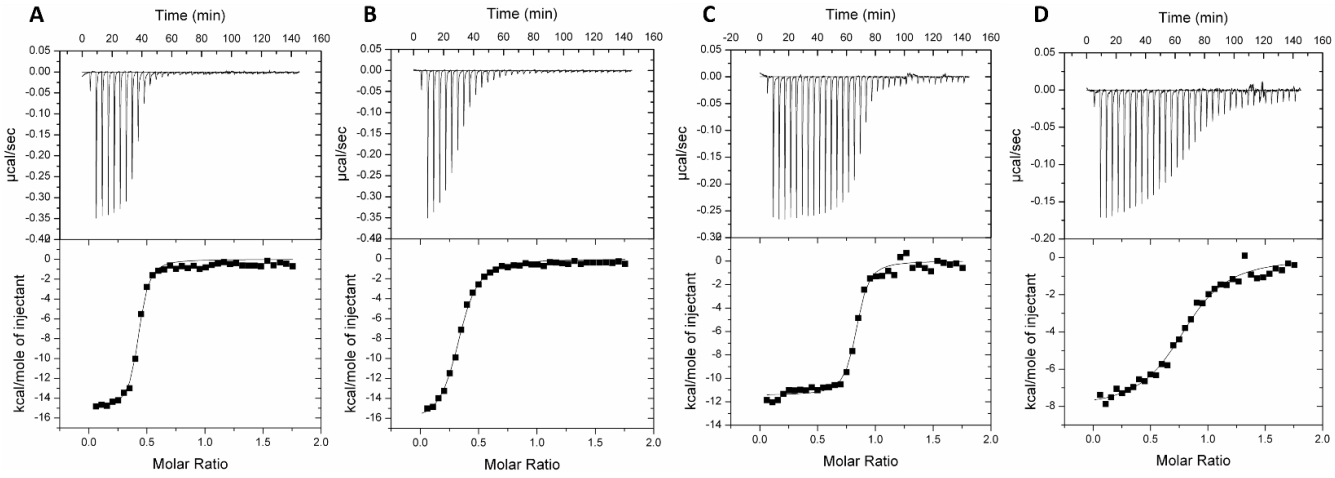

Figure 3.6.2 A-D *ITC measurement at 27ºC of Ca_2/CaBP1 binding to the IQ (**A**) IQ^{WT}, (**B**) IQ^{K1662E}, (**C**) $CaBP1^{E94}$, and (**D**) $CaBP1^{I144E}$.*

The CaBP1 mutation E94K was expected to disrupt the CaBP1 E94 ←→ IQ K1662 salt bridge (**Fig. 3.3.3**), but this mutation had no detectable effect on the IQ binding affinity (K_D^{WT} = 45 ± 9 nM vs K_D^{E94A} = 35 ± 5 nM). This result is further evidence that the structural model with

reversed binding orientation (**Fig. 3.3.3**) is not correct. The IQ mutation K1662E reduced the CaBP1 binding affinity by 4-fold (K_D^{WT} = 45 ± 9 nM vs K_D^{K1662E} = of 220 ± 20 nM). This result is consistent with K1662 forming a salt bridge with D140 from CaBP1 (Fig. 3.5.3). The CaBP1 mutation I144E significantly weakened the IQ binding affinity (K_D^{WT} = 45 ± 9 nM vs K_D^{I144E} = 500 ± 40 nM), consistent with I144 as an important contact for IQ binding. Additionally, CaBP1 mutants F111E and M165E were prepared. These mutants however could not be purified using the CaBP1 purification protocol.

3.7 Ca^{2+}-dependent Activation of $Ca_V1.2$ Promoted by CaBP1

Previous electrophysiology studies on $Ca_V1.2$ suggest that CaBP1 abolishes CDI[36] and causes Ca^{2+}-dependent facilitation (CDF) of channel activity.[9] Also, preliminary electrophysiology studies on $Ca_V1.2$ by Manuel Navedo's lab have shown that ectopic expression of CaBP1 with $Ca_V1.2$ in HEK cells causes an increase in the basal channel open probability (Po) (**Fig. 3.7.1**). This is quite similar to a 3-fold increase in channel Po caused by half-calcified CaM.[90] Based on the similarity of my NMR structures of Ca_2/CaM-IQ (Fig. 2.3.3) and Ca_2/CaBP1-IQ (**Fig. 3.3.2**), it is now clear that Ca^{2+}-bound CaBP1 binding to the IQ-motif can mimic the binding of half-calcified CaM, which may explain how CaBP1 causes increased Po. The competitive IQ binding by Ca_2/CaBP1 and Ca_2/CaM may also explain how CaBP1 can inhibit CaM binding to $Ca_V1.2$ and abolish CDI.[36] However, previous studies on a mutant of CaBP1 that disables Ca^{2+} binding to EF3 and EF4 (D112A/D149A, called $CaBP1_{34}$) indicated that this Ca^{2+}-free mutant only partially restores CDI,[9] which suggested that Ca^{2+}-free apoCaBP1 might bind to $Ca_V1.2$.[36] The partial CDI restoration (rather than full restoration) by $CaBP1_{34}$ is possibly an artifact of the very large overexpression of recombinant $CaBP1_{34}$ protein in these experiments. Indeed, a recent quantitative study showed that recombinant expression of the related CaM mutant (CaM_{34}) in HEK cells was

observed to be expressed at a protein concentration in excess of 10 μM.[90] Such a high concentration of $CaBP1_{34}$ (>10 μM) in HEK cells might be sufficient to allow Ca^{2+}-free apo$CaBP1_{34}$ protein to bind artificially to $Ca_V1.2$ (K_D = 3.8 μM, **Fig. 2.3.1**) and therefore block the binding of endogenous Ca_2/CaM that is present at nanomolar levels under basal conditions.[36] However, it is unlikely that native apoCaBP1 can bind functionally to $Ca_V1.2$ under physiological conditions, because the native free concentration of apoCaBP1 is likely much lower than the micromolar K_D for apoCaBP1 binding to the IQ-motif. The micromolar binding of apoCaBP1 [**Fig. 2.3.1**] would predict about 1% of $Ca_V1.2$ bound to apoCaBP1 under physiological conditions (assuming [CaBP1] = 0.05 μM & Y = 0.05/(4 + 0.05) = 0.012). By contrast, $Ca_V1.2$ binds to Ca_2/CaBP1 with 100-fold higher affinity and would predict ~50% of $Ca_V1.2$ bound to Ca_2/CaBP1 under basal conditions (Y = 0.05/(0.05 + 0.05) = 0.5). Future studies are needed to measure more exact concentrations of native CaBP1 in neurons as well as recombinant $CaBP1_{34}$ versus wild type CaBP1 in HEK cells used for the electrophysiology studies to more accurately assess the fractional binding of apoCaBP1.

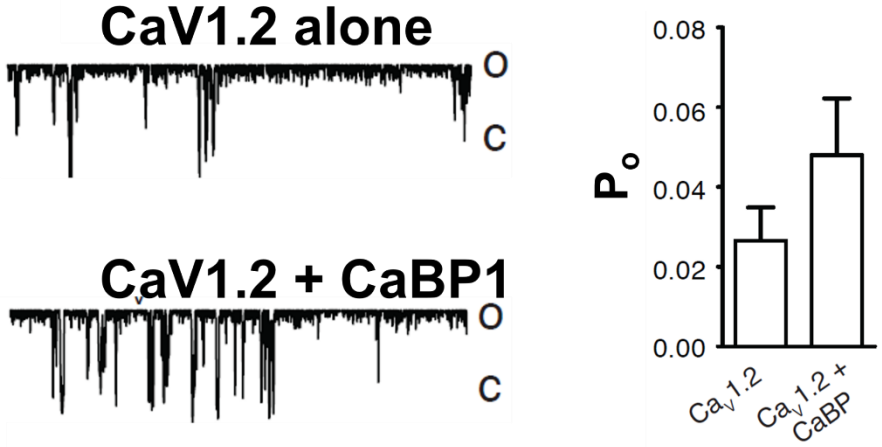

Figure 3.7.1 Preliminary electrophysiology results collected by the Navedo Lab show that ectopic expression CaBP1 with $Ca_V1.2$ in HEK cells causes an increase in the basal channel open probability (Po).

Combining the NMR structure of Ca_2/CaBP1-IQ (**Fig. 3.3.2**) with the known cryoEM structures of $Ca_V1.2$,[11] I propose a new structural mechanism for Ca^{2+}-dependent facilitation (CDF) of $Ca_V1.2$ channel activity promoted by CaBP1 (**Fig. 3.7.2**). $Ca_V1.2$ is proposed to occupy four possible channel states: closed & dissociated from CaBP1 (**Fig. 3.7.2A**), closed & bound to Ca_2/CaBP1 (**Fig. 3.7.2D**), open & dissociated from CaBP1 (**Figs. 3.7.2B-C**), and open & bound to Ca_2/CaBP1 (**Figs. 3.7.2E-F**). Under basal conditions ($[Ca^{2+}]$ = 50-100 nM), 50% of $Ca_V1.2$ channels are estimated to be bound to Ca_2/CaBP1 (**Figs. 3.7.2D-E**) and the remaining channels are not bound to apoCaBP1 (**Figs. 3.7.2A-B**), because apoCaBP1 binds to $Ca_V1.2$ in the micromolar range that is likely higher than physiological CaBP1 levels.[36] Neuronal stimulation produces membrane depolarization that switches the channel from closed (**Figs. 3.7.2A**) to open (**Fig. 3.7.2B**). When the channel first opens, the cytosolic Ca^{2+} concentration is transiently still low (< 100 nM) causing roughly an equal mixture of apoCaBP1 and Ca_2/CaBP1 (at $[Ca^{2+}]$ = 50-100 nM) in which Ca_2/CaBP1 binds to $Ca_V1.2$ (**Fig. 3.7.2E**) but apoCaBP1 is unbound (**Fig. 3.7.2B**). I propose that the binding of Ca_2/CaBP1 to $Ca_V1.2$ switches the channel into an active conformation in which the IQ motif folds back to interact with the channel EF-hand on one side, while Ca_2/CaBP1 is bound to the other side of the IQ helix as seen in the NMR structure of Ca_2/CaBP1-IQ (**Fig. 3.3.2**). The remaining channels (not bound to CaBP1, see **Fig. 3.7.2B**) are assumed to be in the channel inactive state in which the channel EF-hand interacts with the III-IV linker as seen in the cryoEM structure of $Ca_V1.1$ in the inactive state.[10] Prolonged voltage-induced channel opening causes a Ca^{2+} influx in which the cytosolic Ca^{2+} concentration increases to about 1 micromolar (**Figs. 3.7.2C & 3.7.2F**). This rise in Ca^{2+} concentration promotes formation of Ca_2/CaBP1, which binds tightly to the activated channel and switches all channels into the high open probability activated state (**Fig. 3.7.2F**) to produce CDF. By contrast, $Ca_V1.2$ switches into

the inactive channel state when CaBP1 dissociates from the channel at low Ca^{2+} levels (**Fig. 3.7.2B**), which explains why the channel has decreased activity at low cytosolic Ca^{2+} levels when a smaller fraction of $Ca_V1.2$ is bound to Ca_2/CaBP1. An important prediction of this model is that Ca^{2+} binding to CaBP1 should be essential for CDF. Future electrophysiology experiments are needed to test whether the $CaBP1_{34}$ mutant (disables Ca^{2+} binding to EF3 and EF4) will both decrease the basal channel Po and abolish CDF as predicted by the model.

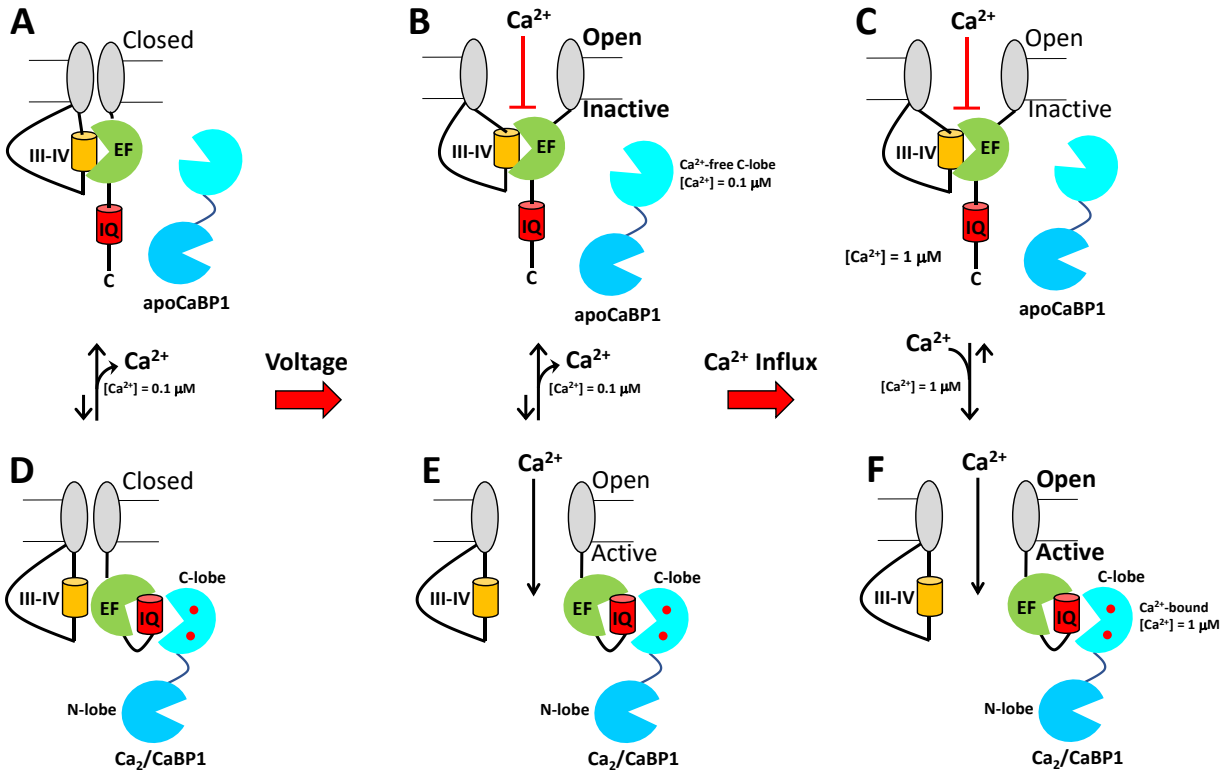

Figure 3.7.2 Structural Mechanism of Ca^{2+}-dependent Facilitation of $Ca_V1.2$ promoted by CaBP1. **A** Closed channel dissociated from apoCaBP1. **B** Open/inactivated channel dissociated from apoCaBP1 at low Ca^{2+} ($[Ca^{2+}] < 100$ nM). **C** Open/inactivated channel at high Ca^{2+} ($[Ca^{2+}] = 1$ µM). **D** Closed channel bound to Ca_2/CaBP1. **E** Open/activated channel bound to Ca_2/CaBP1 at low Ca^{2+} ($[Ca^{2+}] < 100$ nM). **F** Open/activated channel bound to Ca_2/CaBP1 at high Ca^{2+} ($[Ca^{2+}] = 1$ µM). Ca^{2+}-bound CaBP1 (Ca_2/CaBP1) drives formation of the open/active channel at high Ca^{2+} levels (forward arrow between C and F). Ca^{2+}-free CaBP1 (apoCaBP1) dissociates from $Ca_V1.2$ and drives formation of the inactive channel at low Ca^{2+} levels (reverse arrow between B and E). Bound Ca^{2+} (red circles), channel EF-hand (green), IQ-motif (red cylinder), III-IV linker (orange cylinder).

3.8 Experimental Procedures

CaBP1C mutagenesis and purification and IQ peptide for NMR: A cDNA of *Homo sapiens* CaBP1C was subcloned into pET-11b vector (Novagen) that produced recombinant CaBP1C without any extra residues. The mutated complementary DNA was inserted into the NcoI/ BamHI sites of a pET11d vector and verified by automated Sanger sequencing. The recombinant CaBP1C protein was expressed from a pET11d vector in a BL21(DE3) Codon Plus *Escherichia coli* strain (Stratagene) and purified as described previously.[88] The protein concentration was determined using absorbance at 205 nm.[94] The $Ca_V1.2$ IQ peptide ($Ca_V1.2$ residues 1644–1664) was purchased from ChinaPeptides. The peptide was dissolved in d_6-dimethyl sulfoxide to give a peptide concentration of 10.0 mM. The peptide concentration was determined by measuring absorbance at 280 nm with $\varepsilon_{280} = 2980\ M^{-1}\ cm^{-1}$. An aliquot of peptide (1.5 equivalents) was added to a dilute solution of CaBP1C (50 μM protein dissolved in 20 mM 2-amino−2−hydroxymethyl-propane-1,3-diol-d11 [Tris-d_{11}] with 95% H_2O/5% D_2O). The complex was then concentrated to a final concentration of 500 μM in a final volume of 500 μL for NMR experiments using a 3K Amicon concentrator. The 1.5-fold excess of IQ peptide in the NMR sample of CaBP1C -IQ was necessary to minimize the formation of a 2:1 complex, in which two molecules of CaBP1C were bound to one IQ. **Figure 3.8.1** shows a HSQC spectrum with equal concentrations of CaBP1C and IQ peptide. This spectrum includes two distinct peaks for many C-lobe residues of CaBP1C. The most intense peak represented a 1:1 complex (~90% occupancy) and a weaker second peak, which we believe to represent a second CaBP1C molecule bound to opposite side of the IQ-motif in a 2:1 complex (~10% occupancy). Under conditions where the CaBP1C concentration is more than 10-fold greater than that of $Ca_V1.2$, like what exists inside HEK293 cells used in the $Ca_V1.2$ electrophysiological experiment, channel occupation by the 2

separate CaBP1C proteins could reach nearly 100%. The 2:1 complex likely consists of a single IQ peptide that binds tightly to a Ca^{2+}-bound C-lobe on one side of the IQ helix (CaBP1 C-lobe contacting I1654, Y1657, and F1658) as well as a second CaBP1C C-lobe that binds with lower affinity to the opposite side of the IQ helix (CaBP1 C-lobe contacting F1648 and F1652).

Isothermal Titration Calorimetry: ITC experiments were performed using a VP-ITC calorimeter (Micro-Cal) at 27º C and 37º C. The data were acquired and processed with MicroCal software (https://www. originlab.com) as described previously.[33] The first data point from each ITC isotherm was deleted because the amount of $Ca_V1.2$ channel regulation by Ca_2/CaBP1 of injectant delivered during the first injection has significant error caused by a dead volume void in the injection syringe. Samples of Ca_2/CaBP1 (injectant) and IQ peptide (titrant) were prepared by exchanging each into buffer containing 20 mM Tris, pH 7.4, 100 mM KCl, and 1 mM $CaCl_2$. The concentrations of the IQ peptides (WT, I1654A, Y1657D, F1658D, or K1662E) were each 10 μM in 1.5 ml in the sample cell for titration with 0.1 mM Ca_2/CaBP1. Titrations consisted of 35 injections of 10 μl each. For the Ca^{2+} titration in Fig. 3.2.2, the concentration of CaBP1-IQ was 30 μM in 1.5 mL in the sample cell for titration with 0.1 mM $CaCl_2$. Ca^{2+} titrations consisted of 35 injections of 7 μL each.

NMR spectroscopy: All NMR measurements were performed at 303 K using a Bruker Avance III 600 MHz spectrometer equipped with a four-channel interface and triple-resonance cryoprobe. Two-dimensional NMR experiments (heteronuclear single quantum coherence [HSQC] and CT-HSQC) were recorded on samples of 15N-labeled Ca_2/CaBP1 (0.5 mM) bound to unlabeled IQ-peptide (0.75 mM). Each sample was dissolved in 20 mM 2-Amino−2−hydroxymethyl-propane-1,3-diol-d11 (Tris-d_{11} at pH 7.5), 1.0 mM $CaCl_2$, and 95% H_2O/5% D_2O. Backbone resonances were assigned by analyzing HNCA, HNCACB, CBCA(CO)NH, HNCO.[95] Side chain resonances

were assigned by analyzing HCCH TOSCY as described previously.[96] Three-dimensional NMR experiments for assigning backbone and side-chain resonances, and NOESY-derived distance restraints were analyzed as described previously.[63] NMR data were processed using NMRPIPE[64] and NMRFx Analyst[97] and analyzed with SPARKY NMRFAM.[65]

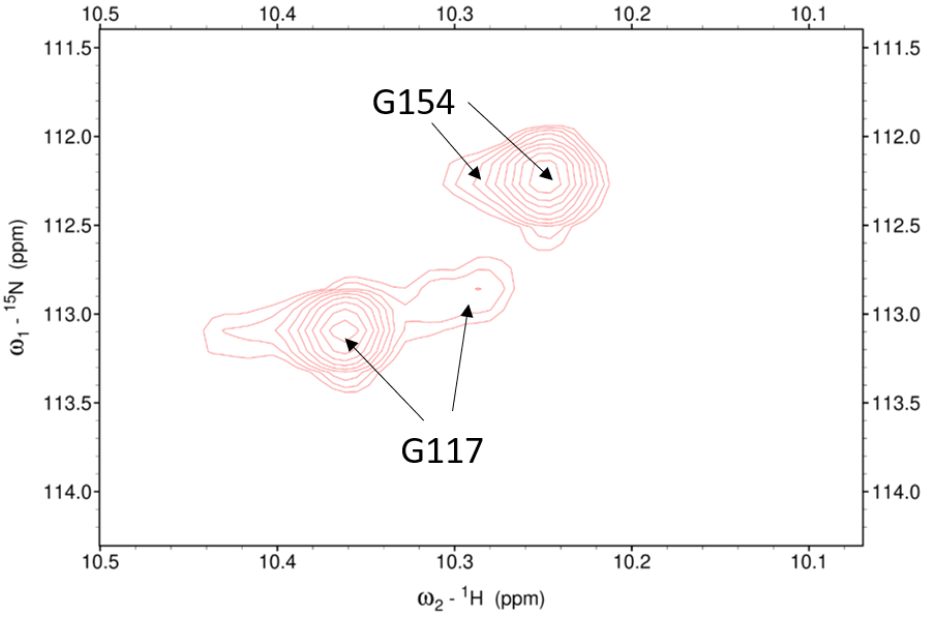

Figure 3.8.1 *HSQC spectrum of 15N-labeled Ca_2/CaBP1 C-lobe (100 μM) bound to unlabeled IQ peptide (100 μM) shows sample heterogeneity. Lower occupancy 2:1 complex CaBP1 C-lobe residues indicated by arrows.*

DOCKING using the HADDOCK2.4 Webserver: The starting structures used for the docking calculation crystal structure of CaBP1 (PDB: 3OX6) and the IQ peptide helix extracted from the structure of apo-calmodulin bound to the calcium voltage gated channel 1.2 IQ-motif (PDB: 6CTB). To create an accessible C-lobe binding surface, the CaBP1 structure was allowed to develop in a simulation with only the linker region defined as flexible. A suitable structure was chosen from these results. CaBP1 residues I99, A107, F111, L132, V136, I144, V148, M164, and M165 and IQ peptide residues I1654, Y1657, F1658, and F1661 were defined as ambiguous interaction restraints (AIRs). No additional segments were defined as flexible or semiflexible. NMR-derived distance restraints were input as unambiguous distance restraints. HADDOCK

initially calculated 2000 structures, the top 400 rigid-body optimization structures continued to simulated annealing. The top 200 simulated annealing structures continue to final refinement and clustering. Structures were clustered based on fraction of common contacts(FCC).

References

(1) Clapham, D. E. Calcium Signaling. *Cell* **2007**, *131* (6), 1047–1058. https://doi.org/10.1016/j.cell.2007.11.028.

(2) Pchitskaya, E.; Popugaeva, E.; Bezprozvanny, I. Calcium Signaling and Molecular Mechanisms Underlying Neurodegenerative Diseases. *Cell Calcium* **2018**, *70*, 87–94. https://doi.org/10.1016/j.ceca.2017.06.008.

(3) Berridge, M. J.; Lipp, P.; Bootman, M. D. The Versatility and Universality of Calcium Signalling. *Nat. Rev. Mol. Cell Biol.* **2000**, *1* (1), 11–21. https://doi.org/10.1038/35036035.

(4) Ames, J. B. L-Type Ca2+ Channel Regulation by Calmodulin and CaBP1. *Biomolecules* **2021**, *11* (12), 1811. https://doi.org/10.3390/biom11121811.

(5) Bezprozvanny, I. Calcium Signaling and Neurodegenerative Diseases. *Trends Mol. Med.* **2009**, *15* (3), 89–100. https://doi.org/10.1016/j.molmed.2009.01.001.

(6) Cain, S. M.; Snutch, T. P. Voltage-Gated Calcium Channels and Disease. *BioFactors* **2011**, *37* (3), 197–205. https://doi.org/10.1002/biof.158.

(7) Catterall, W. A. Voltage-Gated Calcium Channels. *Cold Spring Harb. Perspect. Biol.* **2011**, *3* (8), a003947. https://doi.org/10.1101/cshperspect.a003947.

(8) Andranovits, S.; Beyl, S.; Hohaus, A.; Zangerl-Plessl, E. M.; Timin, E.; Hering, S. Key Role of Segment IS4 in Cav1.2 Inactivation: Link between Activation and Inactivation. *Pflugers Arch.* **2017**, *469* (11), 1485–1493. https://doi.org/10.1007/s00424-017-2038-3.

(9) Findeisen, F.; Minor, D. L. Structural Basis for the Differential Effects of CaBP1 and Calmodulin on CaV1.2 Calcium-Dependent Inactivation. *Structure* **2010**, *18* (12), 1617–1631. https://doi.org/10.1016/j.str.2010.09.012.

(10) Wu, J.; Yan, Z.; Li, Z.; Qian, X.; Lu, S.; Dong, M.; Zhou, Q.; Yan, N. Structure of the Voltage-Gated Calcium Channel Cav1.1 at 3.6 Å Resolution. *Nature* **2016**, *537* (7619), 191–196. https://doi.org/10.1038/nature19321.

(11) Chen, Z.; Mondal, A.; Minor, D. L. Structural Basis for CaVα2δ:Gabapentin Binding. *Nat. Struct. Mol. Biol.* **2023**, 1–5. https://doi.org/10.1038/s41594-023-00951-7.

(12) Yang, C.-F.; Tsai, W.-C. Calmodulin: The Switch Button of Calcium Signaling. *Tzu-Chi Med. J.* **2021**, *34* (1), 15–22. https://doi.org/10.4103/tcmj.tcmj_285_20.

(13) Urrutia, J.; Aguado, A.; Muguruza-Montero, A.; Núñez, E.; Malo, C.; Casis, O.; Villarroel, A. The Crossroad of Ion Channels and Calmodulin in Disease. *Int. J. Mol. Sci.* **2019**, *20* (2), 400. https://doi.org/10.3390/ijms20020400.

(14) Chin, D.; Means, A. R. Calmodulin: A Prototypical Calcium Sensor. *Trends Cell Biol.* **2000**, *10* (8), 322–328. https://doi.org/10.1016/s0962-8924(00)01800-6.

(15) Means, A. R.; VanBerkum, M. F.; Bagchi, I.; Lu, K. P.; Rasmussen, C. D. Regulatory Functions of Calmodulin. *Pharmacol. Ther.* **1991**, *50* (2), 255–270. https://doi.org/10.1016/0163-7258(91)90017-g.

(16) Gilli, R.; Lafitte, D.; Lopez, C.; Kilhoffer, M.-C.; Makarov, A.; Briand, C.; Haiech, J. Thermodynamic Analysis of Calcium and Magnesium Binding to Calmodulin. *Biochemistry* **1998**, *37* (16), 5450–5456. https://doi.org/10.1021/bi972083a.

(17) Linse, S.; Helmersson, A.; Forsén, S. Calcium Binding to Calmodulin and Its Globular Domains. *J. Biol. Chem.* **1991**, *266* (13), 8050–8054.

(18) Ikura, M. Calcium Binding and Conformational Response in EF-Hand Proteins. *Trends Biochem. Sci.* **1996**, *21* (1), 14–17. https://doi.org/10.1016/S0968-0004(06)80021-6.
(19) Roth, S. M.; Schneider, D. M.; Strobel, L. A.; VanBerkum, M. F. A.; Means, A. R.; Wand, A. J. Structure of the Smooth Muscle Myosin Light-Chain Kinase Calmodulin-Binding Domain Peptide Bound to Calmodulin. *Biochemistry* **1991**, *30* (42), 10078–10084. https://doi.org/10.1021/bi00106a003.
(20) Rellos, P.; Pike, A. C. W.; Niesen, F. H.; Salah, E.; Lee, W. H.; von Delft, F.; Knapp, S. Structure of the CaMKIIδ/Calmodulin Complex Reveals the Molecular Mechanism of CaMKII Kinase Activation. *PLoS Biol.* **2010**, *8* (7), e1000426. https://doi.org/10.1371/journal.pbio.1000426.
(21) Ye, Q.; Li, X.; Wong, A.; Wei, Q.; Jia, Z. Structure of Calmodulin Bound to a Calcineurin Peptide: A New Way of Making an Old Binding Mode,. *Biochemistry* **2006**, *45* (3), 738–745. https://doi.org/10.1021/bi0521801.
(22) Vinayagam, D.; Quentin, D.; Yu-Strzelczyk, J.; Sitsel, O.; Merino, F.; Stabrin, M.; Hofnagel, O.; Yu, M.; Ledeboer, M. W.; Nagel, G.; Malojcic, G.; Raunser, S. Structural Basis of TRPC4 Regulation by Calmodulin and Pharmacological Agents. *eLife* **2020**, *9*, e60603. https://doi.org/10.7554/eLife.60603.
(23) Yu, Q.; Anderson, D. E.; Kaur, R.; Fisher, A. J.; Ames, J. B. The Crystal Structure of Calmodulin Bound to the Cardiac Ryanodine Receptor (RyR2) at Residues Phe4246–Val4271 Reveals a Fifth Calcium Binding Site. *Biochemistry* **2021**, *60* (14), 1088–1096. https://doi.org/10.1021/acs.biochem.1c00152.
(24) Bej, A.; Ames, J. B. NMR Structures of Calmodulin Bound to Two Separate Regulatory Sites in the Retinal Cyclic Nucleotide-Gated Channel. *Biochemistry* **2022**, *61* (18), 1955–1965. https://doi.org/10.1021/acs.biochem.2c00378.
(25) Gardill, B. R.; Rivera-Acevedo, R. E.; Tung, C.-C.; Van Petegem, F. Crystal Structures of Ca2+–Calmodulin Bound to NaV C-Terminal Regions Suggest Role for EF-Hand Domain in Binding and Inactivation. *Proc. Natl. Acad. Sci.* **2019**, *116* (22), 10763–10772. https://doi.org/10.1073/pnas.1818618116.
(26) Ben-Johny, M.; Yue, D. T. Calmodulin Regulation (Calmodulation) of Voltage-Gated Calcium Channels. *J. Gen. Physiol.* **2014**, *143* (6), 679–692. https://doi.org/10.1085/jgp.201311153.
(27) Zhang, Y.; Li, Z.; Sacks, D. B.; Ames, J. B. Structural Basis for Ca2+-Induced Activation and Dimerization of Estrogen Receptor α by Calmodulin*♦. *J. Biol. Chem.* **2012**, *287* (12), 9336–9344. https://doi.org/10.1074/jbc.M111.334797.
(28) Sprenger, J.; Trifan, A.; Patel, N.; Vanderbeck, A.; Bredfelt, J.; Tajkhorshid, E.; Rowlett, R.; Lo Leggio, L.; Åkerfeldt, K. S.; Linse, S. Calmodulin Complexes with Brain and Muscle Creatine Kinase Peptides. *Curr. Res. Struct. Biol.* **2021**, *3*, 121–132. https://doi.org/10.1016/j.crstbi.2021.05.001.
(29) Berchtold, M. W.; Villalobo, A. The Many Faces of Calmodulin in Cell Proliferation, Programmed Cell Death, Autophagy, and Cancer. *Biochim. Biophys. Acta BBA - Mol. Cell Res.* **2014**, *1843* (2), 398–435. https://doi.org/10.1016/j.bbamcr.2013.10.021.
(30) Villalobo, A.; Berchtold, M. W. The Role of Calmodulin in Tumor Cell Migration, Invasiveness, and Metastasis. *Int. J. Mol. Sci.* **2020**, *21* (3), 765. https://doi.org/10.3390/ijms21030765.

(31) Zhou, H.; Yu, K.; McCoy, K. L.; Lee, A. Molecular Mechanism for Divergent Regulation of Cav1.2 Ca2+ Channels by Calmodulin and Ca2+-Binding Protein-1*. *J. Biol. Chem.* **2005**, *280* (33), 29612–29619. https://doi.org/10.1074/jbc.M504167200.
(32) Kinoshita-Kawada, M.; Tang, J.; Xiao, R.; Kaneko, S.; Foskett, J. K.; Zhu, M. X. Inhibition of TRPC5 Channels by Ca2+-Binding Protein 1 in Xenopus Oocytes. *Pflüg. Arch.* **2005**, *450* (5), 345–354. https://doi.org/10.1007/s00424-005-1419-1.
(33) Wingard, J. N.; Chan, J.; Bosanac, I.; Haeseleer, F.; Palczewski, K.; Ikura, M.; Ames, J. B. Structural Analysis of Mg2+ and Ca2+ Binding to CaBP1, a Neuron-Specific Regulator of Calcium Channels*. *J. Biol. Chem.* **2005**, *280* (45), 37461–37470. https://doi.org/10.1074/jbc.M508541200.
(34) Oz, S.; Tsemakhovich, V.; Christel, C. J.; Lee, A.; Dascal, N. CaBP1 Regulates Voltage-Dependent Inactivation and Activation of CaV1.2 (L-Type) Calcium Channels*. *J. Biol. Chem.* **2011**, *286* (16), 13945–13953. https://doi.org/10.1074/jbc.M110.198424.
(35) Oz, S.; Benmocha, A.; Sasson, Y.; Sachyani, D.; Almagor, L.; Lee, A.; Hirsch, J. A.; Dascal, N. Competitive and Non-Competitive Regulation of Calcium-Dependent Inactivation in CaV1.2 L-Type Ca2+ Channels by Calmodulin and Ca2+-Binding Protein 1*. *J. Biol. Chem.* **2013**, *288* (18), 12680–12691. https://doi.org/10.1074/jbc.M113.460949.
(36) Findeisen, F.; Rumpf, C. H.; Minor, D. L. Apo States of Calmodulin and CaBP1 Control CaV1 Voltage-Gated Calcium Channel Function through Direct Competition for the IQ Domain. *J. Mol. Biol.* **2013**, *425* (17), 3217–3234. https://doi.org/10.1016/j.jmb.2013.06.024.
(37) Adams, P. J.; Ben-Johny, M.; Dick, I. E.; Inoue, T.; Yue, D. T. Apocalmodulin Itself Promotes Ion Channel Opening and Ca2+ Regulation. *Cell* **2014**, *159* (3), 608–622. https://doi.org/10.1016/j.cell.2014.09.047.
(38) Lian, L.-Y.; Myatt, D.; Kitmitto, A. Apo Calmodulin Binding to the L-Type Voltage-Gated Calcium Channel Cav1.2 IQ Peptide. *Biochem. Biophys. Res. Commun.* **2007**, *353* (3), 565–570. https://doi.org/10.1016/j.bbrc.2006.12.070.
(39) Johny, M. B.; Yang, P. S.; Bazzazi, H.; Yue, D. T. Dynamic Switching of Calmodulin Interactions Underlies Ca2+ Regulation of CaV1.3 Channels. *Nat. Commun.* **2013**, *4* (1), 1717. https://doi.org/10.1038/ncomms2727.
(40) Zühlke, R. D.; Pitt, G. S.; Deisseroth, K.; Tsien, R. W.; Reuter, H. Calmodulin Supports Both Inactivation and Facilitation of L-Type Calcium Channels. *Nature* **1999**, *399* (6732), 159–162. https://doi.org/10.1038/20200.
(41) Peterson, B. Z.; DeMaria, C. D.; Yue, D. T. Calmodulin Is the Ca2+ Sensor for Ca2+-Dependent Inactivation of L-Type Calcium Channels. *Neuron* **1999**, *22* (3), 549–558. https://doi.org/10.1016/S0896-6273(00)80709-6.
(42) Erickson, M. G.; Alseikhan, B. A.; Peterson, B. Z.; Yue, D. T. Preassociation of Calmodulin with Voltage-Gated Ca2+ Channels Revealed by FRET in Single Living Cells. *Neuron* **2001**, *31* (6), 973–985. https://doi.org/10.1016/S0896-6273(01)00438-X.
(43) Turner, M.; Anderson, D. E.; Bartels, P.; Nieves-Cintron, M.; Coleman, A. M.; Henderson, P. B.; Man, K. N. M.; Tseng, P.-Y.; Yarov-Yarovoy, V.; Bers, D. M.; Navedo, M. F.; Horne, M. C.; Ames, J. B.; Hell, J. W. α-Actinin-1 Promotes Activity of the L-Type Ca2+ Channel Cav 1.2. *EMBO J.* **2020**, *39* (5), e102622. https://doi.org/10.15252/embj.2019102622.

(44) Van Petegem, F.; Chatelain, F. C.; Minor. Insights into Voltage-Gated Calcium Channel Regulation from the Structure of the CaV1.2 IQ Domain–Ca2+/Calmodulin Complex. *Nat. Struct. Mol. Biol.* **2005**, *12* (12), 1108–1115. https://doi.org/10.1038/nsmb1027.
(45) Fallon, J. L.; Baker, M. R.; Xiong, L.; Loy, R. E.; Yang, G.; Dirksen, R. T.; Hamilton, S. L.; Quiocho, F. A. Crystal Structure of Dimeric Cardiac L-Type Calcium Channel Regulatory Domains Bridged by Ca2+·calmodulins. *Proc. Natl. Acad. Sci.* **2009**, *106* (13), 5135–5140. https://doi.org/10.1073/pnas.0807487106.
(46) Liu, Z.; Vogel, H. J. Structural Basis for the Regulation of L-Type Voltage-Gated Calcium Channels: Interactions between the N-Terminal Cytoplasmic Domain and Ca2+-Calmodulin. *Front. Mol. Neurosci.* **2012**, *5*, 38. https://doi.org/10.3389/fnmol.2012.00038.
(47) Evans, T. I. A.; Hell, J. W.; Shea, M. A. Thermodynamic Linkage between Calmodulin Domains Binding Calcium and Contiguous Sites in the C-Terminal Tail of CaV1.2. *Biophys. Chem.* **2011**, *159* (1), 172–187. https://doi.org/10.1016/j.bpc.2011.06.007.
(48) Erickson, M. G.; Liang, H.; Mori, M. X.; Yue, D. T. FRET Two-Hybrid Mapping Reveals Function and Location of L-Type Ca2+ Channel CaM Preassociation. *Neuron* **2003**, *39* (1), 97–107. https://doi.org/10.1016/S0896-6273(03)00395-7.
(49) Wu, X.; Bers, D. M. Free and Bound Intracellular Calmodulin Measurements in Cardiac Myocytes. *Cell Calcium* **2007**, *41* (4), 353–364. https://doi.org/10.1016/j.ceca.2006.07.011.
(50) Halling, D. B.; Georgiou, D. K.; Black, D. J.; Yang, G.; Fallon, J. L.; Quiocho, F. A.; Pedersen, S. E.; Hamilton, S. L. Determinants in CaV1 Channels That Regulate the Ca2+ Sensitivity of Bound Calmodulin*. *J. Biol. Chem.* **2009**, *284* (30), 20041–20051. https://doi.org/10.1074/jbc.M109.013326.
(51) Salveson, I.; Anderson, D. E.; Hell, J. W.; Ames, J. B. Chemical Shift Assignments of a Calmodulin Intermediate with Two Ca2+ Bound in Complex with the IQ-Motif of Voltage-Gated Ca2+ Channels (CaV1.2). *Biomol. NMR Assign.* **2019**, *13* (1), 233–237. https://doi.org/10.1007/s12104-019-09883-0.
(52) Fallon, J. L.; Halling, D. B.; Hamilton, S. L.; Quiocho, F. A. Structure of Calmodulin Bound to the Hydrophobic IQ Domain of the Cardiac Cav1.2 Calcium Channel. *Structure* **2005**, *13* (12), 1881–1886. https://doi.org/10.1016/j.str.2005.09.021.
(53) Clore, G. M.; Gronenborn, A. M. NMR Structure Determination of Proteins and Protein Complexes Larger than 20 kDa. *Curr. Opin. Chem. Biol.* **1998**, *2* (5), 564–570. https://doi.org/10.1016/S1367-5931(98)80084-7.
(54) Tjandra, N.; Bax, A. Direct Measurement of Distances and Angles in Biomolecules by NMR in a Dilute Liquid Crystalline Medium. *Science* **1997**, *278* (5340), 1111–1114. https://doi.org/10.1126/science.278.5340.1111.
(55) Shen, Y.; Delaglio, F.; Cornilescu, G.; Bax, A. TALOS+: A Hybrid Method for Predicting Protein Backbone Torsion Angles from NMR Chemical Shifts. *J. Biomol. NMR* **2009**, *44* (4), 213–223. https://doi.org/10.1007/s10858-009-9333-z.
(56) Schwieters, C. D.; Kuszewski, J. J.; Tjandra, N.; Marius Clore, G. The Xplor-NIH NMR Molecular Structure Determination Package. *J. Magn. Reson.* **2003**, *160* (1), 65–73. https://doi.org/10.1016/S1090-7807(02)00014-9.
(57) Finn, B. E.; Evenäs, J.; Drakenberg, T.; Waltho, J. P.; Thulin, E.; Forsén, S. Calcium-Induced Structural Changes and Domain Autonomy in Calmodulin. *Nat. Struct. Biol.* **1995**, *2* (9), 777–783. https://doi.org/10.1038/nsb0995-777.

(58) Kuboniwa, H.; Tjandra, N.; Grzesiek, S.; Ren, H.; Klee, C. B.; Bax, A. Solution Structure of Calcium-Free Calmodulin. *Nat. Struct. Biol.* **1995**, *2* (9), 768–776. https://doi.org/10.1038/nsb0995-768.
(59) Zhang, M.; Tanaka, T.; Ikura, M. Calcium-Induced Conformational Transition Revealed by the Solution Structure of Apo Calmodulin. *Nat. Struct. Biol.* **1995**, *2* (9), 758–767. https://doi.org/10.1038/nsb0995-758.
(60) Laskowski, R. A.; Rullmann, J. A. C.; MacArthur, M. W.; Kaptein, R.; Thornton, J. M. AQUA and PROCHECK-NMR: Programs for Checking the Quality of Protein Structures Solved by NMR. *J. Biomol. NMR* **1996**, *8* (4), 477–486. https://doi.org/10.1007/BF00228148.
(61) Hall, D. D.; Dai, S.; Tseng, P.-Y.; Malik, Z.; Nguyen, M.; Matt, L.; Schnizler, K.; Shephard, A.; Mohapatra, D. P.; Tsuruta, F.; Dolmetsch, R. E.; Christel, C. J.; Lee, A.; Burette, A.; Weinberg, R. J.; Hell, J. W. Competition between α-Actinin and Ca2+-Calmodulin Controls Surface Retention of the L-Type Ca2+ Channel CaV1.2. *Neuron* **2013**, *78* (3), 483–497. https://doi.org/10.1016/j.neuron.2013.02.032.
(62) Liu, H.; Naismith, J. H. An Efficient One-Step Site-Directed Deletion, Insertion, Single and Multiple-Site Plasmid Mutagenesis Protocol. *BMC Biotechnol.* **2008**, *8* (1), 91. https://doi.org/10.1186/1472-6750-8-91.
(63) Lim, S.; Cudia, D.; Yu, Q.; Peshenko, I.; Dizhoor, A. M.; Ames, J. B. Chemical Shift Assignments of Retinal Degeneration 3 Protein (RD3). *Biomol. NMR Assign.* **2018**, *12* (1), 167–170. https://doi.org/10.1007/s12104-018-9802-y.
(64) Delaglio, F.; Grzesiek, S.; Vuister, G. W.; Zhu, G.; Pfeifer, J.; Bax, A. NMRPipe: A Multidimensional Spectral Processing System Based on UNIX Pipes. *J. Biomol. NMR* **1995**, *6* (3), 277–293. https://doi.org/10.1007/BF00197809.
(65) Lee, W.; Tonelli, M.; Markley, J. L. NMRFAM-SPARKY: Enhanced Software for Biomolecular NMR Spectroscopy. *Bioinformatics* **2015**, *31* (8), 1325–1327. https://doi.org/10.1093/bioinformatics/btu830.
(66) Ottiger, M.; Delaglio, F.; Marquardt, J. L.; Tjandra, N.; Bax, A. Measurement of Dipolar Couplings for Methylene and Methyl Sites in Weakly Oriented Macromolecules and Their Use in Structure Determination. *J. Magn. Reson.* **1998**, *134* (2), 365–369. https://doi.org/10.1006/jmre.1998.1546.
(67) Zweckstetter, M. NMR: Prediction of Molecular Alignment from Structure Using the PALES Software. *Nat. Protoc.* **2008**, *3* (4), 679–690. https://doi.org/10.1038/nprot.2008.36.
(68) Tanaka, T.; Ames, J. B.; Kainosho, M.; Stryer, L.; Ikura, M. Differential Isotope Labeling Strategy for Determining the Structure of Myristoylated Recoverin by NMR Spectroscopy. *J. Biomol. NMR* **1998**, *11* (2), 135–152. https://doi.org/10.1023/A:1008212316986.
(69) Nilges, M.; Gronenborn, A. M.; Brünger, A. T.; Clore, G. M. Determination of Three-Dimensional Structures of Proteins by Simulated Annealing with Interproton Distance Restraints. Application to Crambin, Potato Carboxypeptidase Inhibitor and Barley Serine Proteinase Inhibitor 2. *Protein Eng. Des. Sel.* **1988**, *2* (1), 27–38. https://doi.org/10.1093/protein/2.1.27.
(70) Chen, V. B.; Arendall, W. B.; Headd, J. J.; Keedy, D. A.; Immormino, R. M.; Kapral, G. J.; Murray, L. W.; Richardson, J. S.; Richardson, D. C. MolProbity: All-Atom Structure Validation for Macromolecular Crystallography. *Acta Crystallogr. D Biol. Crystallogr.* **2010**, *66* (Pt 1), 12–21. https://doi.org/10.1107/S0907444909042073.

(71) Zhang, Y.; Matt, L.; Patriarchi, T.; Malik, Z. A.; Chowdhury, D.; Park, D. K.; Renieri, A.; Ames, J. B.; Hell, J. W. Capping of the N-Terminus of PSD-95 by Calmodulin Triggers Its Postsynaptic Release. *EMBO J.* **2014**, *33* (12), 1341–1353. https://doi.org/10.1002/embj.201488126.
(72) Tseng, P.-Y.; Henderson, P. B.; Hergarden, A. C.; Patriarchi, T.; Coleman, A. M.; Lillya, M. W.; Montagut-Bordas, C.; Lee, B.; Hell, J. W.; Horne, M. C. α-Actinin Promotes Surface Localization and Current Density of the Ca2+ Channel CaV1.2 by Binding to the IQ Region of the A1 Subunit. *Biochemistry* **2017**, *56* (28), 3669–3681. https://doi.org/10.1021/acs.biochem.7b00359.
(73) Shen, A.; Nieves-Cintron, M.; Deng, Y.; Shi, Q.; Chowdhury, D.; Qi, J.; Hell, J. W.; Navedo, M. F.; Xiang, Y. K. Functionally Distinct and Selectively Phosphorylated GPCR Subpopulations Co-Exist in a Single Cell. *Nat. Commun.* **2018**, *9*, 1050. https://doi.org/10.1038/s41467-018-03459-7.
(74) Perez-Reyes, E.; Castellano, A.; Kim, H. S.; Bertrand, P.; Baggstrom, E.; Lacerda, A. E.; Wei, X. Y.; Birnbaumer, L. Cloning and Expression of a Cardiac/Brain Beta Subunit of the L-Type Calcium Channel. *J. Biol. Chem.* **1992**, *267* (3), 1792–1797. https://doi.org/10.1016/S0021-9258(18)46015-2.
(75) Ellis, S. B.; Williams, M. E.; Ways, N. R.; Brenner, R.; Sharp, A. H.; Leung, A. T.; Campbell, K. P.; McKenna, E.; Koch, W. J.; Hui, A.; Schwartz, A.; Harpold, M. M. Sequence and Expression of mRNAs Encoding the A1 and A2 Subunits of a DHP-Sensitive Calcium Channel. *Science* **1988**, *241* (4873), 1661–1664. https://doi.org/10.1126/science.2458626.
(76) Iacobucci, G. J.; Popescu, G. K. Spatial Coupling Tunes NMDA Receptor Responses via Ca^{2+} Diffusion. *J. Neurosci.* **2019**, *39* (45), 8831–8844. https://doi.org/10.1523/JNEUROSCI.0901-19.2019.
(77) Bartels, P.; Yu, D.; Huang, H.; Hu, Z.; Herzig, S.; Soong, T. W. Alternative Splicing at N Terminus and Domain I Modulates CaV1.2 Inactivation and Surface Expression. *Biophys. J.* **2018**, *114* (9), 2095–2106. https://doi.org/10.1016/j.bpj.2018.03.029.
(78) Sachs, F.; Neil, J.; Barkakati, N. The Automated Analysis of Data from Single Ionic Channels. *Pflüg. Arch.* **1982**, *395* (4), 331–340. https://doi.org/10.1007/BF00580798.
(79) Horn, R. Estimating the Number of Channels in Patch Recordings. *Biophys. J.* **1991**, *60* (2), 433–439. https://doi.org/10.1016/S0006-3495(91)82069-0.
(80) Buonarati, O. R.; Henderson, P. B.; Murphy, G. G.; Horne, M. C.; Hell, J. W. Proteolytic Processing of the L-Type Ca2+ Channel Alpha11.2 Subunit in Neurons. *F1000Research* **2017**, *6*, 1166. https://doi.org/10.12688/f1000research.11808.1.
(81) Davare, M. A.; Hell, J. W. Increased Phosphorylation of the Neuronal L-Type Ca2+ Channel Cav1.2 during Aging. *Proc. Natl. Acad. Sci. U. S. A.* **2003**, *100* (26), 16018–16023. https://doi.org/10.1073/pnas.2236970100.
(82) Hall, D. D.; Feekes, J. A.; Arachchige Don, A. S.; Shi, M.; Hamid, J.; Chen, L.; Strack, S.; Zamponi, G. W.; Horne, M. C.; Hell, J. W. Binding of Protein Phosphatase 2A to the L-Type Calcium Channel Cav1.2 next to Ser1928, Its Main PKA Site, Is Critical for Ser1928 Dephosphorylation. *Biochemistry* **2006**, *45* (10), 3448–3459. https://doi.org/10.1021/bi051593z.

(83) Degasperi, A.; Birtwistle, M. R.; Volinsky, N.; Rauch, J.; Kolch, W.; Kholodenko, B. N. Evaluating Strategies to Normalise Biological Replicates of Western Blot Data. *PLOS ONE* **2014**, *9* (1), e87293. https://doi.org/10.1371/journal.pone.0087293.
(84) Haeseleer, F.; Sokal, I.; Verlinde, C. L.; Erdjument-Bromage, H.; Tempst, P.; Pronin, A. N.; Benovic, J. L.; Fariss, R. N.; Palczewski, K. Five Members of a Novel Ca(2+)-Binding Protein (CABP) Subfamily with Similarity to Calmodulin. *J. Biol. Chem.* **2000**, *275* (2), 1247–1260. https://doi.org/10.1074/jbc.275.2.1247.
(85) Haynes, L. P.; Tepikin, A. V.; Burgoyne, R. D. Calcium-Binding Protein 1 Is an Inhibitor of Agonist-Evoked, Inositol 1,4,5-Trisphosphate-Mediated Calcium Signaling. *J. Biol. Chem.* **2004**, *279* (1), 547–555. https://doi.org/10.1074/jbc.M309617200.
(86) Laube, G.; Seidenbecher, C. I.; Richter, K.; Dieterich, D. C.; Hoffmann, B.; Landwehr, M.; Smalla, K. H.; Winter, C.; Böckers, T. M.; Wolf, G.; Gundelfinger, E. D.; Kreutz, M. R. The Neuron-Specific Ca2+-Binding Protein Caldendrin: Gene Structure, Splice Isoforms, and Expression in the Rat Central Nervous System. *Mol. Cell. Neurosci.* **2002**, *19* (3), 459–475. https://doi.org/10.1006/mcne.2001.1078.
(87) Li, C.; Enomoto, M.; Rossi, A. M.; Seo, M.-D.; Rahman, T.; Stathopulos, P. B.; Taylor, C. W.; Ikura, M.; Ames, J. B. CaBP1, a Neuronal Ca2+ Sensor Protein, Inhibits Inositol Trisphosphate Receptors by Clamping Intersubunit Interactions. *Proc. Natl. Acad. Sci. U. S. A.* **2013**, *110* (21), 8507–8512. https://doi.org/10.1073/pnas.1220847110.
(88) Li, C.; Chan, J.; Haeseleer, F.; Mikoshiba, K.; Palczewski, K.; Ikura, M.; Ames, J. B. Structural Insights into Ca2+-Dependent Regulation of Inositol 1,4,5-Trisphosphate Receptors by CaBP1. *J. Biol. Chem.* **2009**, *284* (4), 2472–2481. https://doi.org/10.1074/jbc.M806513200.
(89) Zhou, H.; Kim, S.-A.; Kirk, E. A.; Tippens, A. L.; Sun, H.; Haeseleer, F.; Lee, A. Ca2+-Binding Protein-1 Facilitates and Forms a Postsynaptic Complex with Cav1.2 (L-Type) Ca2+ Channels. *J. Neurosci. Off. J. Soc. Neurosci.* **2004**, *24* (19), 4698–4708. https://doi.org/10.1523/JNEUROSCI.5523-03.2004.
(90) Bartels, P.; Salveson, I.; Coleman, A. M.; Anderson, D. E.; Jeng, G.; Estrada-Tobar, Z. M.; Man, K. N. M.; Yu, Q.; Kuzmenkina, E.; Nieves-Cintron, M.; Navedo, M. F.; Horne, M. C.; Hell, J. W.; Ames, J. B. Half-Calcified Calmodulin Promotes Basal Activity and Inactivation of the L-Type Calcium Channel CaV1.2. *J. Biol. Chem.* **2022**, *298* (12), 102701. https://doi.org/10.1016/j.jbc.2022.102701.
(91) van Zundert, G. C. P.; Rodrigues, J. P. G. L. M.; Trellet, M.; Schmitz, C.; Kastritis, P. L.; Karaca, E.; Melquiond, A. S. J.; van Dijk, M.; de Vries, S. J.; Bonvin, A. M. J. J. The HADDOCK2.2 Web Server: User-Friendly Integrative Modeling of Biomolecular Complexes. *J. Mol. Biol.* **2016**, *428* (4), 720–725. https://doi.org/10.1016/j.jmb.2015.09.014.
(92) Linge, J. P.; Habeck, M.; Rieping, W.; Nilges, M. ARIA: Automated NOE Assignment and NMR Structure Calculation. *Bioinformatics* **2003**, *19* (2), 315–316. https://doi.org/10.1093/bioinformatics/19.2.315.
(93) Salveson, I.; Ames, J. B. Chemical Shift Assignments of the C-Terminal Domain of CaBP1 Bound to the IQ-Motif of Voltage-Gated Ca2+ Channel (CaV1.2). *Biomol. NMR Assign.* **2022**, *16* (2), 385–390. https://doi.org/10.1007/s12104-022-10108-0.
(94) Scopes, R. K. Measurement of Protein by Spectrophotometry at 205 Nm. *Anal. Biochem.* **1974**, *59* (1), 277–282. https://doi.org/10.1016/0003-2697(74)90034-7.

(95) Ikura, M.; Kay, L. E. A Novel Approach for Sequential Assignment of ’H, 13C,and 15NSpectra of Larger Proteins: Heteronuclear Triple-Resonance Three-Dimensional NMR Spectroscopy. Application to Calmodulint.
(96) Ikura, M.; Spera, S.; Barbato, G.; Kay, L. E.; Krinks, M.; Bax, A. Secondary Structure and Side-Chain Proton and Carbon-13 Resonance Assignments of Calmodulin in Solution by Heteronuclear Multidimensional NMR Spectroscopy. *Biochemistry* **1991**, *30* (38), 9216–9228. https://doi.org/10.1021/bi00102a013.
(97) Norris, M.; Fetler, B.; Marchant, J.; Johnson, B. A. NMRFx Processor: A Cross-Platform NMR Data Processing Program. *J. Biomol. Nmr* **2016**, *65*, 205–216. https://doi.org/10.1007/s10858-016-0049-6.